Comparative Analysis of *Ha-ras* and *B-raf* Mutated Mouse Liver Tumors and Molecular Mechanisms of Phenobarbital-dependent Tumor Promotion

Dissertation

der Mathematisch-Naturwissenschaftlichen Fakultät
der Eberhard Karls Universität Tübingen
zur Erlangung des Grades eines
Doktors der Naturwissenschaften
(Dr. rer. nat.)

vorgelegt von
Benjamin Rignall
aus Böblingen

Tübingen
2011

Tag der mündlichen Prüfung:	19.05.2011
Dekan:	Prof. Dr. Wolfgang Rosenstiel
1. Berichterstatter:	Prof. Dr. Michael Schwarz
2. Berichterstatter:	Prof. Dr. Karl Walter Bock

Acknowledgment

First of all I want to thank my supervisor Prof. Michael Schwarz for the great support and the very interesting thesis, giving me the opportunity to work with several cooperation partners in Berlin and Tübingen.

I also want to thank Dr. Klaus Erich Appel of the Federal Institute for Risk Assessment for his great support.

Special thanks to Dr. Albrecht Buchmann and Dr. Albert Braeuning for proofreading of manuscripts.

Furthermore I want to thank all group members for creating such a pleasant working atmosphere. I also want to acknowledge the excellent technical assistance by Johanna Mahr, Silvia Vetter, Elke Zabinsky and Christine Meckert.

I owe my loving thanks to my girl-friend Izabela for appreciating the little free time during the last months of my thesis work, for her encouragement and understanding.

My special gratitude is due to my parents, sisters and nieces for the enduring and loving support throughout my studies.

RESUME

PERSONAL DATA

Benjamin Rignall
Schwärzlocher Straße 48
72070 Tübingen
07071/946188
brignall@hotmail.com
05.October 1977, Böblingen, Germany

SHORT PROFILE

Bachelor of Science in biochemistry and genetics
Promotion, major subject biochemistry
in advanced education to toxicological specialist

SCHOOL

Gymnasium in den Pfarrwiesen, Sindelfingen, Germany
Graduation: Allgemeine Hochschulreife

STUDIES

02/1999 – 12/2001 University of Otago, Dunedin, New Zealand
Studying biochemistry and genetics
Graduation*:* Bachelor of Science

04/2002 – 07/2006 Eberhard-Karls-Universität Tübingen, Germany
Studying biochemistry with the main subjects: biochemistry, toxicology and analytical chemistry
Diploma thesis: Charakterisierung des G-Protein gekoppelten Rezeptors GPR49 und dessen Einfluss auf den Wnt-Signalweg.
Graduation: Diploma in biochemistry

08/2006 – 02/2011 Eberhard-Karls-Universität Tübingen, Department of Toxicology
Dissertation thesis: Comparative Analysis of *Ha-ras* and *B-raf* Mutated Mouse Liver Tumors and Molecular Mechanisms of Phenobarbital-dependent Tumor Promotion.

Data presented in this work have in part been published:

Rignall , B., *et al*. (2009) Comparative Transcriptome and Proteome Analysis of Ha-ras and B-raf Mutated Mouse Liver Tumors. J Prot. Res. 8 (8):3987-94.

Braeuning , A., **Rignall, B**., *et al*. (2010) Phenotype and growth behavior of residual β-catenin-positive hepatocytes in livers of β-catenin-deficient mice. Histochem. Cell Biol. 134 (5):469-81.

Rignall , B., *et al*. (2011) Tumor formation in liver of conditional β-Catenin-deficient mice exposed to a diethylnitrosamine / phenobarbital tumor promotion regimen. Carcinogenesis 32 (1): 52-57.

Rignall, B., *et al*. Phenobarbital Induces Characteristic Changes in the Liver Proteome of β-Catenin wild-type and β-Catenin null mice. (manuscript in preparation).

Rignall, B., *et al*. Tumor promoting effects of dioxin-like and non-dioxin-like PCBs after combined application. (manuscript in preparation).

Schmid, A., **Rignall, B**., *et al*. Quantitative Analysis of the Growth Kinetics of Chemically-induced Mouse Liver Tumors by Non-invasive Magnetic Resonance Imaging. (manuscript in preparation).

Oral presentations of data presented in this work have been given:

DGPT Jahrestagung 2010 Mainz: Vergleichende Proteomanalyse von Ha-ras und B-raf mutierten Mauslebertumoren.

Baden-Württemberg ToxNet Meeting 2010 Freiburg: Tumor formation in Liver of Conditional β-Catenin-deficient Mice Exposed to a Diethylnitrosamine / Phenobarbital Tumor Promotion Regimen.

Table of Contents

1. Introduction

Cancer is a disease with high incidence, statistically affecting every third person among the European population, male and female in equal proportion (Marquardt and Schäfer, “Lehrbuch der Toxikologie”, 2nd edition, chapters 7-9). Only 25% of all cases affect people younger than 60 years of age, often involving a genetic predisposition to the disease. Therefore, cancer is an illness mainly associated with age.

The process of cancer development in humans is an area of intensive study and the molecular mechanisms are often still unknown. However, the fact that cancer most often affects elderly people and the knowledge that nearly all tumors are epithelial of origin leads to the assumption that carcinogenesis is a long term process consisting of multiple subsequent steps and is most likely caused by environmental factors. Therefore the term chemical carcinogenesis was introduced.

About 60% of all known carcinogens lead to gene mutation, thereby causing the disease pattern. All other experimentally verified carcinogenic substances are negative in genotoxicity testing, acting most likely by a non-genotoxic mechanism. Knowing these molecular mechanisms will help to understand the cause of cancer, also providing tools to develop drugs which specifically target tumor cells.

Most of the chemicals humans are exposed to, e.g. in food, air or at the workplace, are compound mixtures containing multiple substances of diverging potency and potentially affecting different cell populations. Depending on the composition, different organs maybe targeted causing non-additive effects when taking the individual organs into consideration. However, substances targeting the same organ may cause inhibitory, additive or even synergistic effects.

1.1 Liver Physiology

The liver, a central metabolic organ present in every vertebrate, is involved in a number of processes including the biosynthesis of plasma proteins, hormones and urea, the storage of glycogen which can be rapidly released from the liver as glucose to maintain a steady blood glucose level, as well as drug detoxification and xenobiotic metabolism. About 200 billion hepatocytes compose the liver, representing ~80% of the total organ mass. Although the liver is able to regenerate its size after surgery (partial hepatectomy), adult hepatocytes rarely proliferate (only 1/1.000 -

10.000), explaining their relatively long lifespan of about 30 years. Other cell types present in the liver are blood vessel forming endothelial cells, Ito cells that are involved in the storage of vitamin A and collagen, as well as liver-resident macrophages called Kupffer cells.

The histological structure of the liver on a microscopic scale is presented by hexagonally shaped liver lobules that are characterized by a central efferent hepatic vein that is surrounded by afferent portal veins located at the corners of the polygon. Each portal field, attributed to its structure also called portal trias, consists of three vessels: a branch of the hepatic artery supplying oxygen rich blood, a branch from the portal vein delivering xenobiotic substances and nutrients from the gastrointestinal system and an efferent bile duct for the excretion of bile acids. The blood flow is directed from the portal field towards the central vein along sinusoids lined with fenestrated endothelial cells to allow for the exchange of molecular substances smaller than ~250kDa in size between hepatocytes and the passing blood stream. Bile acids, excreted from hepatocytes, move in the opposite direction from the central vein towards the portal field in channels formed by neighboring hepatocytes.

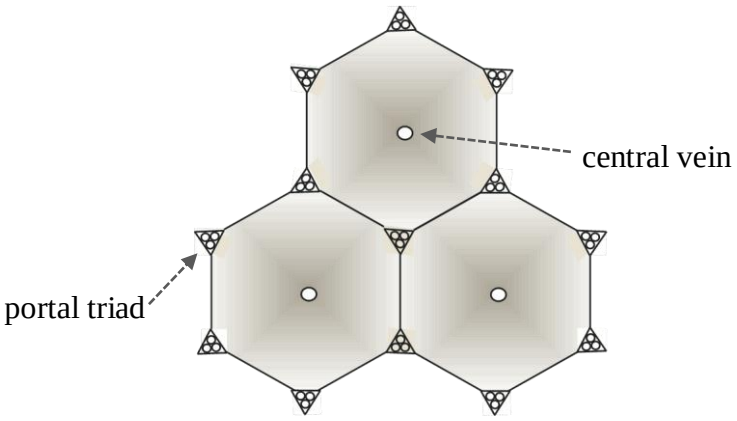

Figure 1: Schematic representation of a hexagonal shaped liver lobule.

1.2 Metabolic Zonation

The liver lobule displays a remarkable functional organization based upon the location of efferent and afferent blood vessels as well as the direction of blood flow. Cells that constitute this setup can be divided into two subpopulations, an upstream periportal population and a downstream perivenous (pericentral) population (for

recent reviews see Gebhardt , 1992; Cavard *et al*., 2008). Periportal cells can be distinguished from periveneous cells based on a difference in function that runs as a gradient from one cell population to the other. Whereas periportal cells exhibit for example a high rate of gluconeogenesis and ammonia detoxification by an active urea cycle pericentral cells have shown to display a high rate of glycolysis, glutamine synthesis as well as xenobiotic and drug metabolizing activity (Katz *et al*., 1977a; Katz *et al*., 1977b; Gebhardt, 1992; Jungermann , 1995).

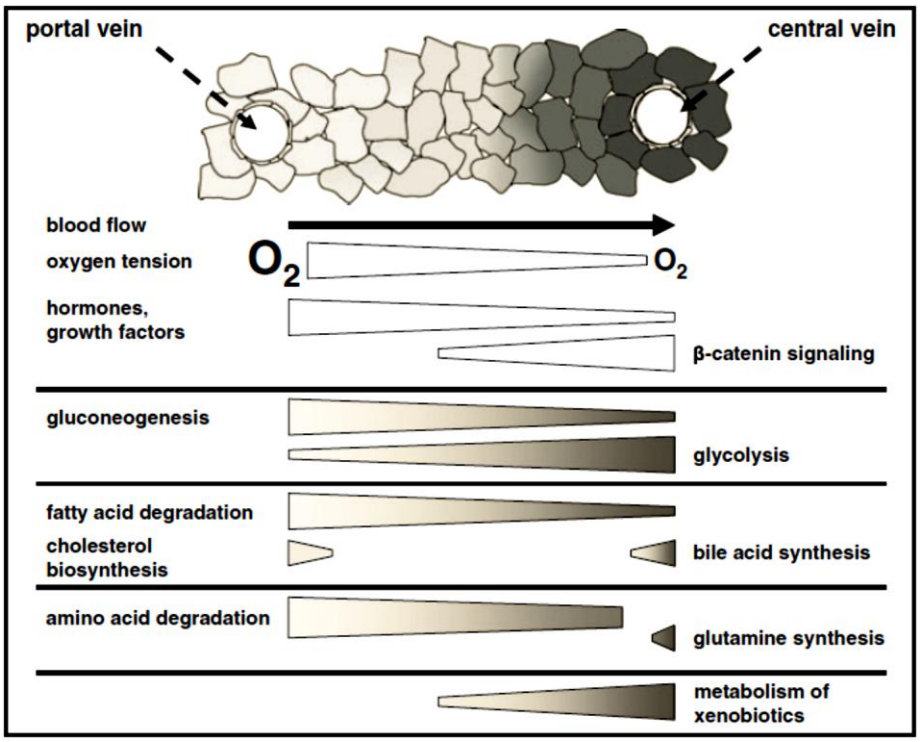

Figure 2: Metabolic zonation of the liver. The liver lobule displays a heterogeneous functional architecture, in which periportally located hepatocytes are involved in gluconeogenesis, fatty acid- and amino acid degradation whereas hepatocytes in vicinity of the central vein show increased glycolysis, bile acid synthesis and expression of xenobiotic metabolizing enzymes as well as glutamine synthesis, the letter based upon high expression of glutamine synthetase which can be used as a marker for pericentral located hepatocytes in immunohistochemical stainings. Figure taken from (Braeuning *et al*., FEBS 2006)

Molecular mechanisms, that have the potential to establish this functional heterogeneity, are still under debate. These include the role of oxygen tension (Jungermann and Katz, 1989), endothelial cell – hepatocyte interaction (Kuo and Darnell, 1991; Gebhardt and Gaunitz, 1997), hormones (Oinonen *et al*., 1993, 2000) and cytokines (Morgan , 2001). Recently the Wnt/β-catenin signaling pathway has been established as a new regulator of zonal gene expression in the murine liver.

Whereas active β-catenin signaling was shown to induce a perivenous gene expression profile (Benhamouche *et al*., 2006; Hailfinger *et al*., 2006; Braeuning *et al*., 2007), loss of β-catenin causes a disruption of perivenous gene expression (Benhamouche *et al*., 2006; Sekine *et al*., 2006; Tan *et al*., 2006). In addition, the periportal expression profile may be regulated by active MAPK/Ras signaling (Braeuning *et al*., 2007) or through inhibition of Wnt-signaling caused by the tumor suppressor APC, a negative regulator of β-catenin stability (Benhamouche *et al*,. 2006).

1.3 Carcinogenesis

The process of tumor formation, also called carcinogenesis, leads to cancer which is the second highest cause of death after cardiovascular disease in the human population worldwide (Marquardt and Schäfer, "Lehrbuch der Toxikologie", 2nd edition, chapters 7-9). The term "cancer" stands synonymous for a malignant tumor characterized by autonomous, invasive growth, often in a metastasizing manner. Benign tumors, as opposed to the rather destructive behaving malignant tumors, show expansive growth only, lacking the malignant phenotype. It is believed that chemical substances in the environment are the cause for the majority of human tumors. Epithelial cells, a type of cell that is often in direct contact to environmental compounds, are the source of 80-90% of all human tumors. In addition, epidemiological studies have shown an association between lifestyle (e.g. nutrition, smoking) and tumor formation (e.g. colon-cancer, lung-cancer). The fact that immigrants from countries with low incidence for a specific type of cancer (e.g. breast-cancer in Asia as opposed to the United States or Europe) adopt the incidence rate of the new environment after only one generation emphasizes the likelihood of chemical carcinogenesis as the main cause of tumor formation in humans. This has also been reflected in occupational medicine, where associations of substance exposure (e.g. polycyclic aromatic hydrocarbons) to disease patterns (e.g. urinary bladder-cancer) have been established.

The mechanism of tumor formation is believed to consist of multiple subsequent steps, starting from initiation of a single cell followed by clonal expansion, a process termed promotion, to a benign tumor and finally malignant progression to result in a malignant cell mass which potentially metastasizes to distant locations in the organism (reviewed in Moolgavkar and Knudson, 1981) and summarized in Figure 3.

The first very rarely occurring event in multistep carcinogenesis, also termed initiation, is the irreversible conversion of a normal cell into a pre-malignant state by i) direct action of a carcinogen, virus or radiation with DNA or via ii) indirect mechanisms of DNA damage caused by reactive oxygen species or inflammation. The molecular mechanisms include mutation of DNA (point mutation, frame-shift) that can affect tumor suppressor genes (gene products often inhibit cell cycle progression and initiate apoptosis or repair damaged DNA) or proto-oncogenes (gene products often activate cell cycle and/or inhibit apoptosis, e.g. *ras*, *raf* and *β-catenin*), genetic instability and aberrant telomerase expression. In very rare occasions, like breast-cancer (BRCA1), familiar adenomatous polyposis coli (FAPC), melanoma (CDK4) and medullary thyroid carcinoma (RET), an inherited genetic defect causes a pre-disposition for the initiation of tumor development. As a result of the initiation process an initiated cell is formed that is still under growth restriction by neighboring normal cells.

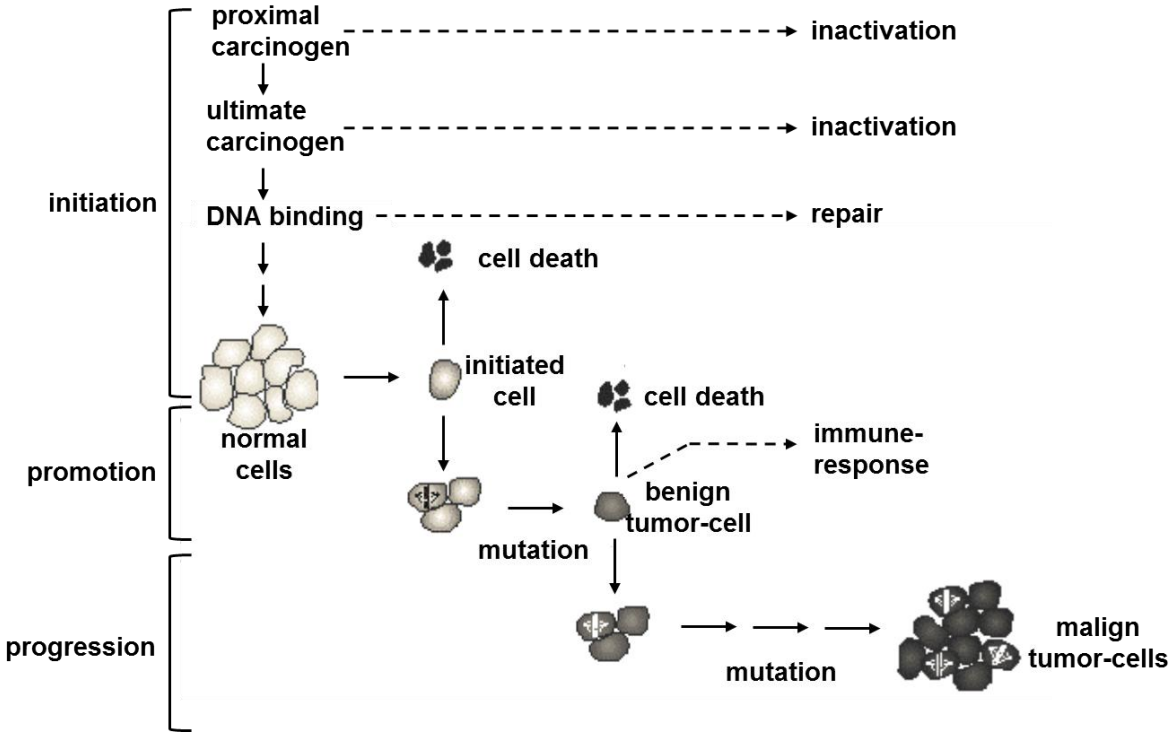

Figure 3: Multistep process of tumor formation adopted from (Schwarz and Bock, 1995).

Clonal expansion of the initiated cell takes place during tumor promotion, a process which is considered to be highly selective and reversible, to form a benign tumor (for a recent review see Klaunig *et al*., 2000). The molecular mechanisms include

epigenetic alteration of DNA (hyper/hypo-methylation, histone de-acetylation), induction of mitosis/regenerative growth, inhibition of apoptosis, inhibition of cell differentiation, sustained receptor activation (e.g. constitutive androstane receptor, aryl hydrocarbon receptor) and generation of oxidative stress. In common to all of these processes is the positive selection of an initiated cell by the tumor promoting agent. Compounds, like inflammatory noxa, capable of simultaneous initiation and promotion are termed complete carcinogens.

Accumulation of additional genetic lesions, especially those that target genes for DNA-damage repair (caretaker genes like p53), as well as epigenetic factors, finally cause the development of an unrestricted growing, malignant and metastasizing phenotype.

1.4 Hepatocarcinogenesis

Hepatocellular carcinoma (HCC) is one of the most frequently occurring human tumors worldwide, with a high incidence of cancer related deaths (Thorgeirsson and Grisham, 2002). The main risk factors for this disease are chronic hepatitis B and C virus infection and aflatoxin B1 exposure as wells as alcohol abuse (Kim *et al*., 2005). The mouse liver is one of the best studied experimental systems for molecular analysis of tumor formation, wherein specific point mutations in the genes coding for *Ha-ras*, *B-raf* or *β-catenin*, depending on the treatment regiment, can be analyzed. For experimental analysis, the mouse strain C3H/N is especially suitable, since it has been demonstrated to harbor a comparatively high background incidence of spontaneous liver tumors (Buchmann *et al*., 1991) and is susceptible to tumor promotion by phenobarbital (Aydinlik *et al*., 2001). While mutations in *Ctnnb1,* the gene coding for β-catenin, are highly prevalent in tumors induced by a treatment regimen including phenobarbital (PB) or a PB-like liver tumor promoter, *Ha-ras* or, alternatively, *B-raf* mutations are seen in up to 70% of spontaneously occurring liver tumors or in tumors induced by exclusive treatment with a genotoxic liver carcinogen like N-nitroso-diethylamine (Buchmann *et al*., 1991; Jaworski *et al*., 2005; Buchmann *et al*., 1991). The situation in human liver cancer, where mainly inactivating mutations in the gene coding for the tumor suppressor protein p53 or activating mutations in *Ctnnb1* but no *ras* or *B-raf* mutations are found, differs in this perspective from that in murine liver (Koehle *et al*., 2008). In addition, there seems to be a lack of tumor promotion in humans when analyzing epidemiological data from clinical application of

PB (IARC 2001). Still, the mouse liver is an indispensable tool to study molecular mechanisms of tumor formation in an *in vivo* situation.

Initiation of liver tumors with N-nitroso-diethylamine: The nitrosamine N-nitroso-diethylamine, also known as diethylnitrosamine or DEN, has been extensively used as an experimental carcinogen in animal experiments. Although there is human exposure to DEN, e.g. through cigarette smoke, an epidemiological association to human carcinogenesis has not been established yet. DEN is a pro-carcinogenic substance that has to be converted into its ultimate DNA alkylating form by catalytic activity of cytochrome P450 enzymes, especially the isoform CYP 2E1 (Kang *et al*., 2007), via α-hydroxylation and subsequent spontaneous de-alkylation. The most relevant targets for DNA modification, thereby inhibiting correct base-pairing of nucleotides and leading to the formation of liver cells with neoplastic potential, are O^6-desoxyGuanine and O^4-desoxyThymine (Verna *et al*., 1996). The molecular targets of DEN in the liver of hepatocarcinogenesis-susceptible juvenile C3H/N mice are *Ha-ras* (~40% of all lesions) and *B-raf* (~18%)(Buchmann *et al*., 2008; Jaworski *et al*., 2005). It is believed that mutation of the *ras* proto-oncogene in this model is an early event (Bauer-Hofmann *et al*., 1992) and that the constitutive activation leads to a proliferative advantage of initiated cells as compared to normal cells (Schwarz *et al*., 1995).

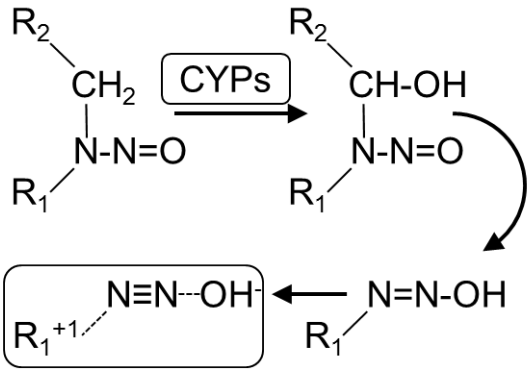

Figure 4: Metabolic activation of DEN through α-hydroxylation, catalyzed by cytochrome P450 enzymes, and subsequent spontaneous de-alkylation, to form a DNA-reactive moiety.

Tumor promotion in the mouse liver with PB: It was first reported in the 1970s that chronic PB treatment promotes hepatocellular carcinoma (HCC) in rodents (Peraino *et al*., 1971). Chronic treatment with PB and PB-like inducers is known to

promote thyroid hypertrophy in humans (Curran and DeGroot, 1991) but not HCC or other types of tumors. PB is a prototypic non-genotoxic carcinogen that causes tumor formation without mutating DNA, although the molecular mechanisms remain virtually unknown. Cell proliferation, as seen in pre-neoplastic cells and caused by non-genotoxic carcinogens, can be either attributed to an increase in cell proliferation of the neoplastic foci or to “mito-suppression” of non-initiated cells surrounding the lesion (Klaunig *et al*., 2000). Sustained treatment with PB seems to act in a mito-suppressing manner, involving an increase in the expression of transforming growth factor β and mannose-6-phosphate/insulin-like growth factor II receptor (Jirtle *et al*., 1994). In addition, a decrease in the rate of apoptosis in foci of rats initiated with N-nitroso-morpholine and chronically treated with PB has been observed (Schulte-Hermann *et al*., 1990). Thus, PB seems to confer a growth advantage of neoplastic foci by a decrease in mitosis of non-initiated cells and at the same time an inhibition of apoptosis in initiated cells. In line with this, acute treatment with PB causes hepatomegaly, an increase in cellular hypertrophy and hyperplasia (Wei *et al*., 2000).

Gap junctions of the liver consist of connexin molecules, the main isoform being connexin32, aligned in a hexameric manner to form a hemi-channel that connects to the hemi-channel of a neighboring cell. Thereby a transmembrane conduit is generated permitting the exchange of small molecular substances. Among these are there are low-molecular-weight messengers that have been linked to regulation of the cell cycle, cell growth and cell death. In fact, it has been demonstrated that during the process of hepatocarcinogenesis gap junctional intercellular communication (GJIC) decreases (Krutovskikh and Yamasaki, 1997). To further analyze the importance of connexin32 in the process of tumor promotion by PB, a connexin32 deficient mouse strain was generated earlier in our laboratory and tested for tumor formation after initiation with DEN followed by chronic treatment with PB. Surprisingly, deficiency in the gap junctional protein inhibited tumor promotion by the barbiturate (Moennikes *et al*., 2000). Therefore, connexin32 is an essential molecule involved in the process of tumor promotion by PB.

Treatment with PB or PB-like tumor promoters leads to the induction of xenobiotic metabolizing enzymes, especially the cytochrome P450 2B (CYP 2B) subfamily. The conversion of PB by CYP 2B has been shown to potentially induce futile cycling of the enzyme which leads to the generation of superoxide anions (Ingelman-Sundberg and Hagbjork, 1982). These reactive oxygen species are possibly genotoxic,

resulting in tumor promotion and progression. The expression of genes coding for CYP 2B family of xenobiotic enzymes is regulated by the constitutive androstane receptor, also known as CAR. PB modulates the activity of the receptor by a yet unknown mechanism that involves the protein phosphatase 2A (PP2A) and de-phosphorylation, maybe catalyzed by PP2A, of a serine residue at position 202 of CAR (Hosseinpour *et al*., 2006). Upon modulation, CAR translocates into the cell nucleus where it heterodimerizes with the 9-*cis* retinoic acid receptor (RXR) and binds to PB-responsive enhancer modules (PBREM) to regulate transcription of multiple genes (Swales and Negishi, 2004). Up-regulation of Mdm2 expression by CAR has been shown to contribute to both increased DNA replication and inhibition of p53-mediated apoptosis (Huang *et al*., 2005). CAR null-mice, initiated with a single dose of DEN followed by chronic treatment with PB, do not show any sign of tumor formation in the liver (Yamamoto *et al*., 2004). Therefore, CAR is another essential molecule for PB-dependent tumor promotion.

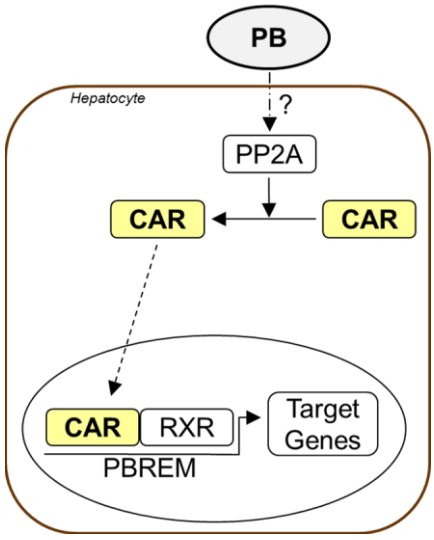

Figure 5: PB-dependent modulation of CAR activity mediated by the protein phosphatase 2A (PP2A). After translocation into the nucleus, CAR heterodimerizes with the 9-*cis* retinoic acid receptor (RXR) to regulate, upon binding to discrete PB responsive enhancer modules (PBREM), target gene transcription. Adopted from (Swales and Negishi, 2004).

In addition, it has been shown that CAR can act independently of PBREM by inhibiting the activity of the transcription factor FoxO1, therefore preventing the expression of gluconeogenetic enzymes (Kodama *et al*., 2004). There is also accumulating evidence that PB alters the methylation pattern of DNA and that these

changes are part of the tumor promotion process induced by the barbiturate (Phillips *et al*., 2007).

Tumor promotion in the mouse liver with a mixture of differently acting PCBs:
In contrast to the situation in the laboratory, where often a single substance in high purity is applied to analyze the associated effects of the test-compound, humans are exposed to a complex mixture of environmental factors that may either act independently of each other or display combined effects. The latter can be antagonistic, additive or synergistic. However, it is still unclear which risk is imposed on humans exposed to these mixtures and concepts for risk assessment are still a matter of debate.

Polychlorinated biphenyls (PCBs) are environmental toxicants characterized by high stability, lipophilicity and persistence. Although PCB production has been banned a long time ago, these substances are still present in the human food chain due to their longevity. PCBs structurally characterized by a backbone consisting of two chlorines in *ortho* position and two *para* chlorines resemble PB in their mode of cytochrome P-450 induction (Denomme *et al*., 1983), presumably acting through the CAR (Waxman , 1999). For dioxin-like substances, which generally contain a planar structure, the mode of action is primarily activation of the aryl hydrocarbon receptor (AhR) (Bandiera *et al*., 1982). PCBs presumably act as tumor promoters in rodent liver by stimulating the outgrowth of initiated cells and there is evidence that, depending on the type of tumor promoting agent used, different subpopulations of cells are acted on.

Most of the studies that experimentally tested the effects of PCBs on tumor promotion *in vivo* have been conducted in rats. However, the molecular mechanisms leading to hepatocarcinogenesis in mice exceed the knowledge we have about the process in other species. PCB 126 is a dioxin-like substance activating the AhR. Constitutive activation of the AhR has been shown to cause hepatocellular tumors (Moennikes *et al*., 2004) which are most often mutated in the *Ha-ras* proto-oncogene (Watson *et al*., 1995) but not in *Ctnnb1* (Devereux *et al*., 1999). The molecular mechanism of dioxin/AhR-dependent tumor promotion, reviewed in Schwarz and Appel, 2005, is partly due to apoptosis inhibition of initiated cells (Stinchcombe *et al*., 1995). In contrast, PCB 153 is a PB-like tumor promoter, positively selecting for tumors with *Ctnnb1* mutations (Strathmann *et al*., 2006). *Ctnnb1* mutated mouse liver

tumors are associated with an over-expression of glutamine synthetase (GS) (Aydinlik *et al*., 2001) and a deficiency in glucose-6-phosphatase (G6Pase) activity (Loeppen *et al*., 2002), which can be used as markers in immunohistological staining for this type of tumor. *Ha-ras* as well as also *B-raf* mutated mouse liver tumors are negative for GS and can therefore be distinguished from *Ctnnb1* mutated tumors.

β-catenin activated hepatoma cells differ considerably from *Ha-ras*- and *B-raf*-mutated hepatocytes with respect to their gene expression profiles. Genes aberrantly expressed in the tumor tissues are the nuclear receptors CAR, AhR and PXR, which are all down-regulated in *Ha-ras*- and *B-raf* mutated hepatomas, while increased in expression in *Ctnnb1*-mutated tumors when compared to normal liver (Stahl *et al*. 2005, and unpublished observations). Since CAR is not expressed in *Ha-ras* and *B-raf*-mutated tumors, hepatocytes carrying these genetic alterations cannot be promoted by PB or a PB-like substance which is in contrast to *Ctnnb1*-mutated hepatocytes expressing CAR (Koehle *et al*., 2008)

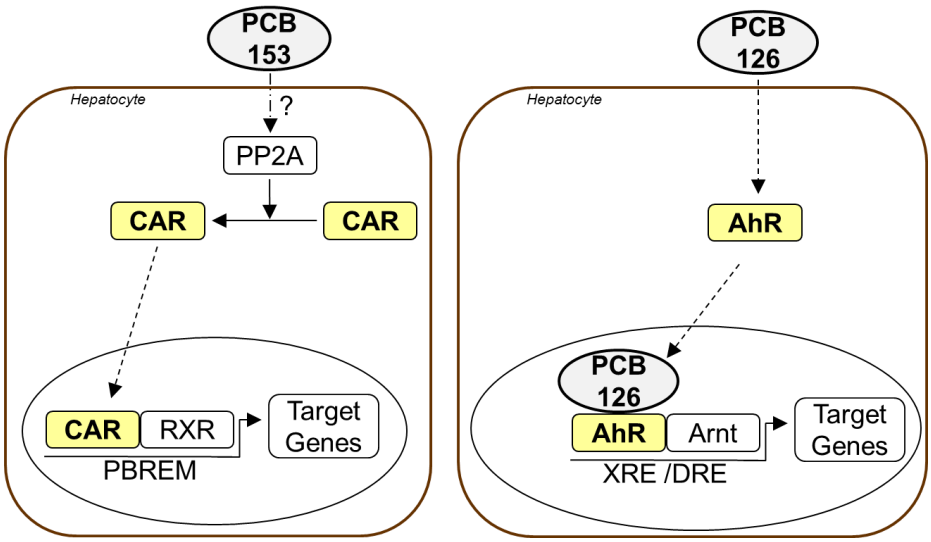

Figure 6: Activation of nuclear receptors by PCB 153 and PCB 126. The PB-like PCB 153 modulates the activity of CAR, thereby altering target gene transcription and promoting the positive selection of *Ctnnb1* mutated cells, after initiation with DEN, by an unknown mechanism. In contrast, dioxin-like PCBs like PCB 126 act via the AhR and promote the outgrowth of different subpopulations of cells. These are mainly mutated in the proto-oncogenes coding for *Ha-ras* or *B-raf*.

Recent studies have lacked a decisive result concerning the combined application of dioxin-like and PB-like acting substances on tumor promotion. In one study the carcinogenic effect was less than additive (Dean *et al*., 2002). In another study, using a comparable experimental setup, PCB 153 in combination with TCDD, PCB 126 and

other dioxins was tested. There was no statistical significant increase in tumor promotion activity when treating animals with mixtures containing PCB 153 together with dioxin-like tumor promoters as compared to animals treated with a mixture of dioxin-like tumor promoters only (van der Plas *et al*., 1999). However, in another study, synergistic effects of tumor promotion using a mixture of PCB 153 and PCB 126 were observed (Bager *et al*., 1995). Therefore, a conclusion concerning the combined exposition to dioxin-like and PB-like carcinogens and the effects on tumor promotion remain unresolved.

1.5 Mitogen Activated Protein (MAP) Kinase Signaling Pathway

The small G-protein *Ha-ras* and the serine/threonine kinase *B-raf* are part of the RAS-RAF-MEK-ERK-MAP kinase pathway that transduces extracellular signals into the cell. The core signaling molecules of the MAP kinase pathway are a set of protein kinases which are sequentially acting on each other: The MAP kinase kinase kinases (MAP3Ks) are serine/threonine specific kinases which are activated by phosphorylation or their interaction with small G-proteins of the Ras/Rac family in response to extracellular stimuli (Krishna and Narang, 2008). MAP3Ks in return activate MAP kinases kinases (MAPKKs) which operate as dual specificity kinases and can phosphorylate MAP kinases (MAPKs) on both serine and tyrosine residues. Once activated MAP kinases phosphorylate their targets on serine and threonine residues. *Ha-ras* functions as a molecular switch potentially enabling various other signal transduction pathways and subsequently activating multiple sets of genes (Malumbres and Barbacid, 2003). *B-raf* is, as to our current knowledge, solely involved in MAP kinase signaling and is therefore able to activate gene expression through MEK and ERK (Wan *et al*., 2004). In normal liver tissue MAP kinase signaling is involved in biological processes like cell proliferation, differentiation and apoptosis. Several factors that influence the activity of MAP kinase pathway enzymes are the presence of bivalent ions (Wu *et al*., 2002; Jin *et al*., 2007; Cullen and Lockyer, 2002), reactive oxygen species (ROS) (Mitsushita *et al*., 2004, Park *et al*., 2004) and the phosphorylation state, the latter being the most intensively studied. An essential effect upon de-phosphorylation is assigned to dual-specificity phosphatase 6 (DUSP6) which is an important regulator of transcriptional feedback regulation of the MAP kinase signaling pathway (Keyse, 2008). DUSP6 is a transcriptional target of ERK dependent pathway activity (Ekerot *et al*., 2008). Mathematical modeling in

Ras transformed cells has found DUSP6 to be a highly likely candidate for configuring the activity of the MAP kinase pathway during cellular transformation caused by the activated *Ras* oncogene (Bluethgen *et al*., 2009).

1.6 Wnt/β-catenin Signal Transduction Pathway

β-Catenin is a multi-functional protein which constitutes a component of the cellular adhesion complex and also acts as a central component in the canonical Wnt/β-catenin signaling pathway, an evolutionarily highly conserved signal transduction cascade regulating differentiation, proliferation and morphogenesis (Lustig and Behrens, 2003). Cellular levels of β-catenin are tightly controlled by a cytosolic multi-protein complex (Behrens *et al*., 1998): In the absence of Wnt-signaling, formation of the complex results in phosphorylation and subsequent proteolytic degradation of β-catenin via the ubiquitin-proteasome pathway. Following stimulation of Wnt-signaling, degradation of β-catenin is inhibited and the protein translocates into the nucleus where it associates with transcription factors of the T-cell-specific transcription factor family and activates target gene transcription (Willert and Nusse, 1998). Deregulation of the β-catenin pathway is frequently observed in human and rodent tumors of the liver and other organs (Behrens and Lustig, 2004). Inappropriate activation of β-catenin signaling is often caused by point-mutations or small deletions affecting the phosphorylation sites in exon 3 of the *Ctnnb1* gene, resulting in stabilization of the onco-protein. As a consequence, Wnt/β-catenin target genes such as glutamine synthetase (GS) are overexpressed in *Ctnnb1*-mutated hepatocellular tumors (Loeppen *et al*., 2002).

1.7 Aims and Objectives

Using a micro-array approach to investigate gene expression differences between *Ha-ras* and *B-raf* mutated mouse liver tumors (Stahl *et al*., 2005; Jaworski *et al*., 2007) have shown the de-regulation of several transcripts within the tumor types but a lack of major gene expression differences between the tumor tissues. To further investigate this high conformity of gene transcription, a proteome analysis was conducted, using 2D-PAGE followed by MALDI-TOF-TOF, to decipher metabolic changes within the tumor types as well as to investigate if the consensus in gene expression is also present on protein level (Project A). In a second project, the effect of β-catenin on PB-dependent tumor promotion was investigated. Tumor initiation-promotion studies, using DEN as initiator and PB as tumor promoter, have pointed towards essential functions of β-catenin (Aydinlik *et al*., 2001) as well as connexin32 (Moennikes *et al*., 2000). To further examine the role of β-catenin in this process, tumor (initiation)-promotion studies using i) a liver specific constitutively active β-catenin mouse strain (Tg(Alb-Cre/βCat^{S33Y}) created earlier in our laboratory (Loeppen *et al*., unpublished data) (Project B) and ii) a liver specific β-catenin knockout mouse strain (β-catenin KO) (Huelsken *et al*., 2001) (Project C) were performed. In addition, differences in protein expression between non-tumor wildtype liver-tissue and liver tissue from β-catenin KO animals were comparatively analyzed, again applying 2D-SDS-PAGE and MALDI-TOF-TOF analysis. Another study addressed the impact of a mixture of PB-like and dioxin-like tumor promoters on tumor promotion in the mouse liver, using PCB 153 as PB-like promoter and PCB 126 as dioxin-acting substance in DEN-initiated mice (Project D). There is no agreement upon the effect of PCB mixtures on tumor promotion in mice or human but there is a major concern that tumor promoting substances acting on the same organ/cell may act, in worst case, synergistically or additively. Again, a comparative proteome analysis followed the initiation-promotion experiment, comparing PCB treated liver samples to non-PCB treated controls or samples from mice treated with differently acting PCBs against each other. In a last experiment, animals with either *Ha-ras*- or *B-raf* mutated liver tumors or tumors with mutations in *Ctnnb1*, the gene coding for β-catenin, were generated for investigation using non-invasive magnetic resonance imaging (Project E) by our co-operation partners Professor Bernd Pichler and Andreas Schmid (Laboratory for Preclinical Imaging and Imaging Technology of the Werner Siemens-Foundation, Department of Radiology, University of Tuebingen).

2. Materials

2.1 Chemicals and Biochemicals

Reagent	Source
10x PCR buffer (for PCR)	MBI Fermentas, St. Leon-Rot, Germany
10x PCR buffer II (for reverse transcription)	Applied Biosystems, Foster City, CA, USA
3,3'-diaminobenzidine	Sigma, Taufkirchen, Germany
3-amino-9-ethylcarbazole	Sigma, Taufkirchen, Germany
acetate	VWR
acetonitrile	Sigma, Taufkirchen, Germany
acrylamide (30%)	Roth, Karlsruhe, Germany
agarose	Peqlab, Erlangen, Germany
albumine bovine fraction V	Serva, Heidelberg, Germany
ammonium bicarbonate	Sigma, Taufkirchen, Germany
ammonium persulfate	Gibco/BRL
AMV reverse transcriptase (10U/µl)	Promega, Mannheim, Germany
ammonia peroxysulfate	Serva, Heidelberg, Germany
aqua RotiPhenol	Roth, Karlsruhe, Germany
bathophenanthroline disulfonate, disodium salt	Alpha Aeasar
BioRad-water	Bio-Rad, Munich, Germany
bisacrylamide	Serva, Heidelberg, Germany
Bradford dye concentrate	Bio-Rad, Munich, Germany
bromophenolblue	Merck
calf intestinal alkaline phosphatase (1U/µl)	Invitrogen, Karlsruhe, Germany
CDP-Star ready to use	Tropix, Weiterstadt, Germany
CHAPS	Bio-Rad, Munich, Germany
chloroform	Merck
cleaning solution	Amersham
collagenase	Sigma, Taufkirchen, Germany
complete mini protease inhibitor cocktail	Roche, Mannheim, Germany
corn oil	Mazola
D-(+)-glucose monohydrate	Merck
de-streak	Amersham Biosciences
dithiothreitol	Sigma, Taufkirchen, Germany
DMSO	Sigma, Taufkirchen, Germany
DNA ladder 1kb	Invitrogen, Karlsruhe, Germany
DNAse I (10U/µl)	Promega, Mannheim, Germany
dNTP mix (10mM each)	MBI Fermentas, St. Leon-Rot, Germany
DTT	Serva, Heidelberg, Germany
EDTA	Sigma, Taufkirchen, Germany
ethoxyresorufin	Sigma, Taufkirchen, Germany
ethanol	Merck
ethidiumbromide	Serva, Heidelberg, Germany
FastRed substrate	KemEnTec, Copenhagen, Denmark
ficoll type 400	Sigma, Taufkirchen, Germany

folie	MoFix
furane	Sigma, Taufkirchen, Germany
glutaraldehyde	Sigma, Taufkirchen, Germany
glycerin	VWR
glycin	Roth, Karlsruhe, Germany
I-block	Tropix, Weiterstadt, Germany
IEF-stripes pH 3-10 NL	Amersham Biosciences
iodoacetamide	Serva, Heidelberg, Germany
IPG buffer	GE Healthcare
isocitrate dehydrogenase	Sigma, Taufkirchen, Germany
isocitrate, sodium salt	Sigma, Taufkirchen, Germany
isopropanol	Merck
LightCycler FastStart DNA Master SYBR Green I	Roche, Mannheim, Germany
magnesium chloride	Merck
methanol	Merck
methylenebisacrylamide	Sigma, Taufkirchen, Germany
milk powder	Roth, Karlsruhe, Germany
N`N`N`N`-Tetramethylethylenediamine (TEMED)	Serva, Heidelberg, Germany
$NADP^+$	Sigma, Taufkirchen, Germany
N-nitrosodiethylamine	Sigma, Taufkirchen, Germany
page ruler prestained protein ladder	MBI Fermentas, St. Leon-Rot, Germany
paraformaldehyde	Sigma, Taufkirchen, Germany
pBR322 DNA-MspI digest (DNA ladder)	NEB, Ipswich, MA, USA
PCB126	gift (Prof. Robertson, Iowa City, USA)
PCB153	gift (Prof. Robertson, Iowa City, USA)
PCR water (Ampuwa)	Fresenius-Kabi, Bad Homburg, Germany
pentoxyresorufin	Sigma, Taufkirchen, Germany
pharmalyte	Amersham Biosciences
phenobarbital	Geyer, Renningen, Germany
phenobarbital-containing diet (0.05% w/v)	Ssniff, Soest, Germany
PhosStop phosphatase inhibitor	Roche, Mannheim, Germany
Plasmid Mini Kit	Qiagen, Hilden, Germany
pleated filter	Neolab
potassium hydroxide	Merck
potassium pentachloro-hydro-ruthenate	Alpha Aeasar
primer oligo d(T)18	Promega, Mannheim, Germany
primer random d(N)6	Roche, Mannheim, Germany
proteinase K	MBI Fermentas, St. Leon-Rot, Germany
QuantiTect Reverse Transcription Kit	Kit Qiagen, Hilden, Germany
reblot plus solution, strong (10x)	Chemicon, Chandler's Ford, UK
restriction endonucleases & buffers	MBI Fermentas, St. Leon-Rot, Germany
RNAeasy Mini Kit	Qiagen, Hilden, Germany
SDS	Serva, Heidelberg, Germany
serdolite MB-1	Serva, Heidelberg, Germany

silicone oil	Amersham Biosciences
sodium ascorbate	Sigma, Taufkirchen, Germany
sodium azide	Sigma, Taufkirchen, Germany
sodium chloride	Sigma, Taufkirchen, Germany
sodium hydroxid solution	Sigma, Taufkirchen, Germany
spermine	Sigma, Taufkirchen, Germany
streptavidin, AP-conjugated	Spa, Milan, Italy
taq polymerase	MBI Fermentas, St. Leon-Rot, Germany
thiourea	Fluka
trifluoric acid	Sigma, Taufkirchen, Germany
tris (base)	Sigma, Taufkirchen, Germany
trizol reagent	Invitrogen, Karlsruhe, Germany
trypsin	Promega, Mannheim, Germany
tween-20	Sigma, Taufkirchen, Germany
urea	Serva, Heidelberg, Germany
α-cyano-4-hydroxycinnamic acid matrix solution	ProteoChem, Denver, USA
β-mercaptoethanol	Sigma, Taufkirchen, Germany

2.2 Primers

All primers listed in the following tables were synthesized by Operon, Cologne, Germany.

2.2.1 Real Time RT-PCR

Gene	Sense primer 5´->3´	Antisense primer 5´->3´
14-3-3 βα	AATAAACAAACCACGGTGTC	AAAGACTGAGAAATTCAGCG
14-3-3 ζδ	GATGACAAGAAAGGAATTGTGG	TCAGGATCTCGTAATAGAACAC
14-3-3 σ	CTACCTGAAGATGAAGGGTG	ATCTCCTTCTTGCTGATGTC
AhR	GTCAAATCCTTCTAAGCGACACA	AACCAGCACAAAGCCATTCA
Aladh	TCCAACCTCATCTATCCCATCTT	ATCATGTCTGACGGAGCTACAAC
Ald1b1	GACCGGAGAACGCTGATACTAGA	GGGATTGGGTTCGGGAGA
Arg1	AAGAAACAGAGTATGACGTGAG	AGTGTTGATGTCAGTGTGAG
Asl	GACTTACAGGAAGACAAGGAG	TTAGTCTCTGCCATGAACAC
Axin2	AGGCTGGCAGAGGTGTCGAA	GGAGCGCGTGGACACTTG
CAR	AACAACAGTCTCGGCTCCAAA	AGCATTTCATTGCCACTCCC
Ctnnb1	GCGTGGACAATGGCTACTCAAG	CCTGACCCTTTTCGGAACGAG
Cyp1A1	TGTCCTCCGTTACCTGCCTA	GTGTCAAACCCAGCTCCAAA
Cyp1A2	ATCCTTTGTCCCCTTCACCAT	GGGAATGTGGAAGCCATTCA
Cyp2B10	TACTCCTATTCCATGTCTCCAAA	TCCAGAAGTCTCTTTTCACATGT
Cyp2E1	CAAGTCTTTAACCAAGTTGGCAAA	CCACGATGCGCCTCTGA
Fdps	GGCTTTCTACTCTTTCTACCT	CCCATAATTCTCCTCTAAGATCTG
Gapdh	ACC ACA GTC CAT GCC ATC AC	TCC ACC ACC CTG TTG CTG TA
Gpr49	AAT CGC GGT AGT GGA CAT TC	GAT TCG GAA GCA AAA ATG GA
GS	GCGAAGACTTTGGGGTGATA	GTGCCTCTTGCTCAGTTTGTC

GSTm3	TGCACTGTGGCTCCCGGT	AGGCCTGGGGCAGCTCC
Oct	TACTCCAAAGGGTTATGAGC	ACTTCATCATCCACTTCTTCTG
Pck1	ATTGAACTGACAGACTCGCCCTAT	TTCCCACCATATCCGCTTCC
Rgn	ATACTTTGCTGGTACCATGG	CATCAATGCACATTCCATCTG
S33Y_Inj	GAGTCGCTCGGTACGATTTA	ATTGTCCACGCTGGATTTT
S33Y_Rec	AACCATGTTCATGCCTTCTTCTT	CAGCTTGAGTAGCCATTGTCCA
UGT1A6	AGAGAGTACAGGAACAACATGATT GTCG	CAACGATGCCATGCTCCCC

2.2.2 RFLP-Analysis and Sequencing (S)

Gene (primer pair used)	**Sense primer 5´->3´**	**Antisense primer 5´->3´**
Braf In15AP/ In15BJ	TTCCTTTACTTACTGCACCTCAGA	AGCAGTCACTAGTTTAGGACTG
Ctnnb1 A1x/ C2	AGCTCAAGCGCAGAGCTGCTG	GAGCGCATGATGGCATGTCTG
Ctnnb1 S1/ S2	ACTCTGTTTTTACAGCTGACCT	CAAGAGCAAGTAGCTGGTAAA
Haras 61A2/ In2B	GAGACATGTCTACTGGACATCCT	GCTAGCCATAGGTGGCTCACCTG

2.2.3 Genotyping

Gene	**Sense primer 5´->3´**	**Antisense primer 5´->3´**
Cre	TTTGCCTGCATTACCGGTCGATGC	TCCATGAGTGAACGAACCTGGTCG
$Ctnnb1^{loxP/loxP}$	ACTGCCTTTGTTCTCTTCCCTTCTG	CAGCCAAGGAGAGCAGGTGAGG
$Ctnnb1^{S33Y}$	ATTATACGAAGTTATCTCGAGTCGCTC	CCTCTTCCTCAGGATTGCCTTTACC

2.3 Antibodies

Antigen: β-catenin	**Cat-No.:** 9587	**Source:** rabbit, polyclonal
Manufacturer: Cell Signaling, Danvers, MA, USA		
Immunohistochemistry:	1: 50 dilution; formalin-fixed cryo sections	

Antigen: BrdU	**Cat-No.:** M0744	**Source:** mouse, monoclonal
Manufacturer: Dako, Glostrup, Denmark		
Immunohistochemistry:	1: 50 dilution; formalin-fixed cryo sections/ Carnoy-fixed paraffin-embedded sections // HRP-conjugated	

Antigen: Cyp1A1	**Cat-No.:** ---	**Source:** mouse, polyclonal
Manufacturer: gift of Dr. P. Beaune, INSERM U75, CHU Necker, Paris		
Western-blotting:	1: 2000 dilution; formalin-fixed cryo sections	

Antigen: Cyp2B1	**Cat-No.:** ---	**Source:** mouse, polyclonal
Manufacturer: gift of Dr. R. Wolf, University of Dundee, Dundee, UK		
Western-blotting:	1: 2000 dilution; formalin-fixed cryo sections	

Antigen: Cyp2E1	**Cat-No.:** MFO-100	**Source:** rabbit, polyclonal
Manufacturer: Stressgen, Victoria, BC, Canada		
Immunohistochemistry:	1: 500 dilution; formalin-fixed cryo sections	

Antigen: GS	**Cat-No.:** G2781	**Source:** rabbit, polyclonal
Manufacturer: Sigma, Taufkirchen, Germany		
Immunohistochemistry:	1: 1,000 dilution; formalin-fixed cryo sections/ Carnoy-fixed paraffin-embedded sections	

Antigen: O^6-ethyl-guanine	**Cat-No.:** ---	**Source:** mouse, polyclonal
Manufacturer: Gift from Dr. J. Thomale, University of Essen, Germany		
Immunohistochemistry:	1: 500-1000 dilution; formalin-fixed cryo sections	

Antigen: phospho-ERK1/2	**Cat-No.:** 4376	**Source:** rabbit, monoclonal
Manufacturer: Cell Signaling, Danvers, MA, USA		
Immunohistochemistry:	1: 100 dilution; Carnoy-fixed paraffin-embedded sections	

Antigen: rabbit IgG	**Cat-No.:** P0217	**Source:** swine, polyclonal
Manufacturer: Dako, Glostrup, Denmark		
Immunohistochemistry:	1: 20 dilution; formalin-fixed cryo sections/ Carnoy-fixed paraffin-embedded sections // HRP-conjugated	

Antigen: rabbit IgG	**Cat-No.:** FR14-61	**Source:** goat, polyclonal
Manufacturer: Spa, Milan, Italy		
Immunohistochemistry:	1: 200 dilution; Carnoy-fixed paraffin-embedded sections // biotin-conjugated	

2.4 Laboratory Equipment

2.4.1 Department of Toxicology, Tübingen, Germany

Appliance	**Manufacturer**	**Type designation**
autoclave	Webeco, Bad Schwartau, Germany	Autoklav C
balances	Sartorius, Göttingen, Germany	Analytic
balances	Mettler, Giessen, Germany	Laborwaage P1200
blotting chamber	Bio-Rad, Munich, Germany	Trans Blot Cell
camera	Zeiss, Göttingen, Germany	AxioCam MRc
CCD camera	Raytest, Straubenhardt, Germany	CSC chemoluminescense
centrifuges	Beckmann, Munich, Germany	J2-21 Centrifuge
centrifuges	Eppendorf, Wesseling, Germany	Centrifuge 5410

centrifuges	Heraeus, Hanau, Germany	Sepatech Biofuge 13
centrifuges	Heraeus, Hanau, Germany	Sepatech Megafuge 1.0 R
centrifuges	Heraeus, Hanau, Germany	Minifuge RF
centrifuges	Hettich , Tuttlingen, Germany	Mikrorapid/K
drying oven	Heraeus, Hanau, Germany	---
electrophoresis	Bio-Rad, Munich, Germany	Mini Protean II
chambers	Gibco BRL, Karlsruhe, Germany	H6
heating appliance	Eppendorf, Hamburg, Germany	Thermomixer 5436
heating appliance	Biometra, Göttingen, Germany	UNO-Thermoblock
incubator	Heraeus, Hanau, Germany	BB 6220 CU
light microscopes	Leitz, Wetzlar, Germany	Labovert FS
light microscopes	Zeiss, Göttingen, Germany	Imager.M1
magnetic stirrers	Janke & Kunkel, Staufen, Germany	IKA-Combimac RCT/ IKA-Mag RH
microtome	Reichert-Jung, Wetzlar, Germany	Frigocut 2800
multiwell plate reader	Perkin Elmer, Waltham, MA, USA	Victor 3V
PCR machines	Perkin Elmer, Waltham, MA, USA	GeneAmp PCR System 2400
PCR machines	Biometra, Göttingen, Germany	Uno-Thermoblock
PCR machines	Roche, Mannheim, Germany	LightCycler
pH-meter	Beckmann, Munich, Germany	F 200 pH-Meter
photometer	Peqlab, Erlangen, Germany	Nanodrop ND-1000
peristaltic pump	Ismatec, Wertheim, Germany	Vario-Pumpsystem
power supplies	Desaga, Wiesloch, Germany	Desatronic 3x500/ 100
power supplies	Pharmacia, Uppsala, Sweden	LKB · EPS 500/ 400
power supplies	Gibco BRL, Karlsruhe, Germany	ST 305/ ST 606 T
shaker	Heidolph, Kelheim, Germany	Titramax 1000
shaker	Bühler, Hechingen, Germany	Swip
shaker	Braun, Melsungen, Germany	Certomat HK
tissue homogenizer	Braun, Melsungen, Germany	Mikrodismembrator II
ultrasound device	Braun, Melsungen, Germany	Ultraschall Labsonic 2000
UV illuminator	Biometra, Göttingen, Germany	Transilluminator TI 1
vortex mixers	Bender & Hobein, Bruchsal	G. Vortex Genie 2 and L
water preparation	Millipore, Schwalbach, Germany	Milli Q Plus

2.4.2 BfR, Berlin, Germany

Appliance	Manufacturer	Type designation
vortex mixer	Heidolph	Reax 1, C-9553
vortex mixer	Heidolph	Reax 2000, C-11923
film welding machine	MEC	ME-300HC
fluoreszenzphotometer	Tecan	Spectra Fluor
freezer	GFL	Type 6483
Investigator Propic	Zinsser Analytic, Frankfurt, Germany	Bund 10049

IPG-elektrophoreses unit	Amersham Biosciences	IPGphor
fridge	Bosch	
proteomic imaging system	Perkin Elmer, Waltham, MA, USA	Proxpress
water preparation	Millipore, Schwalbach, Germany	Milli-QPlus
stiring device	Ikamac	C-10270
stiring device	Ikamac	C-11436
shaker	Heidolph	Promax 2020
shaker	DMG	Thermo Star
SDS-elektrophoreses unit	Amersham Biosciences	Ettan Dalt II
sonifier	Branson	Cell Disrupter B15
ultrasound device	Branson	Branson 3200
ultrazentrifuge	Beckmann, Munich, Germany	Optimus TLX

2.4.3 FMP, Berlin Buch, Germany

Appliance	Manufacturer	Type designation
centrifuges	Beckmann, Munich, Germany	J2-21 Centrifuge
MALDI-TOF/TOF	Applied Biosystems, Framingham, MA, USA	4700 Proteomics analyzer

2.5 Expandable Items

Item	Source	Type designation
1.5ml reaction tubes	Biozym, Oldendorf, Germany	---
6ml polystyrene tubes	BD, Heidelberg, Germany	Falcon 2058
15ml tubes	BD, Heidelberg, Germany	Falcon 2096
15ml centrifuge tubes	Greiner, Frickenhausen, Germany	G.163270
50ml tubes	BD, Heidelberg, Germany	Falcon 2070
cover slips	Langenbrinck, Emmendingen, Germany	cover glasses 24x32 mm
cover slips	Menzel, Braunschweig, Germany	Deckgläser Ø 30 mm
cages	Techniplast, Neumarkt, Germany	Macrolon Typ 2
fluted filter	Macherey-Nagel, Düren, Germany	Faltenfilter Ø 24 cm
Dako Pen	Dako, Glostrup, Denmark	Pen no. S 2002
filter paper	Biometra, Göttingen, Germany	Whatman 3mm Chr
glassware	Schott, Mainz, Germany	---
Pasteur capillary pipettes	WU Mainz, Mainz, Germany	---
cannule (0.90x 40mm)	BD, Heidelberg, Germany	Microlance 3
catheter	Venisystems, London, UK	Abbocath-T
microarray	Affymetrix, Santa Clara, CA, USA	MOE 430A
microscope slides	Langenbrinck, Emmendingen, Germany	---
pipettes and pipet tips	Eppendorf, Hamburg, Germany	---
pipettes and pipet tips	Biozym, Oldendorf, Germany	---

LightCycler capillaries	Roche, Mannheim, Germany	LightCycler Capillaries
PVDF membranes	Millipore, Eschborn, Germany	Immobilon-P (PVDF)
PCR tubes (0.2ml)	Peqlab, Erlangen, Germany	PCR-tubes 0.2 ml
pipettors	Brand, Wertheim, Germany	Accu-jet
reaction tubes (0.5/ 1.5ml)	Eppendorf, Hamburg, Germany	---
silicon grease	Beckmann, Munich, Germany	Vacuum grease silicone
scalpel	Braun, Melsungen, Germany	---
syringes (1, 2, 10, 50ml)	Braun, Melsungen, Germany	Injekt
syringes (1, 2, 10, 50ml)	BD, Heidelberg, Germany	Plastipak
sterile filter 0.20µm	Sartorius, Göttingen, Germany	Minisart
sterile filter 0.22µm	Millipore, Eschborn, Germany	Steritop 0.22 µm
serum syringe filters	Pall, East Hills, NY, USA	Acrodisc
Q-tips	NeoLab, Heidelberg, Germany	---
ZipTip	Millipore, Bedford, MA , USA	C18 RP

2.6 Buffers and Solutions

2.6.1 Protein Isolation and Western Blotting

WCE buffer pH 7.5
- hepes (sodium salt) 1.3g - NaCl 0.88g - glycerol (99%) 10ml - triton X-100 1ml - $MgCl_2$ x 6 H_2O 30mg - EGTA 38mg - NaF 420mg - $Na_4P_2O_7$ 450mg - H_2O_{dest} ad 100ml - store at 4°C - shortly before use, add 1 tablet of Complete Mini protease inhibitor cocktail and 1 tablet of PhosStop phosphatase inhibitor cocktail per 10ml of WCE buffer

2x Lämmli buffer
- tris (base) 1.51g - glycerol (99%) 20ml - H_2O_{dest} 25ml - adjust to pH 6.8 with $HCl_{conc.}$ - SDS 4g - β-mercaptoethanol 10ml - bromophenol blue 4mg - H_2O_{dest} ad 100ml - store at -20°C

10x transfer buffer
- tris (base) 30g

- glycin 144g
- H_2O_{dest} ad 1,000ml
- for 1x transfer buffer: - 10x transfer buffer 100ml
- methanol 200ml
- H_2O_{dest} ad 1,000ml

10x assay buffer
- tris (base) 24.2g - $MgCl_2$ x 6 H_2O 2.03g - adjust tris to pH 9.5, afterwards add $MgCl_2$ - H_2O_{dest} ad 1,000ml

TBS/T
- tris (base) 2.42g - NaCl 8.76g - tween-20 1ml - H_2O_{dest} ad 1,000ml - PBS (pH 7) 1,000ml - tween-20 0.5ml

2.6.2 Electrophoresis

6x loading buffer for agarose gels
- saccharose 50g - SDS 1g - orange G dye 0.5g - H_2O_{dest} ad 100ml

10x loading buffer for acrylamide gels
- bromphenol blue 25mg - xylene cyanol 25mg - ficoll type 400 1.5g - EDTA 0.5M pH 8.0 1ml - H_2O_{dest} ad 10ml

Ethidiumbromide solution
- ethidiumbromide 10mg - H_2O_{dest} ad 1ml - for staining solution, dilute 1: 20,000 with H_2O_{dest}

50x TAE pH 8.5
- tris (base) 242g - EDTA 0.5M pH 8.0 100ml - HAc 57.1ml - H_2O_{dest} ad 1,000ml

5x TBE pH 8.3
- tris (base) 54g - boric acid 27.5g

- EDTA 0.5M pH 8.0 20ml
- H_2O_{dest} ad 1,000ml

10x SDS-PAGE running buffer

- tris (base) 30g
- glycin 144g
- SDS 10g
- H_2O_{dest} ad 1,000ml

0.5M tris buffer pH 6.8

- tris (base) 60.57g
- dissolve in H_2O_{dest}
- adjust to pH 6.8 with HCl_{conc}
- H_2O_{dest} ad 1,000ml

1.5M tris buffer pH 8.9

- tris (base) 181.71g
- dissolve in H_2O_{dest}
- adjust to pH 8.9 with HCl_{conc}
- H_2O_{dest} ad 1,000ml

2.6.3 Proteome Analysis

Lysis buffer

- urea 42.0g
- dissolve in 50ml H_2O_{dest}
- thiourea 15.2g
- serdolyte MB-1 0.5g
- stir for 10 min.
- CHAPS 2.0g
- pharmalyte pH 3-10 2ml
- DTT 1g
- H_2O_{dest} ad 100ml

Rehydration buffer

- urea 18.0g
- thiourea 7.6g
- dissolve in 50ml H_2O_{dest}
- serdolyte MB-1 0.5g
- stir for 10min.
- CHAPS [2%] 0.25g
- DTT 0.1g
- cyrrier-ampholyte/IPG buffer 250µl
- H_2O_{dest} ad 50ml

Acrylamide/Bis-Acrylamide solution

- acrylamide 150g
- methylene bis-acrylamide 4g

- dissolve in 500ml H_2O_{dest}
- serdolyte MB-1 0.5g
- stir for 10 min.

Resolving gel buffer RGB

- tris (base) 90.85g
- SDS 2g
- dissolve in 500ml H_2O_{dest}
- sodium azide 0.05g
- filtrate

Tris HCl, pH 8.8

- tris (base) 118.6g
- dissolve in H_2O_{dest}, adjust pH to 8.8
- H_2O_{dest} ad 1000ml

Displacing solution

- tris HCl pH 8.8
- glycerin 50ml
- bromophenol blue 2mg
- H_2O_{dest} ad 25ml

APS (10%)

- ammonium persulfate 100mg
- H_2O_{dest} ad 1ml

1x SDS-PAGE running buffer

- tris (base) 21.8g
- glycin 112g
- SDS 7.5g
- H_2O_{dest} ad 7500ml

2x SDS-PAGE running buffer

- tris (base) 14.5g
- glycin 74.9g
- SDS 5g
- H_2O_{dest} ad 2500ml

Agarose (0.5%)

- agarose 0.5g
- bromophenol blue 3ml (25mg in 10ml RGB)
- H_2O_{dest} ad 100ml

Gel solution by Goerg

- acrylamide solution 486ml
- RGB 300ml
- glycerin 45.6ml
- H_2O_{dest} ad 360ml

- degas for 10 min.
- APS 3ml
- TEMED 100µl

Equilibration buffer
- urea 90g - H_2O_{dest} ad 125ml - glycerin 75g (=57,5ml) - SDS 5g - RGB 8.4ml - H_2O_{dest} ad 250ml - serdolite MB-1 0.5g - stir for 10 min.

Equilibration buffer I
- DTT 1g - equilibration buffer 100ml

Equilibration buffer II
- iodoacetamide 4g - equilibration buffer 100ml

Fixing solution
- ethanol 900ml - H_2O_{dest} 1800ml - acetic acid 300ml

Washing solution
- ethanol 600ml - H_2O_{dest} 2400ml

Staining solution
- ethanol 600ml - H_2O_{dest} 2400ml - Ruthenium 60µl

De-staining solution
- ethanol 1200ml - H_2O_{dest} 1500ml - acetic acid 300ml

2.6.4 Immunohistochemistry

Carnoy fixative
- ethanol 60ml - chloroform 30ml - glacial acetic acid 10ml

10x citrate buffer 0.1M pH 6
- citric acid (sodium salt) 29.41g - H_2O_{dest} ad 1,000ml - for 1x citrate buffer dilute 1: 10 with H_2O_{dest}

TBS/T for IHC pH 7.4
- tris (base) 6g - NaCl 5.8g - tween-20 1ml - H_2O_{dest} ad 1,000ml

TB buffer pH 8.7
- tris (base) 6g - $MgCl_2$ x 6 H_2O 406mg - H_2O_{dest} ad 1,000ml

PBS/S
- PBS 100ml - BSA 1g - NaCl 2.03g

Acetate buffer
- NaAc 6.48g - HAc 1.21ml - H_2O_{dest} ad 1,000ml

AEC staining buffer
- acetate buffer 14ml - N,N'-dimethylformamide 1ml - 3-amino-9-ethylcarbazole 4mg - H_2O_2 (30%) 15µl

Tris/ maleate buffer 0.2M
- tris (base) 24.2g - maleic acid 23.2g - H_2O_{dest} ad 1,000ml

Mayer's Hämalaun
- hematoxylin 1g - $NaIO_3$ 0.2g - $KAl(SO_4)_2$ x 12 H_2O 50g - dissolve in 1,000ml H_2O_{dest} - chloralhydrat 50g - citric acid x 1 H_2O 1g

G-6-Pase incubation buffer
- tris/ maleate buffer 100ml - H_2O_{dest} 133ml

- 2% lead$_{(II)}$nitrate solution 25ml (add dropwise) - add 250mg glucose 6-phosphate shortly before use

2.6.5 EROD/ PROD Assay

Tris/ Saccharose (10mM/ 250mM) lysis buffer
- tris (base) 1.211g - saccharose 85.575g - H_2O_{dest} ad 1,000ml

Assay buffer
- 1M tris pH 7.4 50µl - 50mM $MgCl_2$ 50µl - 50mM sodium isocitrate 50µl - 5mM $NADP_+$ 50µl - 600µM EDTA 50µl - isocitrate dehydrogenase (10U/µl) 1µl - H_2O_{dest} 70µl

2.7 Mouse Strains

Alb-Cre (B6.Cg-Tg(Alb-Cre)21Mgn/J)

Transgenic mouse expressing Cre recombinase under control of the mouse albumin enhancer/ promoter. Purchased from Jackson Laboratory, Bar Harbor, ME, USA.

C3H/He

Mice from strain C3H/He were purchased from Charles River, Sulzfeld, Germany.

***Ctnnb1*$^{loxP/loxP}$ (Ctnnb1 KO-mice)**

Mouse with mutant Ctnnb1 containing loxP sites introduced into the second and sixth intron of the native Ctnnb1 allele. Cre-mediated recombination results in a deletion/ frame shift mutation (Huelsken et al., 2001). Gift from Dr. Huelsken, Swiss Institute for Experimental Cancer Research, Lausanne, Switzerland.

2.8 Software

Appliance	Manufacturer	Version
GPS Explorer	Applied Biosystems, Framingham, MA, USA	Version 3.5
MASCOT Server	Matrix Science, London, UK	Version 2.0
Windows 7	Microsoft Cooperation,	Version 1.0
Microsoft Office 2010	Microsoft Cooperation,	Version 1.0
Origin Pro 8G	Origin Lab Cooperation, Northampton, MA, USA	V8.0988
CorelDRAW(R) Graphics Suite X5	Corel Corporation, Ottawa, CA	V15.2.0.661
Chromas	Technelysium, USA	Version 1.0
LightCycler Software	Roche	V.3.5

3. Methods

3.1 Animal Breeding and Treatment

3.1.A1 Generation of *Ha-ras* and *B-raf* Mutated Mouse Liver Tumors

3.1.A2 Breeding

All animals used in this experiment were male C3H/N mice (purchased from Charles River, Sulzfeld). Mice were singly housed in macrolon cages and kept on a 12 hour dark/light cycle. Animals received humane care and protocols complied with institutional guidelines.

3.1.A3 Treatment

Tumors used in this study were generated for a previously conducted experiment in our laboratory. In brief, 2 week old male C3H/N mice were injected a single intra-peritoneal dose of N-nitrosodiethylamine (DEN, 10 µg/g body weight) and kept on standard diet and tap water *ad libitum* thereafter. Mice were killed 35 weeks after carcinogen treatment in an airtight chamber flooded with 95% CO_2 and 5% O_2 followed by neck-stretching. The liver was bled by opening the *vena cava* inferior, isolated, washed in cold PBS, weighed and photographed. The color, size and number of tumors was recorded followed by isolation and shock-freezing of those specimens larger than 2 mm in diameter in liquid nitrogen before storage at -75°C. For immunohistochemical analysis, liver lobules were separated and aliquots either frozen on dry-ice or covered in Carnoy solution for subsequent paraffin embedment. In addition, liver probes for DNA-, RNA-, protein- and proteome-analysis were isolated, shock-frozen and stored at -75°C.

Figure 7: Animal treatment for the generation of *Ha-ras*- and *B-raf*-mutated mouse liver tumors. Male C3H/N mice were injected a single intraperitoneal dose of N-nitrosodiethylamine at the age of 2 weeks. Mice were kept on standard diet and water *ad libitum*. Mice were scarified 35 weeks after carcinogen treatment.

3.1.B1 Mice Expressing a Hepatocyte Specific Active Form of β-catenin (Tg(Alb-Cre/βCat^{S33Y})

3.1.B2 Breeding

To analyze the effect of β-catenin in the process of tumor promotion by phenobarbital (PB), a transgenic mouse line (Tg(Alb-Cre/βCat^{S33Y}) carrying a hepatocyte specific active form of the gene coding for β-catenin was used (the strain was generated earlier in our laboratory by Loeppen, S., unpublished data). The mutant carries a point mutation at codon 33 which causes the substitution of a serine residue to tyrosine (S33Y) thereby affecting one of the GSK3β phosphorylation sites, a type of mutation which is frequently seen in chemically-induced mouse hepatoma and expected to stabilize the protein resulting in its constitutive activation. The transgene has to be activated by interbreeding transgene carrier mice (Tg(βCat^{S33Y})) with a strain carrying the viral Cre-recombinase ((Alb-Cre) (Kellendonk *et al*., 2000). The Cre-recombinase catalyzes the excision of DNA flanked by artificial recognition-sequence sites (*flox*-sites). In case of Tg(Alb-Cre/βCat^{S33Y}) mice the excision leads to deletion of a large un-transcribed DNA region between a constitutively active promoter-site and the S33Y-mutated transgene. The approximation of the promoter and the transgene leads to expression of the formerly un-transcribed transgene in the liver. To avoid adverse effects in the development of transgenic embryos, a Cre-recombinase strain under the control of an albumin promoter (Alb-Cre) was used which is expressed from neonatal to adult age only. The Alb-Cre strain and Tg(βCat^{S33Y})-mice were backcrossed for 5 generations into mice of the C3H/N strain leading to a genetic background highly susceptible for PB mediated promotion before intercrossing Alb-Cre and transgene carrier mice to yield transgenic Tg(Alb-Cre/βCat^{S33Y}-C3H/N mice expressing the activated form of β-catenin.

3.1.B3 Genotyping

Animal genotyping was performed via PCR from mouse genomic DNA. For tissue isolation, animals were sedated with furane in an air-isolated chamber. Tissue material was obtained by punching the mouse ear at the outermost end to avoid bleeding and animal suffering. Genomic DNA isolation was achieved by overnight proteinase K digestion (see table 2) and subsequent debris centrifugation. Genotyping was conducted via PCR using Primers given in section 2.2.3 as well as reagents and cycle conditions given in section table 3.

3.1.B4 Treatment

Mice were divided into 4 groups of 15 animals that were either positive for the activated transgene (Tg(Alb-Cre/βCat^{S33Y})) or wildtype (-/βCat^{S33Y}) and received a PB containing diet (Ssniff, Soest) or control diet without the barbiturate. 6 additional animals were assigned to the PB receiving transgenic group in order to check for the appearance of tumors after 20, 25, 30, and 34 weeks of age. PB treatment was started with mice 9 weeks of age, feeding a diet containing 0.05% of the barbiturate until sacrificed 34 weeks later (at the age of 43 weeks). Mice were killed in an airtight chamber flooded with 95% CO_2 and 5% O_2 followed by neck-stretching. The liver was bled by opening the *vena cava inferior*, isolated, washed in cold PBS, weighed and photographed. The color, size and number of tumors was recorded followed by isolation and shock-freezing of those specimen larger than 2 mm in diameter in liquid nitrogen before storage at -75°C. For immunohistochemical analysis, liver lobules were separated and either frozen on dry-ice or covered in Carnoy solution for subsequent paraffin embedment. In addition, liver probes for DNA-, RNA-, and protein-analysis were isolated, shock-frozen and stored at -75°C. The treatment regimen of the experiment is outlined in figure 8.

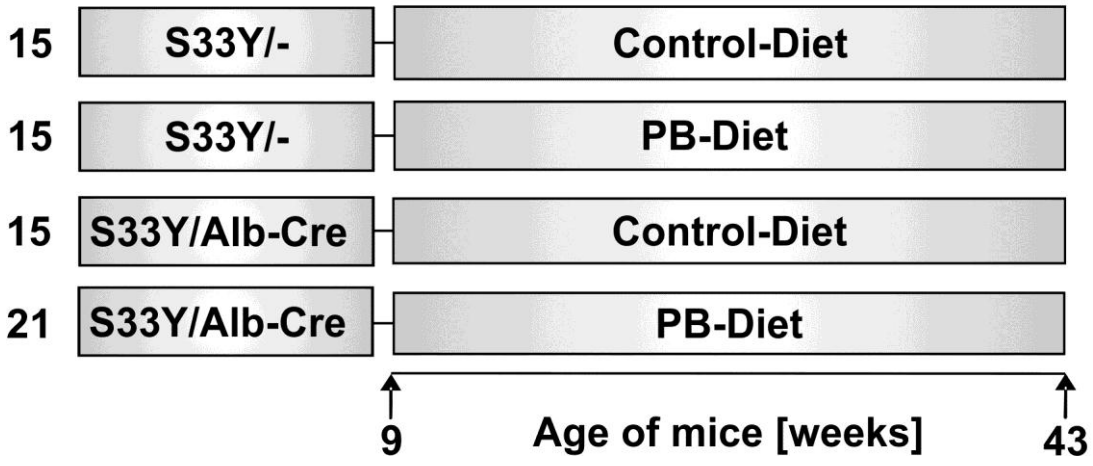

Figure 8: Treatment regimen of transgenic Alb-Cre/βCat^{S33Y} mice and -/βCat^{S33Y} wildtype animals. Transgenic Alb-Cre/βCat^{S33Y} and -/βCat^{S33Y} wildtype animals were either kept on a 0.05% PB containing diet or standard diet and water *ad libitum* from 9 weeks of age until sacrificed 34 weeks later. 6 additional animals were assigned to the PB receiving Alb-Cre/βCat^{S33Y}-group in order to identify the appearance of tumors and to subsequently determine the time point of experiment termination. The number of mice used in the 4 treatment groups is given on the left.

3.1.B5 Statistical Considerations

The number of animals needed per treatment group to reach a significance of 5% was statistically determined using a scheme by J. Bock (J.Bock 1998; “Bestimmung des Stichprobenumfangs”, Oldenburg München).

3.1.C1 Mice Expressing a Hepatocyte Specific Non-Functional Form of β-Catenin (*Ctnnb1*$^{loxP/loxP}$)

3.1.C2 Breeding

Alb-Cre mice (purchased from The Jackson Laboratory, Bar Harbor, ME) expressing Cre-recombinase under control of the hepatocyte-specific albumin promoter and transgenic mice with loxP sites inserted in the introns flanking exons 3 and 6 of *Ctnnb1*$^{loxP/loxP}$ (obtained from Dr. Huelsken) were backcrossed for 5 generations into mice of the C3H/N strain leading to a genetic background highly susceptible for PB mediated promotion (for more details see section 3.1.B2). Mice with hepatocyte-specific knockout of *Ctnnb1* were obtained by interbreeding transgenic mice with Alb-Cre mice. PCR-based genotyping was performed as outlined in table 3. Homozygous *Ctnnb1*$^{loxP/loxP}$ mice carrying a Cre allele, resulting in hepatocyte-specific knockout of *Ctnnb1*, are referred to as ‘*Ctnnb1* knockout (KO) mice’ in the following. The respective wildtype mice are called ‘WT’ hereafter. Mice were kept on a 12 h dark/ light cycle and had access to food and tap water *ad libitum*. Animals received humane care and protocols complied with institutional guidelines.

3.1.C3 Genotyping

Animal genotyping was performed exactly as described elsewhere (section 3.4.3).

3.1.C4 Treatment

For induction of liver tumors, male WT- and KO-mice were intraperitoneally injected with a single dose of DEN (90 µg/g body weight) at 6 weeks of age. After a treatment-free interval of 3 weeks, mice were randomly assigned to 4 experimental groups (15 mice in each of the WT- and 16 mice in each of the KO-groups), which were either kept on a standard diet or on a diet containing 0.05% PB until sacrifice. Liver tumors were isolated 30 weeks after carcinogen treatment. Mice were killed in an airtight chamber flooded with 95% CO_2 and 5% O_2 followed by neck-stretching. The liver was bled by opening the *vena cava inferior*, isolated, washed in cold PBS,

weighed and photographed. The color, size and number of tumors was recorded followed by isolation and shock-freezing of those specimen larger than 2 mm in diameter in liquid nitrogen before storage at -75°C. For immunohistochemical analysis, liver lobules were separated and either frozen on dry-ice or covered in Carnoy solution for subsequent paraffin embedment. In addition, liver probes for DNA-, RNA-, protein- and proteome-analysis were isolated, shock-frozen and stored at -75°C. The study design of the experiment is outlined in figure 9.

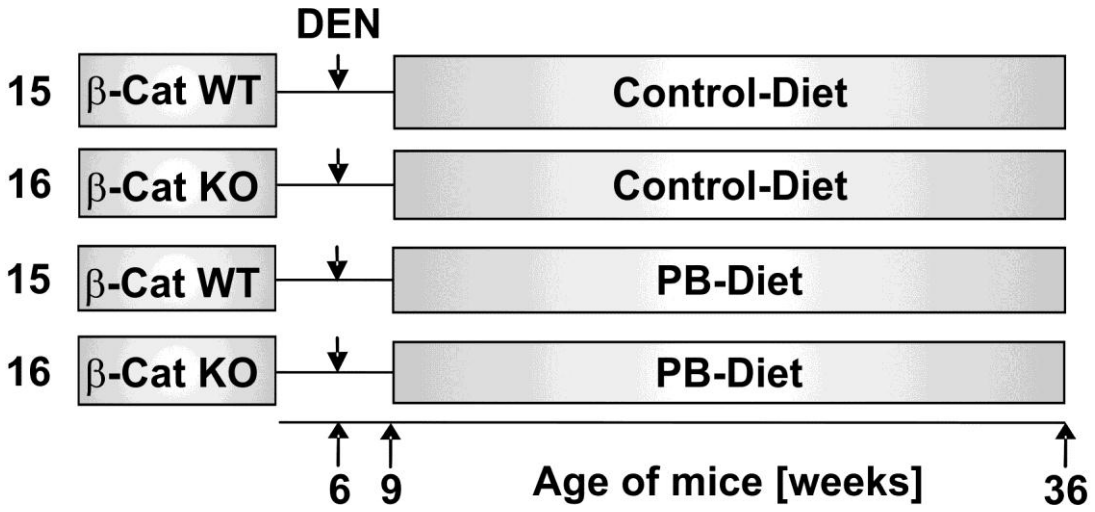

Figure 9: Tumor initiation-promotion regimen of hepatocyte specific β-catenin knockout mice (β-Cat KO) and wildtype animals (β-Cat WT). Transgenic *Ctnnb1*-knockout mice (β-Cat KO) and *Ctnnb1*-wildtype animals (β-Cat WT) were initiated at the age of 6 weeks by single i.p. injection of N-nitrosodiethylamine. Animals were either kept on a 0.05% PB containing diet or standard diet and water *ad libitum* from 9 weeks of age until sacrificed 27 weeks later. The number of mice used in the 4 treatment groups is given on the left.

To analyze metabolic activation of DEN in hepatocytes, male 14 weeks old WT- and KO-mice were i.p. injected with a single dose of DEN (90µg/kg body weight). Animals were sacrificed 4 h later and livers were frozen on dry ice and stored at -75°C before immunohistochemical analysis of O^6-alkylation (see section 3.3).

3.1.D1 Treatment of Mice With a Combination of Dioxin-Like and Non-Dioxin-Like PCBs

3.1.D2 Breeding

All animals used in this experiment were male C3H/N mice (purchased from Charles River, Sulzfeld). Animals were housed in macrolon cages and kept on a 12 hour dark/light cycle. Animals received humane care and protocols complied with institutional guidelines.

3.1.D3 Treatment

Optimal dose effect level finding experiment: C3H/N mice were given either PCB 126 (0, 8, 40, 80µg/kg body weight) or PCB 153 (0, 10, 50, 80mg/kg body weight) (gifts of Prof. Robertson, Iowa City, USA) in duplicates dissolved in corn oil via gauge and sacrificed 4 days later.

Liver PCB content measurement for half-life estimation: In a second experiment C3H/N mice were given PCB 126 or PCB 153 via gauge at day 0 (measurements in duplets), using the following dose ranges: PCB 126; 0, 10, 50, 100, 200µg/kg body weight, PCB 153; 0, 25, 50, 75, 100mg/kg body weight and sacrificed after 4, 21 and 42 days. PCB dependent induction of CYP-mRNA expression was measured in the Tübingen laboratory via RT LC-PCR and PCB-liver contents were assessed in Prof. Robertson´s laboratory via gas chromatography and quantified using the internal standard method.

Tumor initiation-promotion experiment: Animal housing and PCB treatment was conducted in the laboratory of our cooperation partners Prof. Chahoud and Dr. Grote (Inst. of Clinical Pharmacology and Toxicology, Charité University Medical School, Campus Benjamin Franklin). The PCB congeners were applied separately after treatment with the initiator DEN in high dose (groups 3-6, for details see table 1). In addition, the effect after DEN initiation was quantified at half the high dose in treatment groups 7 and 8 (low dose) which was also applied in the groups treated with a mixture of PCB 126 and PCB 153 (groups 9 and 10). Group 1 was used as the vehicle group, whereas group 2 was treated with DEN only and used as reference group for spontaneously occurring tumors. 168 male C3H/N mice (Charles River, Sulzfeld) were intraperitoneally injected with a single dose of DEN (90 µg/g body weight) at 6 weeks of age. After a treatment-free interval of 3 weeks, mice were randomly assigned to experimental groups 2 and 5-9 as outlined in table 1 and kept on a standard diet until sacrifice. In addition 20 male C3H/N mice were randomly assigned to control groups 1, 3, 4, and 10 without DEN initiation. PCB or oil application was performed from 3 weeks until 24 weeks after carcinogen treatment via gauge. Animals were weighed once a week to detect eventual toxic effects caused by the treatment regimen. Liver tumors were isolated 25 weeks and 34 weeks after carcinogen treatment. For assessment of hepatocyte proliferation, BrdU was given orally via drinking water (1mg/ml) for 3 days and detected using a mouse anti-BrdU antibody. 6 animals died during the duration of the experiment without

prevalence for one of the treatment groups. Mice were killed by decapitation. Their livers were isolated, washed in cold PBS, weighed and photographed by me at the laboratory of Prof. Chahoud with assistance of Dr. Grote. The color, size and number of tumors was recorded followed by isolation and shock-freezing of those specimens larger than 2 mm in diameter in liquid nitrogen before storage at -75°C. For immunohistochemical analysis, liver lobules were separated and either frozen on dry-ice or covered in Carnoy solution for subsequent paraffin embedment. In addition, liver probes for DNA-, RNA-, protein- and proteome-analysis were isolated, shock-frozen and stored at -75°C. All probes were sent to the Tübingen laboratory for subsequent analysis.

Table 1: Biometric scheme of project D

Group #	DEN-Initiation[a]	PCB 153	PCB 126	# Mice	
				Time point 1	Time point 2
1	-	-	-	-	5[e]
2	+	-	-	14 (+2)[d]	14
3	-	+[b]	-	-	5[e]
4	-	-	+[b]	-	5[e]
5	+	+[b]	-	10 (+2)[d]	10
6	+	-	+[b]	9 (+2)[d]	9
7	+	+[c]	-	13 (+2)[d]	14
8	+	-	+[c]	13 (+4)[d]	14
9	+	+[c]	+[c]	14 (+4)[d]	14
10	-	+[c]	+[c]	-	5[e]
Total				**73 (16)**	**95**

[a] Onetime i.p. injection of 90µg/g b.w. at the age of 6 weeks
[b] PCB-application once a week via gauge; High-dose
[c] PCB-application once a week via gauge; Low-dose (1/2 high-dose)
[d] Additional animals allocated to define the optimal time of termination
[e] Descriptive animals only

3.1.D4 Statistical Considerations

The biometric setup and evaluation of the animal experiment was conducted by our cooperation partner Dr. Kopp-Schneider (central unit for Biostatistics, DKFZ, Heidelberg).

3.1.E1 Mouse Liver Tumor Generation for Non-invasive Magnetic Resonance Imaging

3.1.E2 Breeding

All animals used in this experiment were male C3H/N mice (purchased from Charles River, Sulzfeld). Mice were singly housed in macrolon cages and kept on a 12 hour dark/light cycle. Animals received humane care and protocols complied with institutional guidelines.

3.1.E3 Treatment

Ha-ras and *B-raf* mutated tumors were initiated by injecting a single i.p. dose of DEN (10 µg/g of body weight) into 2 weeks old male C3H/N mice. Magnetic resonance imaging was performed from week 16 until the end of the experiment every second week. Mice were killed 35 weeks after carcinogen treatment in an airtight chamber flooded with 95% CO_2 and 5% O_2 followed by neck-stretching. The liver was bled by opening the *vena cava inferior*, isolated, washed in cold PBS, weighed and photographed. The color, size and number of all tumors were recorded. Liver lobules were separated and either frozen on dry-ice or covered in Carnoy solution for subsequent paraffin embedment and immunohistochemical analysis.

For the generation of β-catenin mutated tumors 6 weeks old male C3H mice were injected a single i.p. dose of DEN (90 µg/g of body weight). After a treatment-free period of 2 weeks mice were fed a 0.05% PB-containing diet until sacrifice. Magnetic resonance imaging was conducted and performed at the laboratory of Prof. Pichler by Andreas Schmid (Laboratory for Preclinical Imaging and Imaging Technology of the Werner Siemens-Foundation, Department of Radiology, University of Tuebingen) from week 16 until the end of the experiment every second week. Mice were killed 30 weeks after carcinogen treatment at the department of toxicology by me in an airtight chamber flooded with 95% CO_2 and 5% O_2 followed by neck-stretching. The liver was bled by opening the *vena cava inferior*, isolated, washed in cold PBS, weighed and photographed. The color, size and number of all tumors were recorded. Liver lobules were separated and either frozen on dry-ice or covered in Carnoy solution for subsequent paraffin embedment and immunohistochemical analysis.

3.2 Measurement of Liver and Lipid PCB Content

The concentration of PCB in liver and lipid for establishing the pharmacokinetics of PCB 126 and PCB 153 were measured in the laboratory of our cooperation partner Prof. Robertson, Iowa City, USA, using gas chromatography and quantified using the internal standard method (Rignall *et al*., 2011, in preparation).

3.3 Immunohistochemistry

3.3.1 Formaldehyde Fixation

Serial sections (10µm thickness) were prepared from frozen livers. For immunohistochemical stainings slices from frozen liver samples were fixed with 3% formaldehyde. Unspecific binding was blocked by incubation with swine serum (1:30 dilution; Dako, Glostrup, Denmark).

3.3.2 Carnoy Fixation

Liver slices were incubated in Carnoy fixative o/n. The fixative was removed by o/n incubation in isopropanol followed by embedding of the tissue samples in paraffin.

3.3.3 HRP & Biotin-Steptavidin-AP Staining

Horse-Radish-Peroxidase (HRP)-staining: Endogenous peroxidase activity in paraformaldehyde-fixed cryo sections or paraffin-embedded Carnoy-fixed sections was inactivated by incubation for 15 min. in a mixture of methanol / 0.15% H_2O_2. Primary antibody was bound o/n at 4°C, HRP-conjugated secondary antibody diluted in PBS/S for 60min at room temperature. Detection of enzymatic activity was carried out by approximately 30 min. incubation in AEC buffer at room temperature.

Biotin-streptavidin-alkaline phosphatase (AP)-staining: After binding of biotinylated secondary antibody diluted in TBS/T +3% BSA, liver slices were incubated with streptavidin-AP complexes for 30 min. at room temperature followed by FastRed staining for approximately 40 min. In case of double staining for glutamine synthetase (HRP-staining) and phospho-ERK1/2 (AP-staining), AP-staining was performed first. Nuclei were counterstained using Mayer's Hemalaun.

3.3.4 Glucose 6-Phosphatase Staining

Glutaraldehyde-fixed tissue was incubated for 20 minutes in G6Pase incubation buffer. The reaction product was precipitated by incubation in 1% $(NH_4)_2S$ solution followed by a second glutaraldehyde fixation step as described previously (Wachstein *et al.*, 1957).

3.3.5 Quantification of Enzyme Altered Lesions

The sizes of enzyme-altered liver lesions in G6Pase- and GS-stained sections were quantified by means of a computer-assisted digitizer system consisting of a Zeiss Axio Imager microscope and a Wacom Cintiq 21UX pen display. Areas of liver sections and of enzyme-altered tumor intersections therein were determined and the volume fractions of altered lesions (which are equivalent to the area fractions) were calculated.

3.3.6 Assessment of Hepatocyote Proliferation Using BrdU-Specific Antibodies

For assessment of hepatocyte proliferation, BrdU was given orally via the drinking water (1mg/ml) for 3 days prior to organ isolation. BrdU incorporation into nuclei of DNA was determined immunohistochemically in H&E counterstained paraffin sections (2µm) as recently described (Stinchcombe *et al.*, 1995).

3.4 PCR and LC RT-PCR

3.4.1 Quantification of Nucleic Acids

Optical density (OD) of DNA/ RNA solution was measured at 280nm and 260nm using a Nanodrop photometer. OD260 was used for calculation of concentration, OD260/OD280 quotient for purity estimation.

3.4.2 Isolation of Genomic DNA

From ear scrap: A small part of ear scrap or liver tissue was digested by 20µg of proteinase K in a volume of 40µl 1x PCR buffer o/n at 56°C. Proteinase K was heat inactivated at 95°C for 15min. Cell debris was pelletized by centrifugation (13,000xg, 5min). Supernatant containing genomic DNA was directly used for PCR.

Table 2: Proteinase K digestion

Reagent	**Conc.**	**End-conc.**	**Vol. [µl]**
Water			35
TAQ-Buffer (+$MgCl_2$)	10x	1x	4
Proteinase K	20mg/ml	0,5mg/ml	1
Total Volume			**40**
Centrifugation step	13.000 rpm	10 sec	
Incubation step	56°C	3 h or over night	
Inhibition step	95°C	15 min	
Centrifugation step	13.000 rpm	5 min	

From tumor material: Tumor material of approximately 1mm^3 in size was powderized under liquid nitrogen in a mortar and extracted with sodium-acetate/phenol (1:1) and isoamyl-alcohol/chloroform (1:25). Subsequentyl DNA was precipitated with Ethanol, washed, dissolved in 50µl TE-buffer and quantified.

From liver slides: Liver sections were prepared and stained with hemalaun/eosin, mounted on dialysis bags and stained for the marker enzyme glucose-6-phosphatase (G6Pase) which is known to be absent from pre-neoplastic and neoplastic cancer cells (Wachstein *et al*.,1957). Negatively stained areas were punched out with sharpened cannulas and used for PCR and RFLP analysis.

3.4.3 Standard PCR

5µl aliquots of isolated genomic DNA were amplified by 1U Taq polymerase in 1x PCR buffer in a final volume of 50µl using the following PCR programs and conditions:

Table 3: PCR-protocol used for β*Cat*^{S33Y}, *Ctnnb1*$^{loxP/loxP}$, *Ctnnb1*, *B-raf* and *Ha-ras* amplification

PCR Reaction Mix Reagent	**Conc.**	**End-conc.**	**Vol. [µl]**
Water			33
Taq Buffer (+15mM $MgCl_2$)	10x	1x	5
dNTPs (10 mM)	10mM	0,2mM	1
Primer 1 (10 µM)	10µM	0,5µM	2,5
Primer 2 (10 µM)	10µM	0,5µM	2,5
Volume			**44**
DNA (0,1 mg/ml)	0,1mg/ml	0,01mg/ml	5
Taq Polymerase	5U	0,5U	1
Total Volume			**50**

PCR Conditions	
βCat^{S33Y}	95°C, 60sec. / 66°C, 60sec. / 72°C, 60sec. 35 cycles
Ctnnb1$^{loxP/loxP}$ **(KO-allele)**	95°C, 60sec. / 60°C, 60sec. / 72°C, 60sec. 35 cycles
Ctnnb1 **(WT-allele)**	95°C, 60sec. / 58°C, 60sec. / 72°C, 60sec. 40 cycles
B-raf	95°C, 60sec. / 55°C, 60sec. / 72°C, 60sec. 40 cycles
Ha-ras	95°C, 60sec. / 65°C, 60sec. / 72°C, 60sec. 40 cycles

Table 4: PCR-protocol used for *Alb-Cre* amplification.

PCR Reaction Mix Reagent	**Conc.**	**End-conc.**	**Vol. [µl]**
Water			25
Taq Buffer (-$MgCl_2$)	10x	1x	5
$MgCl_2$	25mM	2mM	4
dNTPs (10 mM)	10mM	0,4mM	2
Primer 1 (10 µM)	10µM	0,8µM	4
Primer 2 (10 µM)	10µM	0,8µM	4
Volume			**44**
DNA (0,1 mg/ml)	0,1mg/ml	0,01mg/ml	5
Taq Polymerase, recombinant	5U	0,5U	1
Total Volume			**50**
PCR Condition			
Alb-Cre	95°C, 60sec. / 68°C, 60sec. / 72°C, 60sec. 35 cycles		

3.4.5 DNA-Sequencing

Sequencing of genomic DNA was performed by 4baseLab, Reutlingen, Germany. For sequencing primers, see section 2.2.2.

3.4.6 Isolation of RNA

Total RNA was extracted from tissue or cell cultures by use of the Trizol reagent (PeqLab) following the manufacturer's instructions.

3.4.7 Reverse Transcription

Reverse transcription of 375ng RNA per assay was performed using 4U avian myeloblastosis virus reverse transcriptase (Promega) and oligo $d(T)_{18}$ and random $d(N)_6$ primers for 1h at 42°C followed by a 15 minutes heat-inactivation step at 95°C. Liver tissue samples were reverse transcribed using the QuantiTect Reverse Transcription Kit (Quiagen) following the manufacturer's instructions.

3.4.8 LightCycler Real-Time (LC RT) PCR

A capillary-based Roche LightCycler was used for expression analysis. Amplification was monitored by fluorescence using the FastStart DNA Master SYBR Green I Kit (Roche).

3.5 RFLP Analysis

PCR products of *B-raf* and *Ha-ras* mutated tumor material or G6P-ase negatively stained areas from fixed liver lobule specimens were screened for mutations by restriction fragment length polymorphism (RFLP) analysis as recently described (Buchmann *et al*., 2008). Three of the *Ha-ras* codon 61 mutations analyzed generate new restriction enzyme recognition sites which can be detected by the following enzymes (mutated codon 61 sequences are given in parenthesis): TaqI (C**G**A), XbaI (C**T**A) and BspHI (C**A**T), whereas the mutated sequence AAA leads to the loss of a Hpy188III recognition site. The known hotspot mutation in *B-raf* codon 637 (mutated sequence G**A**G), as well as other types of possible mutations within this codon, lead to the loss of a *TspRI* recognition site. PCR products were digested with the respective restriction enzymes (New England Biolabs, Frankfurt, Germany, or Fermentas, St. Leon-Roth, Germany), separated on 10% polyacrylamide gels, and visualized by staining with ethidiumbromide. Each mutation detected was confirmed by an independent PCR/RFLP analysis.

3.6 Protein Analysis

3.6.1 Protein Isolation for 2D-PAGE

2D-PAGE analysis was performed at the laboratory of our cooperation partner Dr. Appel (Federal Institute for Risk Assessment, Center for Experimental Toxicology, Berlin) with assistance from Dr. Paal and Ms. Meckert at the first analysis and from then on by myself. In brief, frozen tissue samples were homogenized in liquid

nitrogen and the resulting tissue powder was transferred into a reaction cup, containing a mixture of lysis buffer (7 M urea, 2 M thiourea, 4% CHAPS, 1.2% DeStreak Reagent (GE Healthcare Bio- Sciences, München, Germany), 2% IPG Puffer 3–10 NL and 20 mM spermin) and proteinase inhibitors (Protease Inhibitor Coctail III, Calbiochem – VWR Deutschland, Darmstadt, Germany), and mixed immediately (approximately 10 mg of tissue powder/250 mL of lysis buffer). After stepwise sonification, the extracts were spun at 100 000 x g and the supernatant was collected and stored at –80°C.

3.6.2 Bradford Assay

Protein concentrations were estimated using the Bradford assay. Maximum absorption of Coomassie Brilliant Blue G250 dye shifts from 465nm to 595nm in the presence of proteins and was assessed photometrically. Protein content was calculated relative to a BSA standard curve.

3.6.3 2D SDS-PAGE

The separation in the first dimension was carried out using IPG-strips (3–10 NL, 24 cm, GE Healthcare Bio-Sciences) on an IPGphor® IEF-separation unit (GE Healthcare Bio-Sciences). Samples were loaded by active in-gel rehydration (rehydration solution: 7 M urea, 2 M thiourea, 4% CHAPS, 1.2% DeStreak Reagent (GE Healthcare Bio-Sciences) and 0.5% IPG Puffer 3–10 NL under 30 V for 15 h during reswelling). The proteins were focused at <50 µA *per* strip at 20°C using progressively increasing voltage up to 8000 V for a total of 68 000 Vh. Each gel strip was loaded with 150 µg of protein extract and each sample was applied in three technical replicates. These three replicates were analyzed in different runs according to an experimental design with 12 different samples per run, in order to reduce bias due to uncontrollable inter-day or day-to-day technical variations. Following IEF, the gel strips were equilibrated in SDS, reduced with DTT, and alkylated with iodoacetamide. The second dimension, SDS-PAGE, was performed with 12.5% acrylamide gels using an ETTAN Dalt II®separation unit (GE Healthcare Bio-Sciences). Fixation of the gels was carried out in aqueous 10% acetic acid/30% ethanol overnight and gels were stained for 6 h with 10 nM Ruthenium II Tris. Gels were then washed with water (twice for 10 min), destained in 10% acetic acid/40% ethanol overnight, washed again with water (twice 10 min), and stored in 20% ethanol. Imaging was performed by use of the ProXPRESS® ProFinder fluorescence

imaging workstation (ProXPRESS 2-D Proteomic Imaging System fluorescence imaging workstation, PerkinElmer Lifesciences, Boston, MA, USA). Spot detection and quantification were performed automatically using ProteinMine TM 2-DE image analysis software (Version 1.5.0, BioImagene, San Mateo, CA, USA). The most representative gel image was selected as a reference image for subsequent image alignment and spot matching. Match tables were generated and formatted for further statistical evaluation.

3.6.4 Data Evaluation and Statistical Analysis

Data evaluation and statistical analyses of protein expression were carried out using the software package R (Version 2.2.0 (R-Development-Core-Team, 25) by our cooperation partner Dr. Weimer (central unit for Biostatistics, DKFZ, Heidelberg). Match tables were imported, overall match statistics and histograms of intensity values for each gel image were visualized for quality control. A groupwise scale normalization was conducted for the $\log_2$ transformed intensity values resulting in equal median intensity values for every gel image from tissues of the same treatment/phenotype group. Pairwise comparisons of treatment/phenotype groups were performed by two-sided Wilcoxon rank sum tests considering only the median of intensity values of the technical replicates of each animal. This analysis was restricted to spots quantified in at least two of the three technical replicates of at least 80% of the biological replicates per group. Changes in spot intensity were quantified by the $\log_2$ ratio of median intensities of both groups and visualized together with the corresponding p-values of the Wilcoxon rank sum tests in volcano plots. All spots with a p-value ≤ 0.05 and $|\log_2 \text{ ratio}| \geq 1$ (studies A and C) or ≥ 0.6 (study D) were selected for further investigation. Furthermore, all spots were selected which could be detected exclusively in one of two comparison groups (absent–present search). For each of the selected spots, the intensity values of the technical replicates and the median intensity values were visualized in a barplot to investigate individual spot intensities of all gel replicates.

3.6.5 Spot Selection and Spot Picking

The list of differentially expressed spots obtained by the statistical analysis was further evaluated according to the criterion that localization of the spot allows its removal from the gel without contamination with any neighboring spot. Spots fulfilling this criterion were picked by the Investigator™ Pro- Pic™ workstation (Genomic

Solutions, Zinsser Analytic, Frankfurt, Germany) at the laboratory of Dr. Appel by me and used for protein identification. In certain cases, multiple spots of identical location were picked from different gels. In these cases, the identity of the respective proteins was always verified.

3.6.6 In-gel Digestion and Sample Preparation

Sample preparation for subsequent analysis was performed at the laboratory of our cooperation partner Dr. Krause (Leibniz Institute for Molecular Pharmacology (FMP), Berlin Buch) with assistance from Dr. Stefanovic by me. The excised protein spots were washed with 50% v/v ACN in 50 mM ammonium bicarbonate, shrunk by dehydration in ACN, dried in a vacuum centrifuge, and incubated with 50 ng of trypsin (sequencing grade, Promega, Madison, WI, USA) in 10 mL of 5 mM ammonium bicarbonate at 37°C overnight. To extract the peptides, 2.5 mL of 0.5% v/v TFA in water were added. The supernatant was separated and the peptides were purified on a C18 RP minicolumn (ZipTip C18; Millipore, Bedford, MA, USA). Purification was performed according to the manufacturer's recommendations with the exception that peptides were eluted directly onto the MALDI target plate using 0.8 mL of α-cyano-4-hydroxycinnamic acid matrix solution consisting of 5 mg of matrix dissolved in 1 mL of 0.3% TFA in ACN/water (60:40 v/v).

3.6.7 Protein Identification by Peptide Mass Fingerprint Analysis

MS and MS/MS measurements were performed using a MALDI-TOF/TOF instrument (4700 Proteomics analyzer, Applied Biosystems, Framingham, MA). MS spectra were acquired in positive ion reflector mode by accumulation of 5000 consecutive laser shots. A maximum of 5 precursor ions for MS/MS fragmentation were selected automatically. The GPS Explorer (version 3.5, Applied Biosystems) was used for processing the spectra. After exclusion of contaminant ions (known matrix and human keratin peaks), the data were submitted to the MASCOT server (version 2.0, Matrix Science, London, U.K.) for in-house search against the Swiss-Prot database. The maximum of one missed cleavage was allowed and the mass tolerance of sequence and precursor ions was set to 20 ppm and 0.15 Da. Allowed variable modifications were carbamidomethylation on cysteine and methionine oxidation. The proteins were identified by a combined search using the peptide mass fingerprint data and MS/MS spectra. A protein was accepted as identified if the total protein score was higher than the significance threshold indicated by MASCOT, whereby the

MS/MS data confirmed the identification. Single protein identifications from multiprotein families were based on the detection of particular masses and MS/MS confirmation of specific peptide sequences differentiating the given protein from the other members of the family.

3.6.8 Statistical Analysis for Protein to RNA Comparison

For comparison between mRNA expression and protein expression in *Ha-ras* versus *B-raf*-mutated mouse liver tumors, microarray data from a previous analysis conducted in our laboratory (Stahl *et al.*, 2005) were re-evaluated with assistance from our cooperation partner Dr. Ittrich (central unit for Biostatistics, DKFZ, Heidelberg). Statistical evaluations were carried out using the software package Origin (version 6.1) (OriginLab Corp., Northampton, MA). Correlations between data sets from different groups were analyzed by linear regression analysis and correlation coefficients and significance values were calculated.

3.7 Ethoxyresorufin/Pentoxyresorufin Dealkylase Assay

Measurements of ethoxyresorufin-O-dealkylase (EROD) as well as pentoxyresorufin-O-dealkylase (PROD) activity are established markers of exposure to either CYP1A1/2- or CYP2B10 inducing agents, respectively (Prough *et al.*, 1978; Burke *et al*., 1974). In principle, a substrate (ethoxy- or pentoxyresorufin) is converted to a fluorescence emitting product by CYP1A1/2 or CYP2B10, which can be quantified by use of a standard curve. Enzymatic activity is given is nmol resorufin converted / µg protein / minute.

Table 5: Reaction mix for the EROD/ PROD-Assay

Reaction Mix Reagent	**Conc.**	**End-conc.**	**Vol. [µl]**
Water			79
Tris-HCl pH 7,4	1M	100mM	50
$MgCl_2$	50mM	5mM	50
Isocitrate-Na^+	50mM	5mM	50
$NADP^+$	5mM	500µM	50
EDTA	600µM	60µM	50
Isocitrate Dehydrogenase	3U/mg		1
Ethoxy/Pentoxyresorufin	75µM	1,5µM	10
Liver homogenate			50
Total Volume			**550**

The reaction was started by adding 10µl of either ethoxy- or pentoxyresorufin to 37°C pre-warmed reaction mix and stopped by adding 1ml of ice-cold methanol. Measurements were conducted in duplicates at time points 0 (here methanol was added before the substrate), 7.5 minutes and 15 minutes after substrate addition. After centrifugation, 150µl of probe were transferred onto a 96-well plate and measured using an excitation wavelength of 550nm and an emission wavelength of 585nm.

3.8 Electrophoresis

3.8.1 Agarose Gel Electrophoresis

Agarose was dissolved in 1x TAE buffer by boiling. 3µl of ethidiumbromide solution per 10ml of total volume were added directly to the solution before gel poring. Samples were applied to the gel in the appropriate loading buffer. Gels were run at 90V for 30-60min. DNA separation was monitored under UV (254nm) irradiation.

3.8.2 Polyacrylamide Gel Electrophoresis (PAGE)

Samples were diluted in the appropriate loading buffer and applied to the gel. Polyacrylamide gels were run at 300V for approx. 90min in 1x TBE buffer. Afterwards, gels were dyed in ethidiumbromide staining solution for 10min to allow visualization of separated DNA fragments under UV (254nm) irradiation.

4. Results

Chemically induced mouse liver tumors are frequently mutated in the genes encoding *Ha-ras*, *B-raf* or *Ctnnb1*, leading to constitutive activation of signaling pathways downstream of the respective regulatory proteins affected by mutation of their genes. While *Ctnnb1* mutations are highly prevalent in tumors induced by a treatment regimen including PB or a PB-like liver tumor promoter (Aydinlik *et al*., 2001; Calvisi *et al*., 2004; Strathmann *et al*., 2006) *Ha-ras* or alternatively *B-raf* mutations are seen in up to 70% of spontaneously occurring liver tumors or in tumors induced by exclusive treatment with a genotoxic liver carcinogen like DEN (Buchmann *et al*., 1991; Jaworski *et al*., 2005; Buchmann *et al*., 2008). The molecular mechanisms of tumor promotion by PB are still unknown, however some molecules are essential for the tumor promoting activity of PB. One of these molecules, which is involved in the exchange of small molecular substances between neighboring cells, was shown to be the channel forming protein connexin32. In previous works conducted in our laboratory it was shown that connexin32 knockout in livers of male mice inhibits the tumor promoting activity of PB (Moennikes *et al*., 2000). Another molecule linked to PB-dependent tumor promotion and activated by PB by a jet unknown mechanism that involves the protein phosphatase 2A, is the constitutive androstane receptor (CAR) (Swales and Negishi, 2004). *In vivo* knockout of either connexin32 or CAR inhibits tumor promotion by PB.

The overall scopes of the thesis were to

A. analyze the protein expression pattern of *Ha-ras* and *B-raf* mutated mouse liver tumors on a global scale in order to gain additional information about the molecular mechanisms of constitutive activation of either of the two proto-oncogenes.

B. investigate the importance of β-catenin in PB-dependent tumor promotion using a liver specific β-catenin active mouse strain (Tg(Alb-Cre/βCat^{S33Y})

C. analyze, in direct comparison to B., the role of β-catenin in PB-dependent tumor promotion using a liver specific β-catenin knockout mouse strain (β-catenin KO).

D. examine the tumor promotion effect of PB-like and non-PB-like tumor promoters after combined application in mice after DEN initiation.

E. study the feasibility of tumor imaging *in vivo* using magnetic resonance tomography and position election tomography.

4A. Comparative Transcriptome and Proteome Analysis of *Ha-ras* and *B-raf* Mutated Mouse Liver Tumors

Ha-Ras and B-Raf are proteins participating in signal transduction of the MAPK (mitogen activated protein kinase) family pathway. The B-Raf kinase, which specifically phosphorylates serine/threonine residues, is downstream of the small monomeric G-protein Ha-Ras and is thought to signal primarily through the MAPK pathway (Hagemann and Rapp, 1999; Mercer and Pritchard, 2003; Wellbrock *et al*., 2004). Ras proteins can potentially activate signaling pathways other than MEK/ ERK and thus have a broader spectrum of downstream effectors than Raf kinases (for reviews see Malumbres and Barbacid, 2003; Downward , 2003). Hence, constitutive activation of *Ha-Ras* in mouse liver tumors would be expected to impact on the activity of a broader range of transcriptional regulators and therefore lead to gene expression that differs from *B-raf* mutated tumors. The results of a recent microarray analysis conducted in our laboratory did not reveal any significant transcriptome differences between *Ha-ras* and *B-raf* mutated tumors (Jaworski *et al*., 2007). This would suggest that the transcriptional regulators activated by mutated *Ha-Ras* and *B-Raf* are largely identical. However, the expression of certain proteins is known to be regulated primarily at the transcriptional level, whereas the expression of numerous others is further controlled by complicated post-transcriptional mechanisms including alterations in mRNA stability, translation kinetics, or post-translational modifications affecting protein stability and enzymatic activity, leading to considerable discrepancies between mRNA and protein expression patterns (Chen *et al*., 2002; Schmidt *et al*., 2007; Griffin *et al*., 2002; Washburn *et al*., 2003; Maziarz *et al*., 2005; Unwin and Whetton, 2006). Therefore a comparative analysis between the proteome expression of *Ha-ras* and *B-raf* mutated mouse liver tumors was conducted in order to discriminate between the two tumor genotypes based on their protein expression patterns. In addition, changes in the transcriptome of *Ha-ras* and *B-raf* mutated liver

tumors as detected in earlier studies from our group (Jaworski *et al*., 2007; Stahl *et al*., 2005) was compared to the proteome data.

Proteome analysis: 2D-gel-electrophoresis and subsequent statistical analysis of the fluorescence stained gels revealed, on average, 2513 protein spots per run in the tissue samples (for representative examples, see Figure 10).

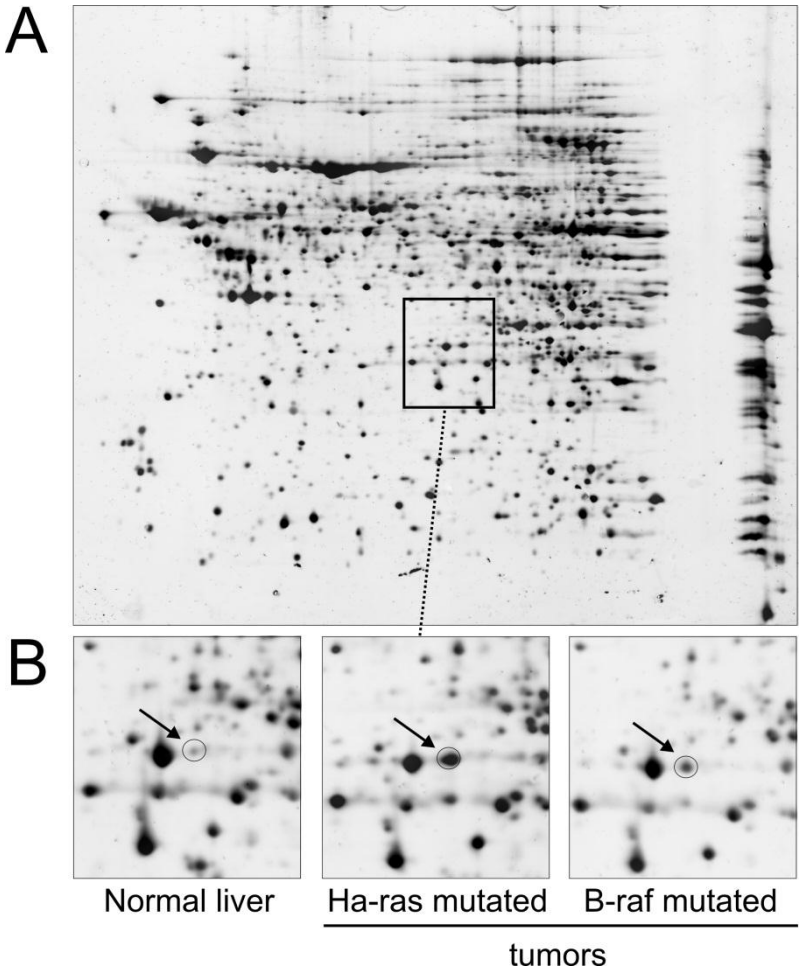

Figure 10: Representative examples of 2-D gel electrophoresis images. (A) Image of a stained 2-D gel with protein extracts from a control liver. (B) Zoomed regions of gel images with protein preparations from normal liver and *Ha-ras* and *B-raf* mutated tumors. The arrows point towards a spot representing Aldoketoreductase 1C18 (Q8K023) which is overexpressed in both *Ha-ras* and *B-raf* mutated tumors when compared to normal liver. Taken from (Rignall *et al*., 2010).

When applying threshold levels of $p \leq 0.05$ and $|\log_2 \text{ratio}| \geq 1$, there was a total of 156 significantly altered protein spots in *Ha-ras* mutated tumor samples of which 65 were down-regulated and 91 up-regulated when compared to normal liver tissue. The respective numbers for the *B-raf* mutated tumors were quite similar: 135 protein spots were de-regulated in total of which 66 were under-expressed and 69 over-expressed.

A summary of these results is given in the Volcano plots shown in Figure 11 A,B where the significantly altered protein spots are located in the gray-shaded areas of the plots.

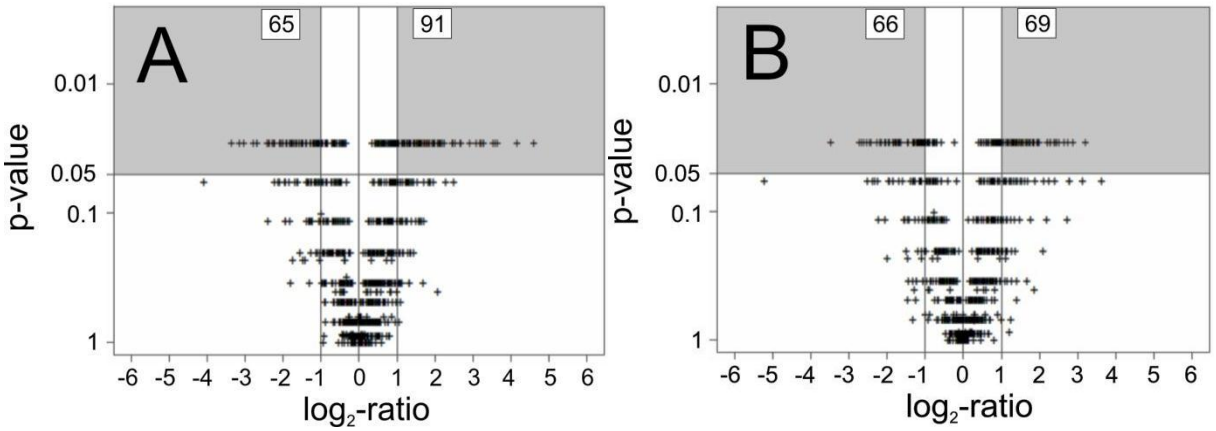

Figure 11: Protein expression in liver tumors with distinct genotypes. Differences in protein expression are demonstrated in the form of Volcano plots. (A) *Ha-ras* mutated tumors versus normal liver; (B) *B-raf* mutated tumors versus normal liver. Significantly altered spots with a $|\log_2$ expression ratio$| \geq 1$ and a p-value ≤ 0.05 are represented in the gray shaded areas of the graphs. The numbers of proteins with significant differences in expression between groups are also indicated. Taken from (Rignall *et al.*, 2010).

In addition, a comparison between the protein expression patterns from *Ha-ras* mutated tumors with those from their *B-raf* mutated cousins was performed. Here, only 2 spots showed significant differences at the threshold levels of $p \leq 0.05$ and $|\log_2$ ratio$| \geq 1$ (Figure 12). To verify this finding, all significantly changed spots were manually rechecked for correct matching between gels assigned by the software package. Upon this second analysis, the two spots that had been identified as significantly different between *Ha-ras* and *B-raf* mutated tumors did no longer reach the level of significance indicated above, and therefore, there remained no significant differences in protein patterns between *Ha-ras* and *B-raf* mutated tumors.

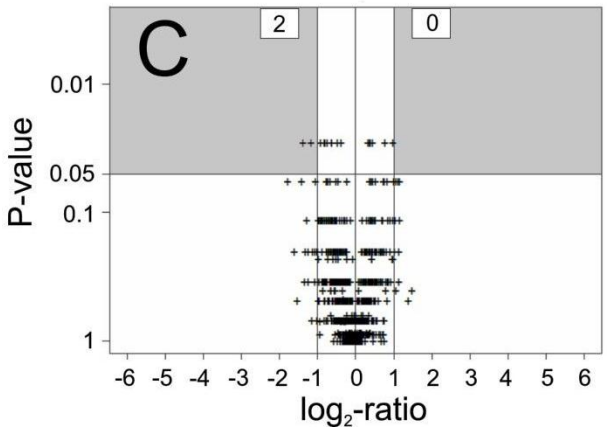

Figure 12: *B-raf* mutated versus *Ha-ras* mutated tumors. Significantly altered spots with a $|\log_2$ expression ratio$| \geq 1$ and a p-value ≤ 0.05 are represented in the gray areas of the graphs. The numbers of proteins with significant differences in expression between groups are also indicated. Taken from (Rignall *et al.*, 2010).

Subsequently, applying MALDI-TOF-TOF mass spectrometry, the identification of proteins with significant different expression was performed. For this purpose, all significantly altered protein spots were isolated and in-gel digested with trypsin. In the next step, the fragments were loaded on a MALDI target plate to be analyzed by peptide mass fingerprint and MS/MS sequence analysis. Out of the 291 digested protein spots, 131 were definitely assigned to individual proteins. Of these, 39 were identified in two or more spots, probably representing post-translationally modified forms (for the complete list of all identified protein sequences see Rignall *et al*., 2010). Taking into account that some proteins were identified more than once, the numbers of proteins and variants thereof significantly de-regulated in either *Ha-ras* or *B-raf* tumor tissues were 104 and 111, respectively, of which 45 were significantly altered in both tumor types.

In order to correlate changes in the protein expression between *Ha-ras* and *B-raf* mutated liver tumors, $\log_2$ protein expression ratios of the two tumor types were plotted against each other (Figure 13), showing that the protein expression patterns in *B-raf* and *Ha-ras* mutated tumors are highly significantly correlated. Equal changes in both tumor types would lead to data distribution on a straight line with a slope of 1, as indicated by the diagonal in Figure 13, and the majority of proteins showed comparatively little deviation from this line. Moreover, all proteins were located in the lower left and upper right quadrant of the diagram, demonstrating that all of them were de-regulated in the same direction in *Ha-ras* and *B-raf* mutated tumors when compared to normal liver.

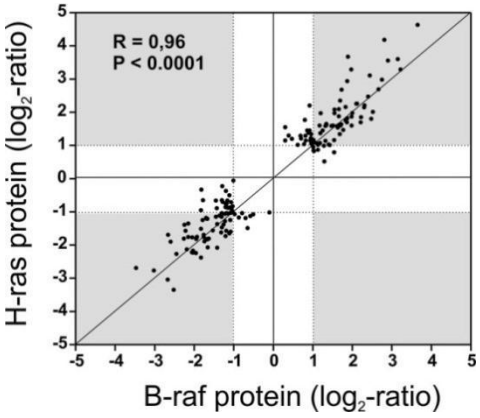

Figure 13: Comparison of protein expression in *B-raf* and *Ha-ras* mutated liver tumors. Each dot represents one protein spot. The extent and direction of the expression changes relative to normal liver were very similar in *B-raf* and *Ha-ras* mutated tumors. Protein spots with $|\log_2$ expression ratio$| \geq 1$ are represented in the gray shaded areas of the graph. Taken from (Rignall *et al.*, 2010).

A hierarchical cluster analysis of protein expression data from the *Ha-ras* and *B-raf* mutated tumors and the normal liver samples is presented in Figure 14. The blue and red scales in the figure indicate decreased or increased expression (on a logarithmic scale) relative to the mean expression in all tissues investigated. The resulting heat map confirms the high conformity in protein expression between *Ha-ras* and the *B-raf* mutated tumors as compared to normal liver. Only in very few cases there was a complete change in scaling (blue to red or vice versa), which, however, was mostly apparent in only one out of the 8 tumor samples, indicating a low level of heterogeneity between the individual tumors analyzed.

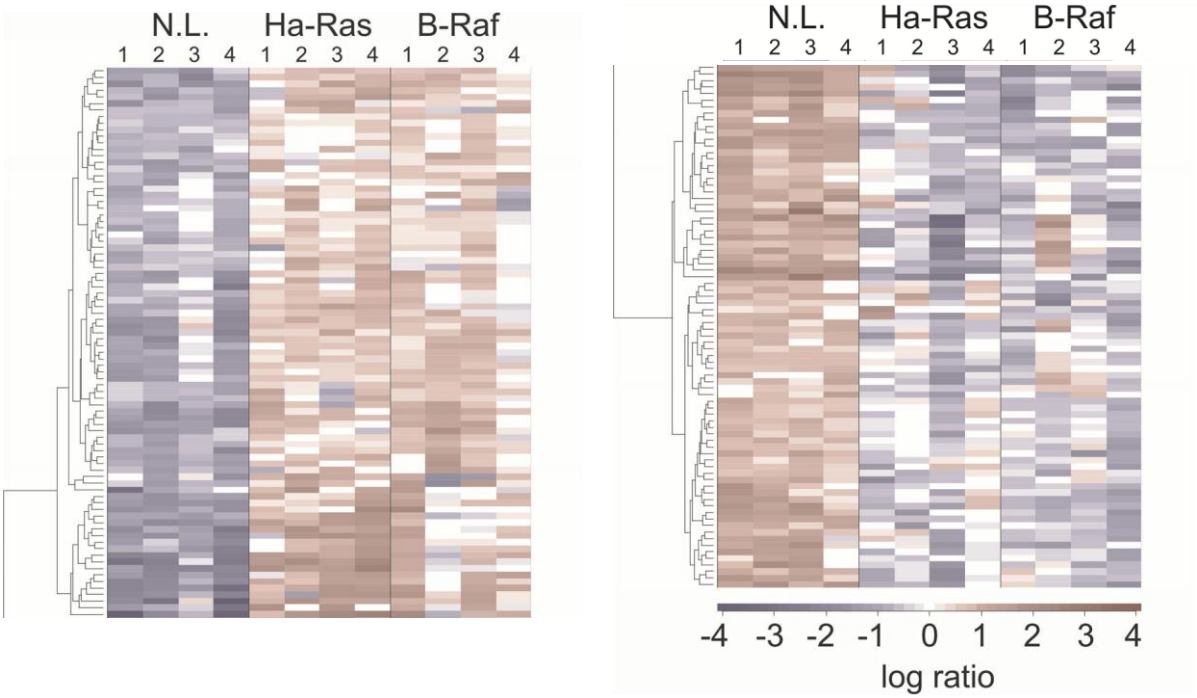

Figure 14: Hierarchical cluster analysis (manhattan metric + complete linkage) of the 170 protein spots showing significant expression changes in *Ha-ras* or *B-raf* mutated liver tumors relative to normal liver (N.L.). For each of the proteins, changes in expression ($\log_2$-ratios) relative to the mean of values from all 12 tissues of the study (4 *Ha-ras* and 4 *B-raf* mutated tumors, and 4 normal liver tissues) are scaled by differences in color (blue, low expression; red, high expression). Taken from (Rignall *et al.*, 2010)

To compare the observed changes of protein expression in *Ha-ras* and *B-raf* mutated liver tumors with their mRNA expression levels, data sets from two microarray analyses that had previously been conducted in our laboratory were used. In one of the studies, *B-raf* and *Ha-ras* mutated tumors and normal liver samples were investigated (Jaworski *et al*., 2007) while only *Ha-ras* mutated tumors and normal liver (plus *Ctnnb1* mutated tumors) were analyzed in the other study (Stahl *et al*., 2005). Starting from the Swiss-Prot/NCBI classification numbers of the proteins showing significant expression changes in *Ha-ras* and/or *B-raf* mutated tumors, the corresponding mRNAs were identified and their $\log_2$ expression ratios (tumor versus normal liver) were taken from the data sets of the two microarray studies. To get some impression on how well the mRNA expression data from the two data sets matched each other, the *Ha-ras*-tumor/normal liver $\log_2$-ratios of the two studies were plotted against each other. The result is shown in Figure 15, demonstrating a very high degree of correlation between both *Ha-ras* mRNA data sets.

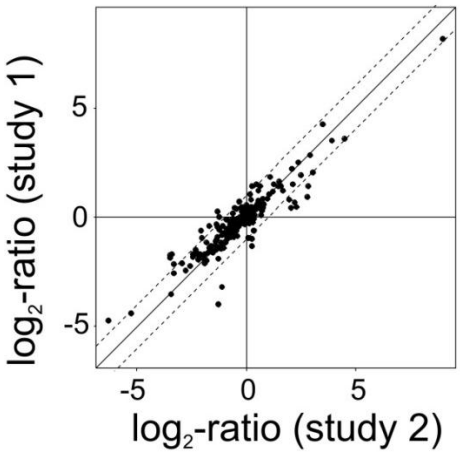

Figure 15: Correlation between two data sets on aberrant mRNA expression in *Ha-ras* mutated liver tumors. The data were taken from two recently published microarray studies conducted in our laboratory (study one: Stahl, S. et al., 2005 and study two: Jaworski, M. et al., 2007) and log2-ratios (*Ha-ras* mutated tumor versus normal liver) of mRNA expression detected in the two studies were plotted against each other. Each data point represents one transcript. Taken from (Rignall *et al.*, 2010)

Therefore, the two studies were regarded as equivalent in quality and all available data from the two studies were combined for the comparison with changes in protein expression levels in *Ha-ras* mutated liver tumors. The results obtained upon comparison between changes in mRNA and protein expression in *Ha-ras*-mutated tumors and *B-raf*-mutated tumors are shown in Figure16, panels A and B, respectively. Overall, changes in protein and mRNA expression largely appeared well-correlated, both in *Ha-ras* and *B-raf* mutated tumors, but there were also considerable variances in magnitude and several of the altered (mainly up-regulated) proteins did not show accompanying changes in their mRNA expression levels. In around 85% of the cases (data points located in the lower left and upper right

quadrant in Figure 16), expression of proteins and their mRNAs in tumors was de-regulated in the same direction (either up or down relative to normal liver), although mRNA changes were not always significant. In the 15% of the remaining cases, protein and mRNA expression were altered in opposite directions, and interestingly, most of them were up-regulated at the protein level, but mRNA expression was unchanged or even slightly lowered. Moreover, the data points in Figure 16 seem to cluster closer towards the x-axis, indicating a bias towards smaller changes in transcript expression than for the corresponding proteins. This may be explained by the use of two independent techniques, 2D-SDS-PAGE for the quantification of protein expression and microarray analysis for the corresponding mRNA quantification, leading to different degrees of absolute expression values. An extreme example for this is the secretory protein kininogen-1 precursor (see Figure 16A), which is ~25-fold up-regulated in *Ha-ras* mutated tumors (log_2 = 4.63), while the corresponding mRNA is up-regulated less than 2-fold, only (log_2 = 0.55-0.96). The opposite, however, was also found. Aldoketoreductase 1C18 (20-alpha-hydroxysteroid dehydrogenase, [EC 1.1.1.149]) was detected in two different protein spots, potentially representing post-translationally modified versions of the same protein (Figure 16A). The mRNA of the protein was increased in the *Ha-ras*-mutated tumors by a factor of ~250-500 (log_2-ratio ~8 to 9, depending on study); the two protein forms, however, were only ~3- to ~12-fold increased (corresponding to log_2-ratios of 1.55 and 3.56, respectively).

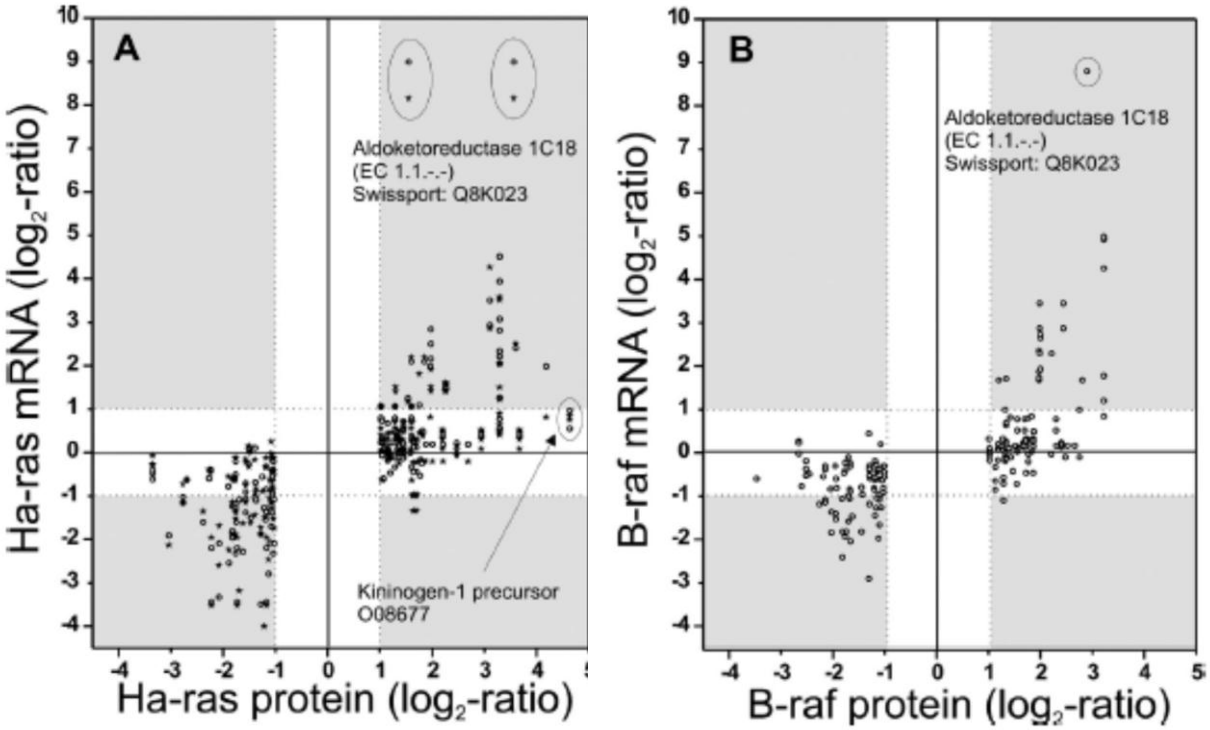

Figure 16: Correlation between protein and mRNA expression in (A) *Ha-ras* and (B) *B-raf*-mutated tumors. Expression data on proteins with significant alterations in *Ha-ras* and *B-raf* mutated tumors from the present study were compared with two data sets on aberrant mRNA expression from two earlier studies conducted in our laboratory. Stars (A) indicate mRNA data from the study of Stahl *et al.*, 2005 while open circles (A and B) indicate data from the study of Jaworski *et al.*, 2007. Data points with |log2 expression ratios| ≥ 1 for protein and corresponding mRNA are represented in the gray areas of the graph. Taken from (Rignall *et al.*, 2010)

Immunohistochemistry: Ras proteins and Raf kinases are known to transmit their signals via the MAPK pathway. To analyze activation of this pathway in *Ha-ras* and *B-raf* mutated tumors, immunostainings with tumor containing mouse liver sections using a phospho-specific antibody, that specifically detects the activated (threonine^{202}/tyrosine^{204} phosphorylated) forms of ERK1/2 was performed. The mutation analysis was performed by use of punched tissue biopsies taken from parallel sections. As exemplified in Figure 17, *Ha-ras* mutated tumors showed the expected positive staining for p-ERK1/2, both in the cytosol and in the nucleus of the hepatoma cells. Surprisingly, however, *B-raf* mutated tumors completely lacked p-ERK1/2 staining, indicating a major difference in signal transduction between *Ha-ras* and *B-raf* mutated tumors. In total, 20 tumors were studied from 11 mice. Six of them showed activating mutations in codon 61 of *Ha-ras* and all of these tumors were strongly positive for p-ERK1/2. Four tumors contained activating mutations in codon 637 of *B-raf* (but no *Ha-ras* mutations) and all of these tumors were negative for p-ERK1/2 staining. No mutations were detectable in the remaining 10 tumors which were also negative for p-ERK1/2 or showed only very faint staining, not comparable at all to the immunoreaction seen with the *Ha-ras* mutated tumors.

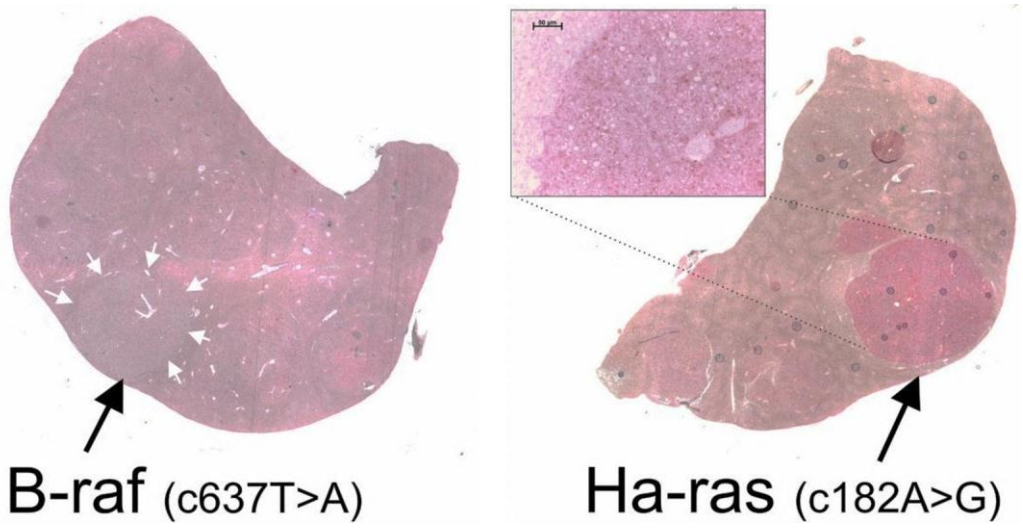

Figure 17: Immunohistochemical demonstration of differences between *B-raf* and *Ha-ras* mutated tumors in the activation status of extracellular signal regulated kinase (ERK). Liver sections were immunostained for the phosphorylated (activated) form of ERK (p-ERK1/2). Arrows point towards a *B-raf* mutated (left) and a *Ha-ras* mutated (right) tumor. There is a strong positive staining of the *Ha-ras* mutated tumor which is entirely absent in its *B-raf* mutated cousin. The inset in the right part of the figure shows the p-ERK1/2-positive tumor at a higher magnification, demonstrating a homogeneous cytoplasmic and nuclear staining throughout the entire tumor. Taken from (Rignall *et al.*, 2010)

4B. The Importance of β-catenin in PB-Dependent Tumor Promotion Analyzed by Using a Liver Specific β-catenin Active Mouse Strain (Tg(Alb-Cre/βCat^{S33Y})

Hepatocyte proliferation is known to be strongly affected by β-catenin-dependent signaling. Transgenic expression of an N-terminally truncated version of β-catenin results in increased hepatocyte proliferation and hepatomegaly (Cadoret *et al*., 2001), while livers from conditional β-catenin knockout mice show reduced weight (Sekine *et al*., 2006) and delayed regeneration (Tan *et al*., 2006). Recent studies in our laboratory have also shown that up to 80% of chemically induced mouse liver tumors initiated by a single DEN dosage and promoted by subsequent PB treatment carried activating point mutations in the *Ctnnb1* gene (Aydinlik *et al*., 2001). Since β-catenin is positively selected by PB, an analysis regarding the importance of the proto-oncogene in PB-dependent tumor promotion was carried out.

For the analysis, a transgenic mouse strain expressing a mutant version of β-catenin specifically expressed in the liver (Tg(Alb-Cre/βCat^{S33Y}) was used, which was recently generated in our laboratory (Loeppen *et al*., Dissertation). The mutant carries a point mutation at codon 33 affecting one of the GSK3β phosphorylation sites, a type of mutation frequently seen in chemically-induced mouse hepatomas and expected to stabilize the protein resulting in its constitutive activation. In the livers of the transgenic mice, expression of β-catenin target genes including GS and CYP2E1 was observed, but only in a subpopulation of hepatocytes scattered throughout the liver lobules (Figure 18).

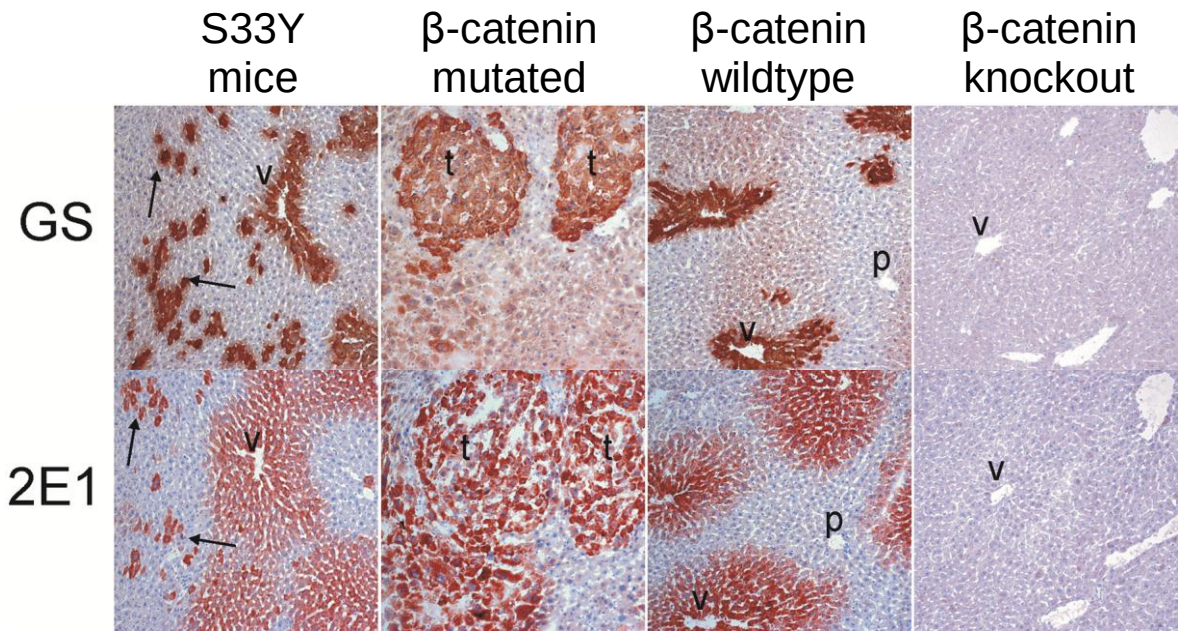

Figure 18: Immunohistochemical staining of liver slices of Tg(Alb-Cre/βCat^{S33Y}), wild-type mice with and without *Ctnnb1*-mutated tumors (t) and conditional *Ctnnb1*-knockout mice. Frozen liver slices were probed with antibodies as described in the materials and methods section. Expression of active β-catenin simultaneously elevated protein levels of glutamine synthetase (GS), a known direct target gene of activated β-catenin and of the cytochrome P450 isoform CYP2E1 (2E1). Scattered stained hepatocytes with abnormal localization within the liver lobule are indicated by arrows. v, central vein; p, portal vein (Schreiber *et al.*, unpublished).

To study the importance of β-catenin in tumor promotion by PB, an experiment, feeding Tg(Alb-Cre/βCat^{S33Y}) mice a PB-containing diet for 34 weeks to stimulate the outgrowth of tumors from the transgenic hepatocytes, was conducted. As expected, tumor response was very low in the control diet groups in absence of tumor-initiating or -promoting agents, resulting in an average of 0.27 and 0.14 tumors per animal in the wildtype (WT) and Tg(Alb-Cre/βCat^{S33Y}) groups, corresponding to a total number of 4 and 2 tumors in each group, respectively (Figure 19A). Feeding with PB promoted tumor development in mice from both genotypes. The highest average number of tumors per mouse was achieved in the Tg(Alb-Cre/βCat^{S33Y}) group (1.67; corresponding to a total of 25 tumors), while only 1.00 tumors per animal (corresponding to a total of 14 tumors) were found in their WT littermates (Figure 19A). This effect, however, missed the criteria of statistical significance (Wilcoxon rank sum test, p=0.107). Remarkably, only 3 out of these 14 tumors (21%) exceeded the size of 1mm in the WT goup, whereas 9 out of 25 tumors (36%) from Tg(Alb-Cre/βCat^{S33Y}) mice showed this characteristic (Figure 19B). Thus, Tg(Alb-

Cre/βCat^{S33Y}) mice displayed a tendency towards the development of more and larger tumors under PB treatment, as compared to WT controls. In order to rule out the occurrence of spontaneous mutations of the murine *Ctnnb1* gene, tumor DNA was isolated and analyzed for *Ctnnb1* mutations. No mutations of murine *Ctnnb1* were found in PB-promoted tumors from Tg(Alb-Cre/βCat^{S33Y}) mice.

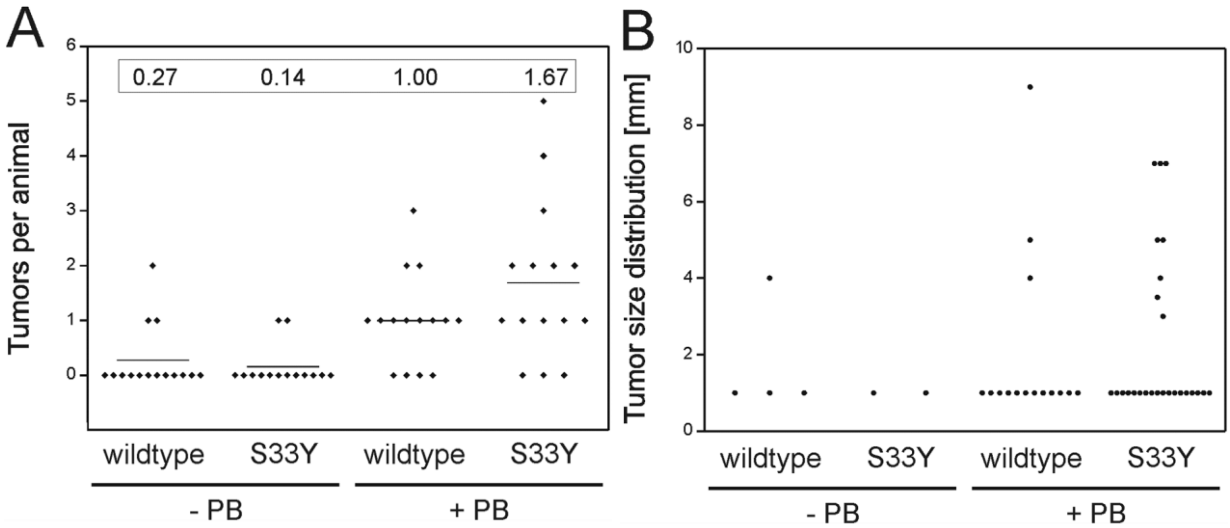

Figure 19: Tumor promotion by phenobarbital (PB) in livers from Tg(Alb-Cre/βCat^{S33Y}) (S33Y) mice and wildtype controls. (A) The number of tumors per animal is slightly increased in PB-treated Tg(Alb-Cre/βCat^{S33Y}) mice, as compared to wildtype controls. Each animal is represented by a single dot in the diagram. Mean of the distribution is given as a black line. Numbers on top of the panel indicate mean tumor number per mouse from each group. (B) Size distribution of tumors. Each tumor ≥1mm diameter is represented by a single dot. A slightly higher number of big (>2mm) tumors is observed in Tg(Alb-Cre/βCat^{S33Y}) after treatment with PB. Group sizes: wildtype, control diet: n=15 mice; Tg(Alb-Cre/βCat^{S33Y}), control diet: n=14; wildtype, PB-containing diet: n=15; Tg(Alb-Cre/βCat^{S33Y}), PB-containing diet: n=15.

Recent work in our laboratory demonstrated that overexpression of GS is associated with β-catenin-mutations in mouse liver tumors during promotion of hepatocarcinogenesis by PB (Loeppen *et al*., 2002). To examine if GS overexpression also occurs in mouse liver tumors of Tg(Alb-Cre/βCat^{S33Y}) animals feeding a PB containing diet as well as if this effect is dependent on the βCat^{S33Y} transgene, frozen mouse liver tissues of Tg(Alb-Cre/βCat^{S33Y}) and WT animals either receiving PB or control diet were analyzed for the expression of GS. In total, 11 GS altered lesions were identified originating from 7 animals. Within the Tg(Alb-Cre/βCat^{S33Y}) / PB treatment group 40% of all lesions were GS positive (2/5) whereas 80% (4/5) of lesions belonging to control animals receiving PB containing diet

showed this staining pattern. Although the number of lesions was too small to represent a comprehensive picture, the low incidence of GS positive lesions in the Tg(Alb-Cre/βCat^{S33Y}) / PB treatment group was different when comparing the incidence to a recent study (Aydinlik *et al*., 2001).

To further investigate the overall low number of liver lesions as well as the low incidence of GS positive liver lesion in transgenic animals treated with PB, the content of recombined transgene-DNA in comparison to the non-recombined fraction in isolated tumors ≥1mm in size and corresponding normal liver tissue of Tg(Alb-Cre/βCat^{S33Y}) animals receiving PB was assessed (Figure 20).

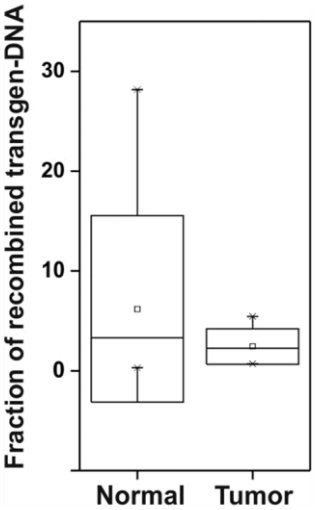

Figure 20: Amount of recombined transgene-DNA relative to the non-recombined fraction, given in percent, between tumor tissue of Tg(Alb-Cre/βCat^{S33Y}) animals receiving PB and corresponding non-tumors tissue (normal). There is no statistical significant difference in the recombined transgene-DNA fraction, rather slightly higher recombination-levels in non-tumor tissues. Overall the average recombination levels are very low (6,1% within non-tumor tissue; 2,4% in tumor tissue). The Box plot is represented by the average value (small center box), median (center line), standard deviation (large box) as well as minimum and maximum outliers. Group sizes: n=8 for both non-tumor tissue and tumor tissue.

Transgene recombination is a pre-requisite for transgene expression. Apparently there was no statistically significant difference in the fraction of recombined transgene-DNA between non-tumor tissue (normal) and tumor tissue. More strikingly was the fact that the percentage of recombined transgene-DNA was, for both types of tissue, very low and also higher in non-tumor tissue (6,1% within non-tumor tissue; 2,4% in tumor tissue).

In addition, quantitative gene expression analysis, assessed by LC RT-PCR in combination with standard row measurement, of endogenous *Ctnnb1*, transgene *β-catenin^{S33Y}*, *Cre recombinase*, the enzyme responsible for transgene recombination as well as *GS* and *GPR49*, both β-catenin target genes, was performed (Figure 21).

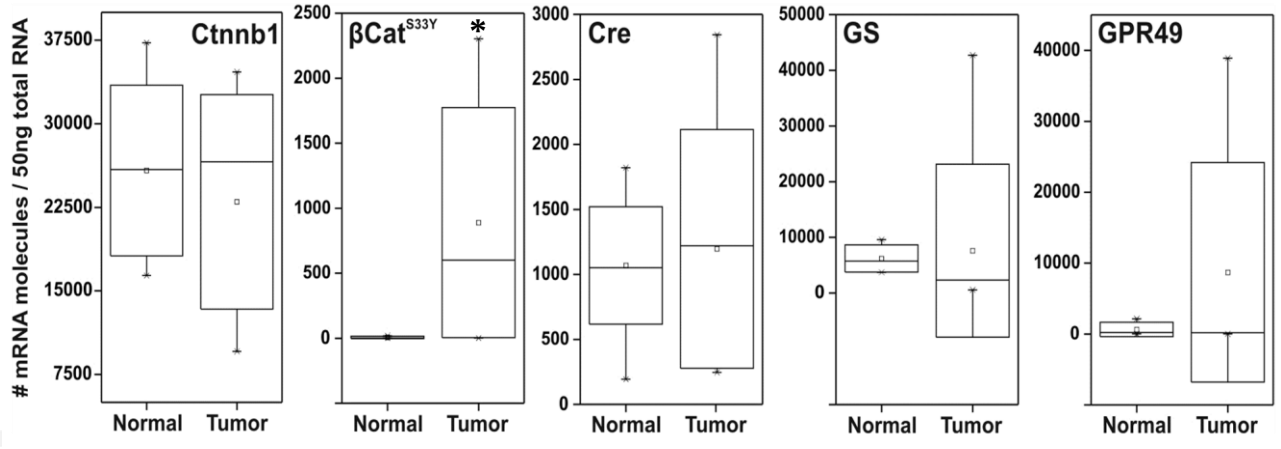

Figure 21: Quantitative mRNA expression levels, expressed as number of molecules per 50ng of total RNA, between tumor tissue of Tg(Alb-Cre/βCat^{S33Y}) animals receiving PB and corresponding non-tumors tissue (normal). *Ctnnb1* is highly expressed in both types of tissue. β*Cat^{S33Y}* transgene expression is statistically significant higher with p ≤ 0.05 in tumor tissue as compared to non-tumor tissue, when applying Student´s t-test, but the overall expression level is still very low. Cre recombinase, GS as well as GPR49 display no significantly different expression levels between the tissue types. Group sizes: n=9 for both non-tumor tissue and tumor tissue.

Although there was a statistical significant increase in transgene-mRNA expression between non-tumor tissue and tumors of Tg(Alb-Cre/βCat^{S33Y}) animals receiving PB at p≤0,05 the up-regulation was not accompanied by a statistical significant increase in GS and GPR49 mRNA.

4C. The Importance of β-catenin in PB-Dependent Tumor Promotion Analyzed by Using a Liver Specific β-catenin Knockout Mouse Strain (β-catenin KO-mice)

To further analyze the importance of β-catenin in PB-dependent tumor a β-catenin knockout mouse strain was used in which the β-catenin signaling pathway is specifically inactivated in hepatocytes (Huelsken *et al*., 2001; Braeuning *et al*., 2009).

Demonstration of O^6-ethylguanine formation: DEN, the tumor initiator in the experiment, requires metabolic activation through cytochrome P450 (CYP)-mediated α-hydroxylation to exert its carcinogenic effect. CYP2E1 is involved in the catalysis of this reaction since Cyp2e1 knockout-mice develop less liver tumors than WT-mice

(Kang *et al*., 2007). To investigate activation of DEN in liver, an antibody specifically directed against O^6-ethylguanine, a pro-mutagenic adduct formed in liver DNA of DEN-exposed mice (Pegg *et al*., 1977) was used. Frozen liver sections from WT- and β-catenin knockout (KO)-mice treated with a single injection of DEN were double-stained for the presence of O^6-ethylguanine and GS. The latter staining was used for the identification of central venules which are exclusively surrounded by GS-positive hepatocytes (Gebhardt *et al*., 1983). The results shown in Figure 22 demonstrate that O^6-ethylguanine adducts from DEN are formed in hepatocytes from both WT- and KO-mice, but also that the zonality of DNA-alkylation in WT-mice which has been lost in livers of KO-mice. In WT-mice, perivenous hepatocytes stained strongly positive while periportal hepatocytes displayed only very faint staining. By contrast, KO-mice showed staining of nuclei in all hepatocytes, albeit with somewhat weaker intensity than in WT-mice. The loss of O^6-ethylguanine-zonality in KO-mice was not unexpected since various CYP-isoforms lose zonal expression in liver in the absence of β-catenin; for review see (Braeuning and Schwarz, 2009). The result clearly demonstrated that DEN is metabolized to its ultimate carcinogenic form in liver of KO-mice and, as a side result, it also showed that CYP2E1 cannot be the only CYP-isoform responsible for this metabolic step since expression of CYP2E1 is strongly reduced in liver of Ctnnb1 KO-mice (Braeuning *et al*., 2009, Sekine *et al*., 2006).

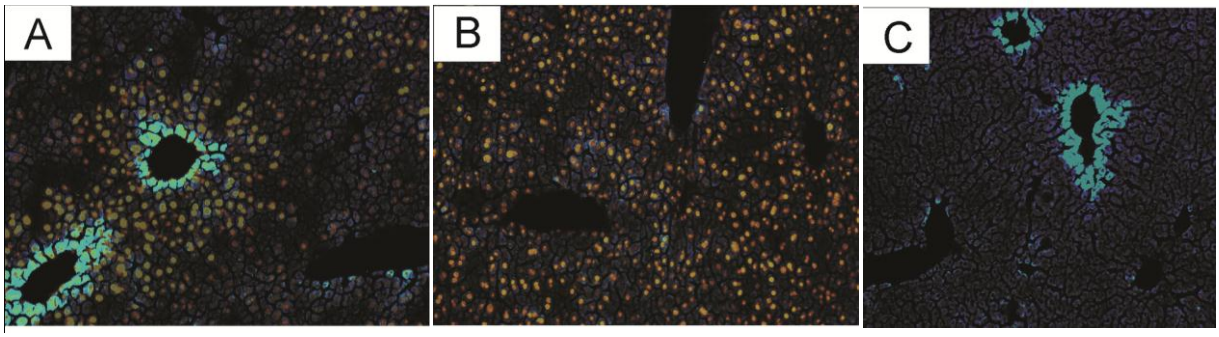

Figure 22: Immunohistochemical demonstration of O^6-ethylguanine-adducts in DNA of (A) DEN-treated WT-mice, (B) DEN-treated KO-mice, (C) untreated WT-mice. Note that nuclear staining for the DNA-adduct (orange fluorescence) is preferentially in perivenous hepatocytes in WT-mice as opposed to a more homogeneous staining pattern in liver of KO-mice. Staining for GS (green fluorescence) labels a ring of hepatocytes around the central veins, marking the perivenous areas of the liver lobules in WT-mice. Taken from (Rignall *et al*., 2011)

Tumor initiation-promotion study: The tumor initiation-promotion study was conducted using DEN as initiator and PB as tumor promoter. At the beginning of the experiment, KO-mice had a slightly reduced body weight when compared to WT-mice, which remained lower during the entire study period (Figure 23). Ten of the KO-mice (6 on control diet and 4 PB-treated mice) died during the experiment, in contrast to only one in the WT-groups, indicating a much higher vulnerability of the KO-mice. PB-treatment led to an increase in the liver/body weight ratio both in WT- and in KO-mice, but the effect was somewhat smaller in KO-mice (Figure 23). The more pronounced increase in mean liver/body weight ratio in PB-treated WT-mice was not solely due to the well-known liver-enlarging effects of PB but also to a much stronger liver tumor burden in this group.

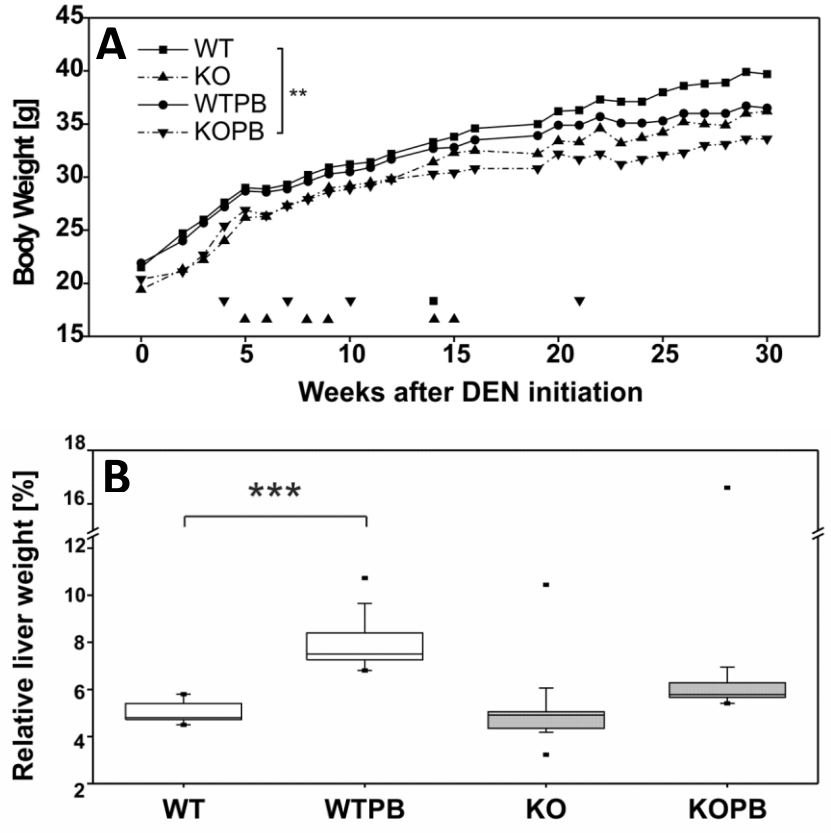

Figure 23: The initiation-promotion study. (A) Body weight gain of animals in the 4 experimental groups. The time points of premature death of some of the animals are also indicated. Differences between groups at the end of the experiment were significant ($p<0.001$; Kruskal-Wallis test). Significant differences in Dunn´s multiple comparison test are indicated by 2 asterisks ($p<0.01$). (B) Liver/body weight ratios (relative liver weight in percent) of mice of the 4 groups. Kruskal-Wallis test was significant with $p<0.0001$. Statistical significances in Dunn´s multiple comparison test are indicated by 3 asterisks ($p<0.001$). Taken from (Rignall *et al.*, 2011)

After termination of the experiment, tumors visible on the surface of the liver were counted. Tumor multiplicity (mean number of tumors/mouse) in the 4 treatment groups is given in Figure 24. The results clearly demonstrated that (i) the tumor response was, in the absence of PB, much higher (although not statistically significant at $p<0.05$) in KO- (0.14 tumors/mouse) than in WT-mice (1.0 tumor/mouse) and that (ii) PB was very active as a tumor promoter in WT- but not in KO-mice. These findings are illustrated in detail in Figure 24 where the size class distribution of tumors in the 4 groups is shown. While only 2 tumors with a diameter between 1 and 2 mm were observed in the 14 mice of the WT minus-PB group, KO-mice had tumors in all 3 diameter classes, both in the PB and non-PB treatment groups. Moreover, tumor response was strongly enhanced in PB-treated WT-mice in all 3 diameter classes.

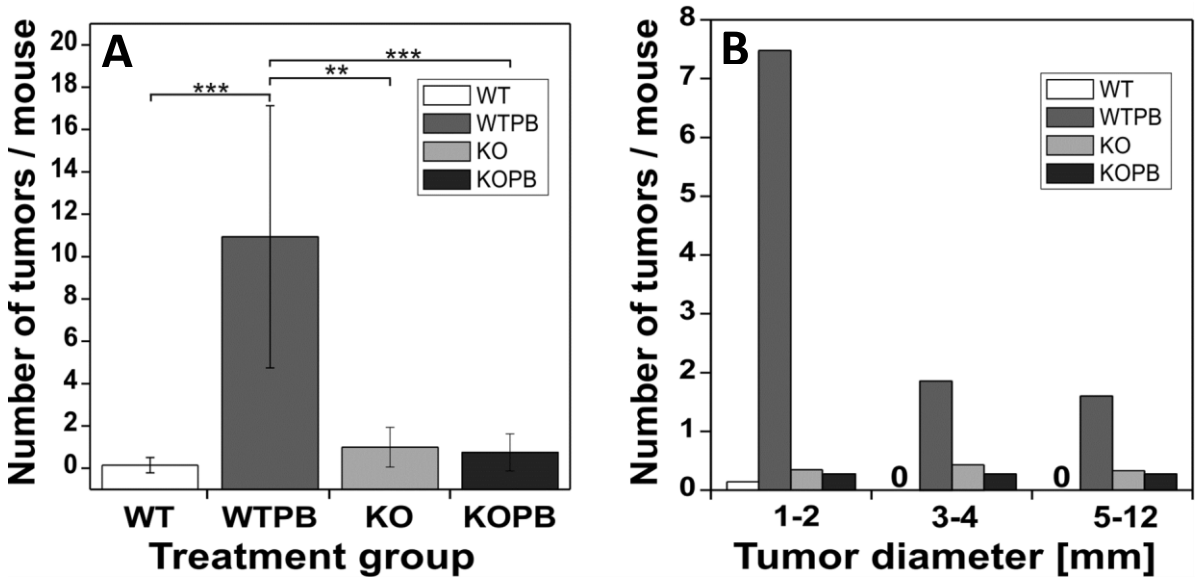

Figure 24: Frequency of macroscopically visible liver tumors. (A) Average number of tumors per mouse visible on the surface of the liver in the 4 treatment groups. Differences between groups were highly significant (p<0.0001;Kruskal-Wallis test). Statistical significances in Dunn´s multiple comparison test are indicated by asterisks (p<0.01; *** p<0.001). (B) Number of tumors per mouse in the indicated diameter size classes. Taken from (Rignall *et al.*, 2011)**

To further analyze the effect of PB in β-catenin knockout mice, serial sections were prepared from frozen livers and stained for G6Pase and GS. Tumors were identified in the stained sections by an alteration in G6Pase-activity (mostly negative) and/or alteration in GS staining-intensity (mostly positive) relative to the surrounding normal tissue. In most instances, compression of the surrounding normal liver tissue was

also seen. Representative examples of tumors identified by the two markers in the liver of a PB-treated WT-mouse are shown in Figure 25.

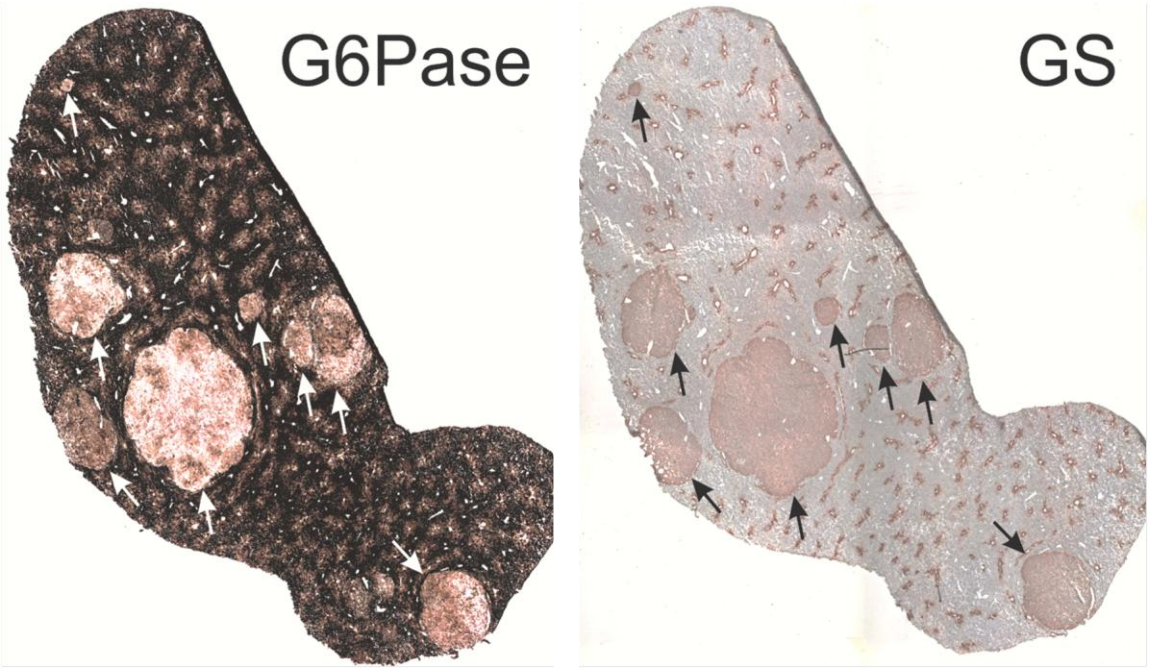

Figure 25: Enzyme- and immunohistochemical localization of liver tumors in G6Pase- and GS-stained tissue sections. The example shows two serial sections from a PB-treated *Ctnnb1* WT-mouse. Arrows indicate tumors identified by the two markers. Taken from (Rignall *et al.*, 2011)

The two-dimensional sizes of intersections of tumors identified by alterations in G6Pase-activity and/or GS-content were determined thus allowing the quantification of the percentage of tumor tissue in the animals. The volume fraction, which is equivalent to the area fraction, is the most reliable parameter, since it can be determined without bias-sensitive stereological procedures. The results of this analysis are summarized in Table 6, showing that the by far strongest carcinogenic response occurred in livers of PB-treated WT-mice, and that most of the lesions were G6Pase-negative and also GS-positive. Non-PB-treated KO-mice were somewhat more susceptible with respect to the formation of enzyme-altered lesions than WT-mice. A promoting effect of PB, however, was not seen in KO-mice.

Table 6: Quantification of enzyme-altered liver lesions in G6Pase- and GS-stained sections.

			Volume fraction of lesions in liver (%)			
			G6Pase		GS	
Group	Genotype/ treatment	Effective # of mice	negative[a]	positive or patchy[a]	negative[b]	positive[a]
1	WT	14	0.34 ±1.25	0 ±0.00	0.34 ±1.25	0 ±0.00
2	WTPB	15	9.57[c] ±9.23	3.27[d] ±3.85	1.25[e] ±2.00	11.59[f] ±11.49
3	KO	10	0.46 ±1.40	0.15 ±0.47	0.60 ±1.43	0 ±0.00
4	KOPB	12	0 ±0.00	0.62 ±1.38	0.32 ±1.10	0.30 ±0.94

Relative fractions (%) of tumor tissue of the respective phenotype are given as mean ±SD
[a]Kruskal-Wallis test is significant with p<0.0001
[b]Kruskal-Wallis test is significant with p<0.05
[c]significantly different from groups 1,4 (p<0.001) and 3 (p<0.01); Dunn´s multiple comparison test
[d]significantly different from groups 1,3 (p<0.001) and 4 (p<0.01); Dunn´s multiple comparison test
[e]significantly different from group 1 (p<0.05) and 4 (p<0.01); Dunn´s multiple comparison test
[f]significantly different from groups 1,3 and 4 (p<0.001); Dunn´s multiple comparison test.

Mutation analyses. Tumors with diameters of >3 mm were isolated and analyzed for the presence of mutations in codon 61 of *Ha-ras*, codon 637 of *B-raf*, and exon 3 of *Ctnnb1*. In total, 14 tumors from non-PB-treated mice were analyzed, of which 3 (two from KO-mice and one from a WT-mouse) were *Ha-ras*-mutated, all of the type c.181C>A. *B-raf*- or *Ctnnb1*-mutations were not detected in these tumors. Of the 10 tumors analyzed from PB-treated WT-mice, 9 showed activating point-mutations in *Ctnnb1*, all affecting the well-known hot-spot positions in the gene region encoding exon 3 (Aydinlik *et al*., 2001). Surprisingly, 2 out of 6 tumors isolated from PB-treated KO-mice were also *Ctnnb1*-mutated. A consistency-check unequivocally demonstrated the hepatocyte-specific *Ctnnb1*-knockout in these mice (for a possible explanation for this finding see discussion).

Histopathological findings in non-tumorous tissue. In haemalum/eosin-stained sections, we detected clear signs of a fibrotic process in livers from KO-mice which was accompanied by massive infiltration of cells of the immune system. To further characterize and specify these effects, we performed a histological Masson-Goldner-trichrome stain which allows the discrimination between hepatocytes (Figure 26A/C, red staining) and fibrotic tissue (Figure 26A/C, greenish staining). Some of the livers

showed areas consisting of hepatocytes demonstrating massive lipid storage (Figure 26E) and other areas consisting of strongly enlarged hepatocytes of a preneoplastic phenotype (Figure 26F). The hepatocytes, arranged in nodular structures surrounded by fibrotic tissue (Figure 26A), appeared to store glycogen as indicated by the Periodic Acid Schiff's stain, but in a somewhat scattered manner (Figure 26B/D).

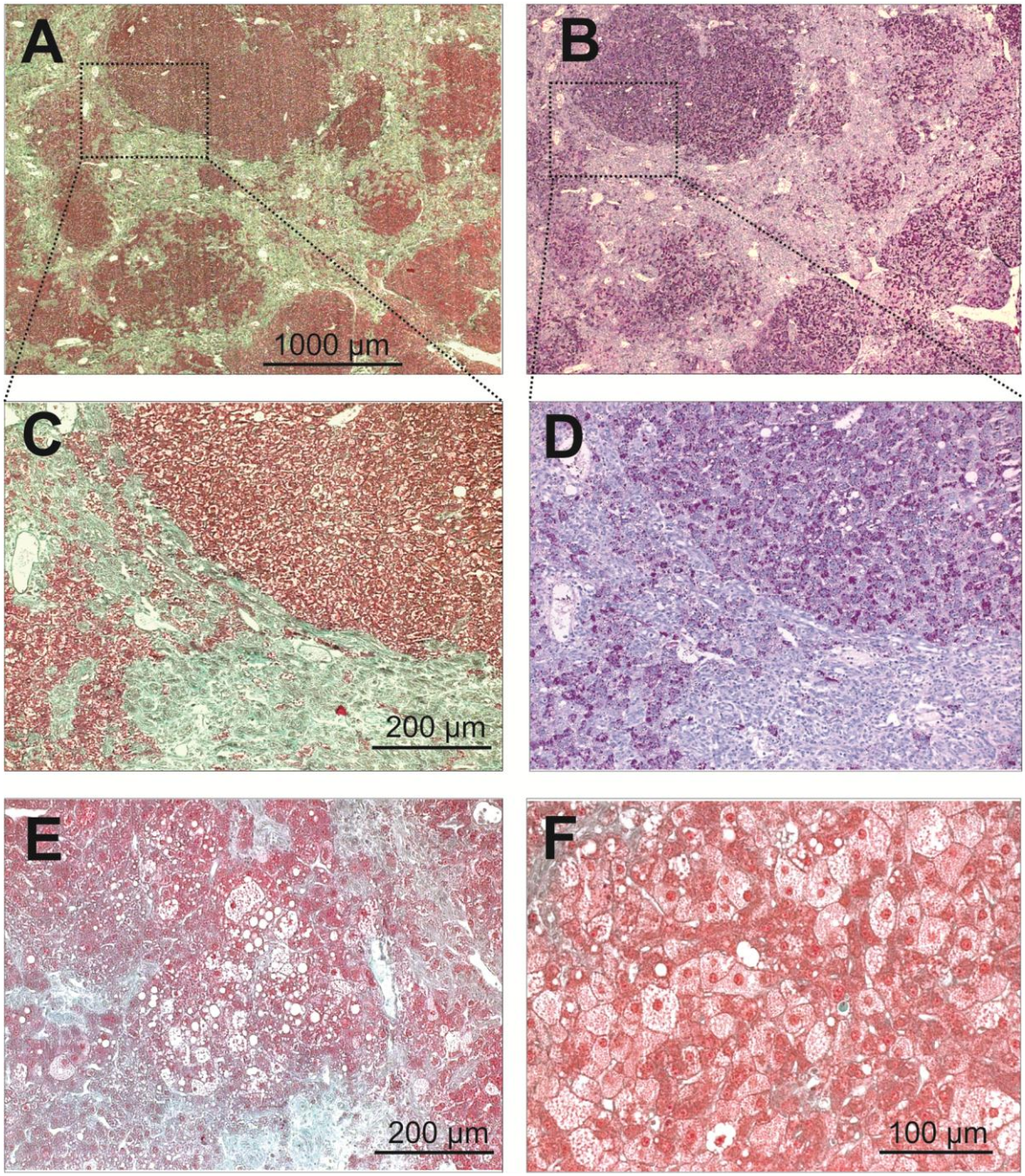

Figure 26: Fig. 5. Histological abnormalities in liver of KO-mice. (A,C,E,F) Masson-Goldner-trichrome stain. (A) Pre-cirrhotic alterations in liver from a PB-treated KO-mouse characterized by a nodular arrangement of hepatocytes (stained red) surrounded by fibrotic tissue (greenish). (B) Parallel section stained for glycogen using the Periodic Acid Schiff's stain. Note the extensive glycogen storage in hepatocytes scattered within the various nodular structures. (C,D) Higher magnifications of (A) and (B), respectively. (E) Demonstration of a cluster of hepatocytes showing extensive storage of lipids in large vacuoles. (F) Characteristic cluster of strongly enlarged hepatocytes of a pre-neoplastic phenotype. Taken from (Rignall *et al.*, 2011)

These histopathological abnormalities were only seen in KO-, but not in WT-mice. The response, however, was very variable and differed between PB-treated and non-PB-treated groups. Some KO-mice showed almost no signs of liver fibrosis/cirrhosis, whereas this abnormality was very evident in others. Strong differences in the degree of fibrotic appearance were observed even between different lobes of one and the same animal (not shown). Notably, KO-mice of the PB-treatment group were more frequently affected: half of the mice of this group showed more or less pronounced signs of fibrosis (6 out of 12), while only 1 out of 10 of the non-PB-treated mice showed (albeit in this case very strong) liver fibrosis.

Proteome analysis: In a next step, proteome changes were analyzed in livers of WT- and KO-mice treated with PB or control diet by 2-D gel-electrophoretic separation of proteins followed by their identification by mass spectrometry. 2D-gel-electrophoresis and subsequent statistical analysis of the fluorescence stained gels revealed, on average, 2602 protein spots per run in the tissue samples. When applying threshold levels of $p \leq 0.05$ and $|\log2 \text{ ratio}| \geq 1$, a total of 72 proteins that were significantly altered in intensity in KO as compared to WT mice were found; the majority of these (56) were lower in intensity in KO mice. Short-term PB treatment of WT mice resulted in deregulation of only 10 proteins (6 up- and 4 down-regulated by the barbiturate). By sharp contrast, PB treatment altered the intensity of 59 proteins in KO mice, 47 of which were up- and 12 down-regulated in comparison to non-PB treated KO mice. Interestingly, of the 56 proteins which were down-regulated in KO as compared to WT mice, 20 were up-regulated by PB in KO mice, but, except for one (glutathione S-transferase mu1), not in PB-treated WT mice. The number of 20 would even increase to 25 if allowing for protein isoforms (for example: keratin, type 1, cytoskeletal 10, reduced in KO versus WT and the keratin isoform type 18 induced by PB in KO mice). On the other hand, the levels of 7 of the 16 proteins, which were

higher in expression in KO than in WT mice, were lowered by PB treatment in liver of KO mice but not so in liver of PB-treated WT mice. A list of all proteins which were found to be affected both by the KO genotype and by PB-treatment is presented in table 7.

Table 7: Proteins altered by phenobarbital treatment in knockout mice

Proteins with levels: KO<WT AND KO plus PB>KO minus PB

Protein Name	EC-Number	Swiss-Prot	Log_2 ratio KO<WT	Log_2 ratio KOPB>KO
10-formyltetrahydrofolate dehydrogenase	1.5.1.6	Q8R0Y6	2,243	2,824
26S proteasome non-ATPase regulatory subunit 13	-	Q9WVJ2	2,399	2,935
Carboxymethylenebutenolidase homolog	3.1.-.-	Q8R1G2	3,643	3,408
Delta-aminolevulinic acid dehydratase	4.2.1.24	P10518	6,937	3,74
Eukaryotic initiation factor 4A-I	3.6.4.13	P60843	3,031	3,053
Farnesyl pyrophosphate synthetase	2.5.1.1/10	Q920E5	3,814	2,535
			3,973	2,844
FK506-binding protein 4	5.2.1.8	P30416	2,098	2,46
Glutathione S-transferase A4	2.5.1.18	P24472	2,857	3,152
			2,428	
Glutathione S-transferase Mu 1	2.5.1.18	P10649	2,77	4,911
			4,213	8,299
			7,195	16,283
Liver carboxylesterase 31	3.1.1.1	Q63880	3,01	4,398
Phenazine biosynthese-like domain-containing protein	5.1.-.-	Q9CXN7	2,398	2,177
Phosphoglycerate mutase 1	5.4.2.1/4, 3.1.3.13	Q9DBJ1	2,312	2,665
Proteasome activator complex subunit 1	-	P97371	2,353	2,56
Proteasome subunit beta type-1	3.4.25.1	Q9R1P4	2,95	2,468
Proteasome subunit beta type-4	3.4.25.1	P99026	3,178	4,012
Regucalcin	-	Q64374	8,266	2,774
Ribosyldihydronicotinamide dehydrogenase [quinone]	1.10.99.2	Q9JI75	2,273	2,611
S-adenosylmethionine synthetase isoform type-1	2.5.1.6	Q91X83	2,4	3,433
			3,432	2,617
Thioredoxin domain-containing protein 4	-	Q9D1Q6	2,412	3,18
			2,973	
Thiosulfate sulfurtransferase	2.8.1.1	P52196	3,318	2,035

Proteins with levels: KO>WT AND KO plus PB<KO minus PB

Protein Name	EC-Number	Swiss-Prot	Log_2 ratio KO>WT	Log_2 ratio KOPB<KO
Aldehyde dehydrogenase X, mitochondrial	1.2.1.3	Q9CZS1	3,856	2,195
Arginase 1	3.5.3.1	Q61176	2,499	2,044
Argininosuccinate lyase	4.3.2.1	Q91YI0	2,535	2,296
Fumarylacetoacetase	3.7.1.2	P35505	2,771	2,261
Ornithine carbamoyltransferase, mitochondrial	2.1.3.3	P11725	2,004	2,116
Phosphoenolpyruvate carboxykinase, cytosolic [GTP]	4.1.1.32	Q9Z2V4	2,418	3,435
Succinate dehydrogenase [ubiquinone] flavoprotein s.u., mt	1.3.5.1	Q8K2B3	2,189	2,196

A synopsis on expression changes of intermediary metabolism enzymes observed in *Ctnnb1* KO mice is illustrated in figure 27.

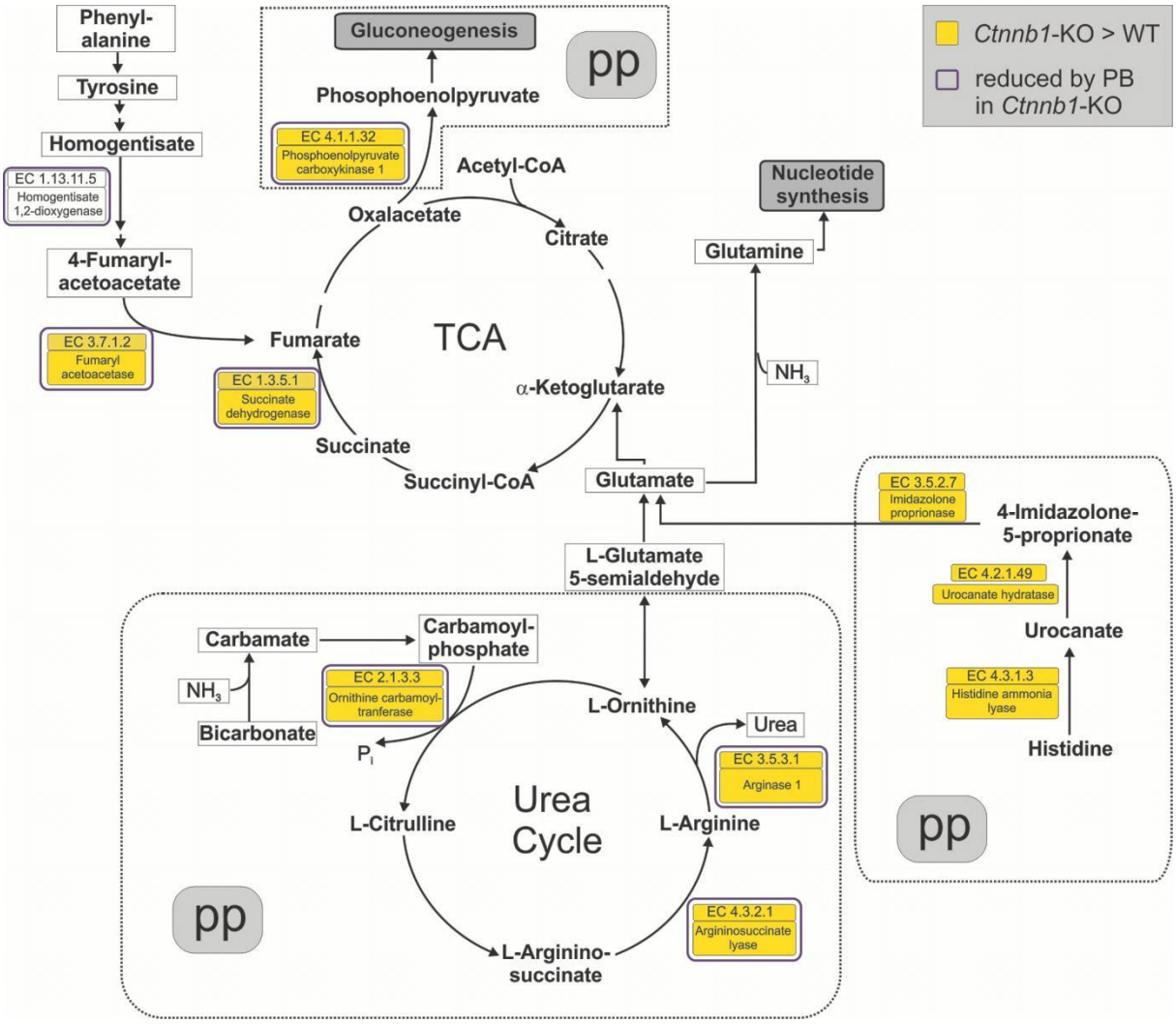

Figure 27: Proteins significantly up-regulated in KO-mice as compared to WT animals and the impact of PB upon the expression levels. Several enzymes involved in catabolism of phenylalanine, tyrosine and histidine or gluconeogenesis or the urea cycle are up-regulated in *Ctnnb1* knockout animals, indicating negative regulatory effects of β-catenin in wildtype animals (yellow boxes). Upon PB treatment the expression of 6 out of 9 proteins formerly up-regulated in *Ctnnb1* knockout animals is reversed to nearly wildtype level, indicating a β-catenin mimetic effect in the absence of *Ctnnb1* (blue boxes). Most interestingly, 7 out of 10 proteins significantly de-regulated are reported to be periportally located (pp) which would support the theory that β-catenin is a modulator of zonation and negatively regulates periportal protein expression. Taken from (Rignall *et al.*, in preparation)

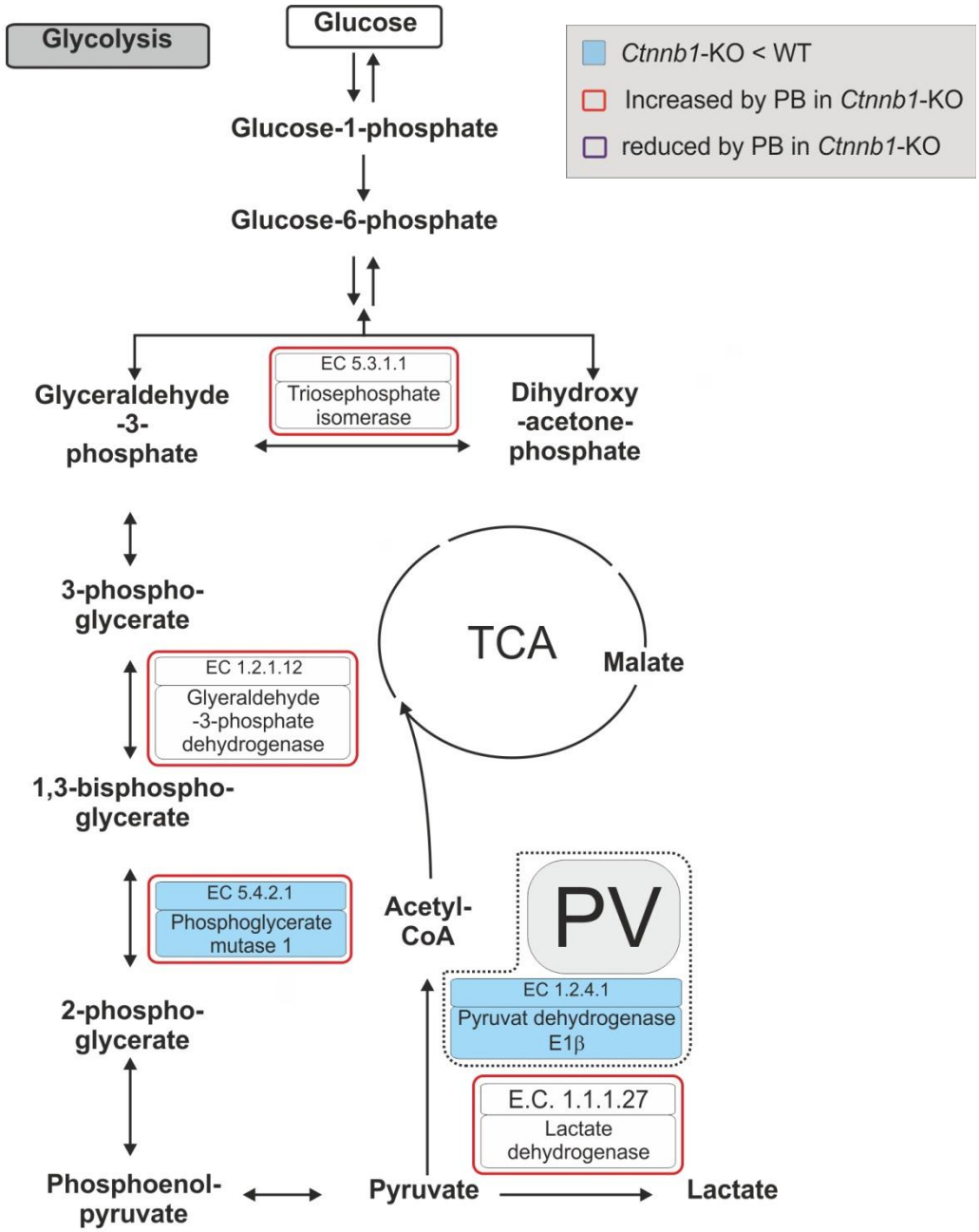

Figure 28: Proteins significantly up-regulated in KO-mice as compared to WT animals and the impact of PB upon the expression levels. (continued). Two enzymes of the glycolytic pathway were significantly down-regulated in liver of KO as compared to WT mice, namely pyruvate dehydrogenase and phosphoglycerate mutase 1 (illustrated by the blue color). The level of the latter enzyme and 3 other enzymes within the metabolic pathway, namely triosephosphate isomerase, glyceraldehydes-3-phosphate dehydrogenase and lactate dehydrogenase, were statistically significant up-regulated by PB. The levels of these latter 3 enzymes were not significantly decreased in KO as compared to WT mice at an individual basis. However, when analyzing the 4 PB-regulated enzymes as a group the decrease in KO as compared to WT mice became highly significant ($p<0.05$). (Rignall *et al.*, in preparation)

Gene-expression analysis. In order to analyze if changes identified by the proteome analysis are due to a change in gene expression, LC RT-PCR analysis was carried out. The expression of 5 target genes with up-regulated protein levels in KO-mice compared to WT-mice was tested. The outcome of this analysis is given in Figure 29. In 4 out of 5 cases there is an obvious correlation between protein and mRNA expression, although changes in transcript levels do not reach statistical significance. In addition the expression of 3 target genes with reduced protein levels in KO-mice relative to their WT mates was tested. Here, only one of the 2 transcript levels resembled those seen in the protein expression analysis.

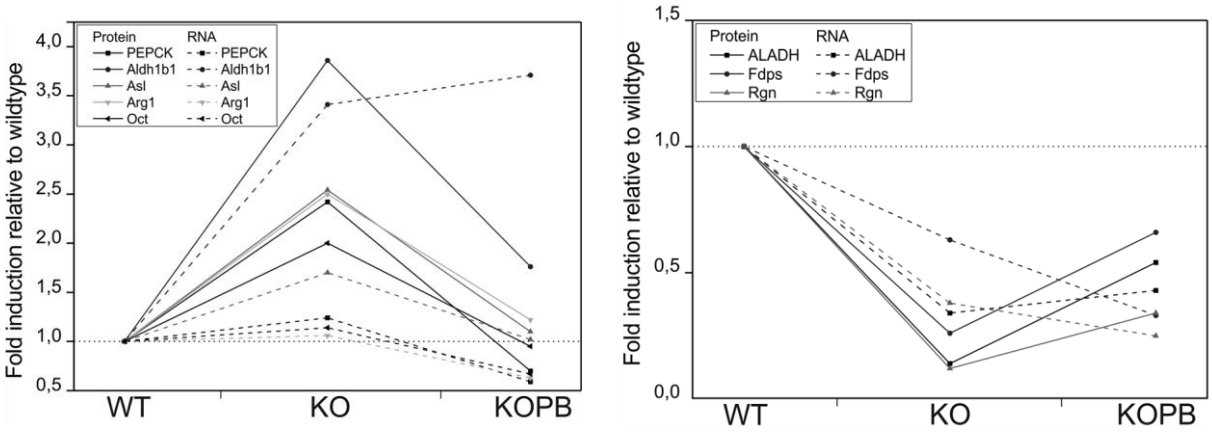

Figure 29: Expression of mRNAs in livers from wild-type and *Ctnnb1* knockout mice, either treated with PB or control diet as determined by real-time RT-PCR. Expression of target genes up-regulated (A) or down-regulated (B) in livers of knockout animals as compared to wildtype controls and the resulting effect upon the expression level measured in tissue of knockout animals treated with PB. Abbreviations: Delta-aminolevulinic acid dehydratase (Alad), Aldehyde dehydrogenase 1b1 (Aldh1b1), Arginase 1 (Arg1), Argininosuccinate lyase (Asl), Farnesyl pyrophosphate synthetase (Fdps), Glyceraldehyde-3-phosphate dehydrogenase (Gapdh), Ornithine carbamoyltransferase (Oct), Phosphoenolpyruvate carboxykinase (Pck1), Regucalcin (Rgn). Taken from (Rignall *et al*., in preparation)

4D. Tumor promotion effects of PB-like and non-PB-like tumor promoters after combined application in mice after DEN initiation.

Polyhalogenated dibenzo-p-dioxins and –furans as well as polyhalogenated biphenyles (PCB) are carcinogenic when applied at high doses in animal experiments. The mode of action is most likely a tumor promoting effect which is based on positive selection of initiated cells. The tumor promoting activity is mediated by cellular receptors. For dioxins, furans and dioxin-like PCBs the mode of action is activation of the aryl hydrocarbon receptor (AhR). Non-dioxin-like PCBs (PB-like), act mainly by signal transduction via the CAR or pregnane-X-receptor (PXR). PCBs occur in the environment as complex mixtures, often in combination with dioxins and furans. It is still unclear which risk is imposed on humans by uptake of foreign compound mixtures and concepts for risk assessment are still a matter of debate.

The objective of this project was to study the combined effect of a compound mixture that consisted of PCB 126 (dioxin-like) and PCB 153 (non-dioxin-like) on tumor promotion in mice initiated with a single intraperitoneal dose of DEN. The PCB congeners act via two distinctive cellular receptors, the AhR (PCB 126) and CAR (PCB 153). Recent studies have shown no decisive result concerning the tumor promoting effect of combined PCB 126 and PCB 153 application. In one study the carcinogenic effect was antagonistic (Dean *et al*., 2002). In another study there was no statistical significant increase in tumor promotion activity when treating animals with a compound mixture containing PCB 153 compared to animals treated with the same mixture but without PCB 153 (van der Plas *et al*., 1999). However in another study synergistic effects of tumor promotion using PCB 153 and PCB 126 were observed (Bager *et al*., 1995).

PCB 153 and PCB 126 induce the activation of separate nuclear receptors with different potencies. One aim of the experiment was to apply equipotent doses in order to compare resulting effects without the need of potency extrapolation. Therefore, two preliminary experiments had to be conducted before the main experiment. The first experiment was carried out to determine equipotent doses of PCB 153 and PCB 126. A second experiment was conducted to identify the half-life of the two PCB congeners in liver of mice in order to determine an initial PCB dose as well as weekly sustaining doses to maintain a constant PCB level during the

duration of the main experiment. Recent studies have shown that PCB potency is well correlated to cytochrome P450 induction in the liver. Therefore specific induction of cytochrome P450 isoforms 1a1 and 2b10 were used as endpoints for PCB 126 and PCB 153 activity, respectively. The result of the first experiment, depicted in Figure 30, shows that PCB 126 is the far more potent CYP inducer with a lowest CYP induction dose of 40µg/kg b.w. as compared to PCB 153 which induces comparable effects at 50mg/kg b.w.. From this figure it is also clear that both congeners induce specifically only one of the two cytochrome P450 isoforms without cross-activation.

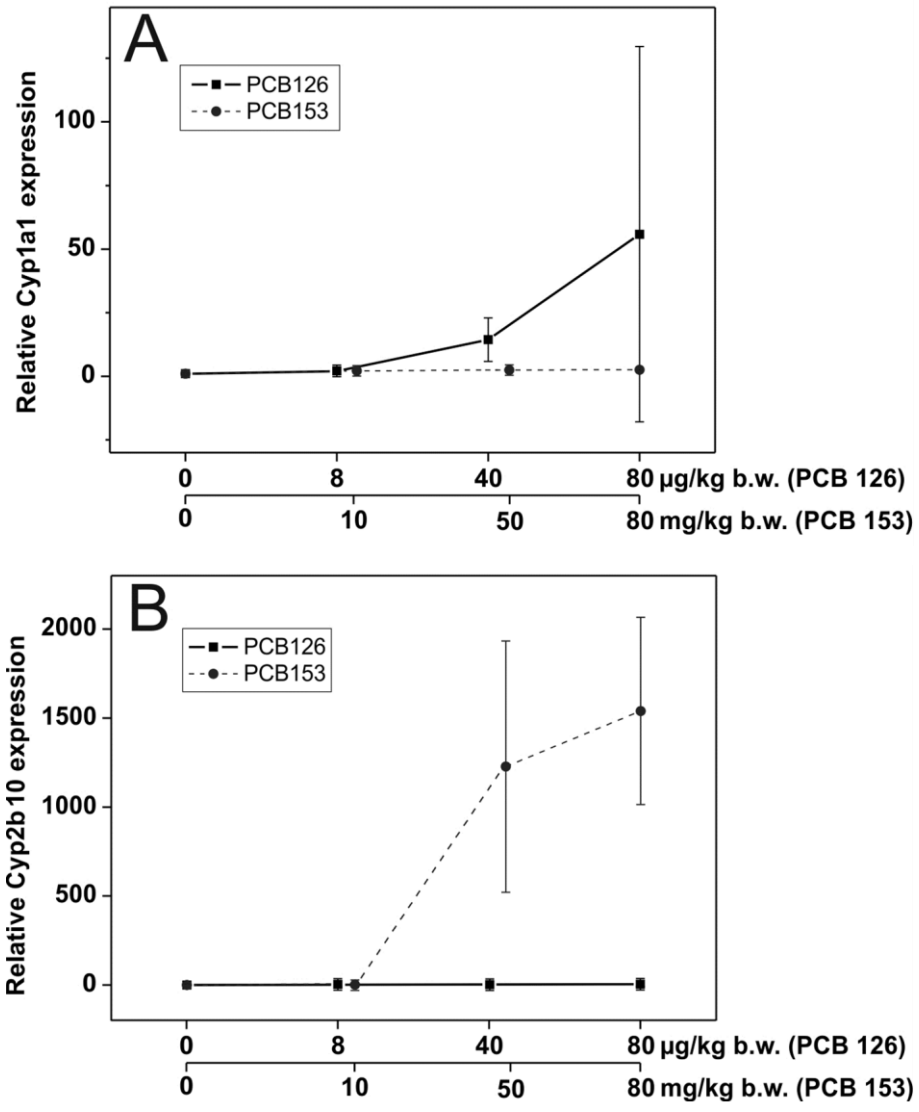

Figure 30: Dose-response relationship between PCB application, relative Cyp1a1 mRNA expression (A) and relative Cyp2b10 mRNA expression (B). PCB 126 specifically induces the expression of Cyp1a1 mRNA but not Cyp2b10 mRNA when compared to control animals receiving oil only. Contrarily PCB 153 induces Cyp2b10 mRNA expression only but no Cyp1a1 mRNA induction. Abbreviation: b.w. body weight. Group sizes: n=3 for controls, n=2 per dose.

In the second experiment, animals were either given PCB 153, PCB 126 or corn oil only as control in 5 concentrations ranging from 0; 10; 50; 100; 200µg/kg b.w. (PCB 153) or 0; 25; 50; 75; 100mg/kg b.w. (PCB 126) in volumes of 200µl at day 0. Two animals each were killed at 4, 21 and 42 days after treatment. The PCB concentration in liver and adipose tissue for each point in time was determined as was the induction of cytochrome P450 enzymes. Figure 31 exemplarily illustrates the outcome for 100µg/kg b.w. PCB 126 and 75mg/kg b.w. PCB 153 PCB application.

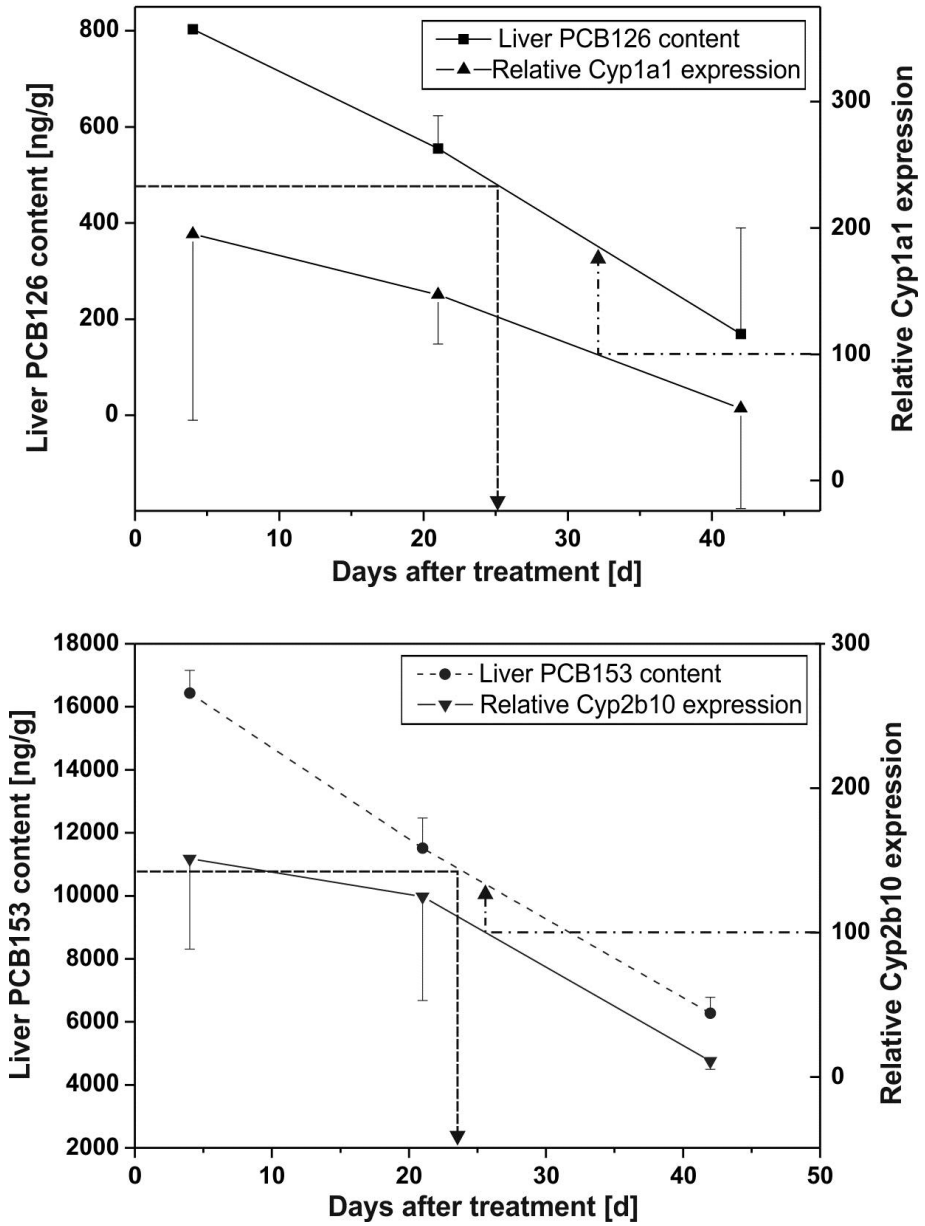

Figure 31: Relationship between CYP induction and liver PCB content (–·–) as well as liver PCB half-life estimation (––). Relative Cyp1a1 (PCB 126) and Cyp2b10 (PCB 153) induction of 100 were extrapolated to liver PCB content for equipotent PCB-dose computation in the main experiment. PCB half-life was estimated from liver PCB decay after one time PCB application (see text for details). Group size: n=2. Bars indicate standard deviation.

It is clearly visible that induction of cytochrome P450 enzymes was strongly associated with the amount of accumulated PCB in the liver. In addition, the half-life of liver PCB and the concomitant induction of the respective cytochrome P450 isoenzymes were for both PCB congeners about 25 days.

Main experiment: Equipotent doses of PCB 153 and PCB 126 were applied in the main experiment in order to generate comparable effects in the liver of mice. As outlined earlier, cytochrome P450 induction is a good measure for PCB activity. On the basis of dose response relationships between PCB application and CYP induction measured in the preliminary experiments and as outlined in figure 32, a relative Cyp1a1- (PCB 126) or Cyp2b10 induction (PCB 153) of 100 was set as equipotent which lies well within the respective dose response curves.

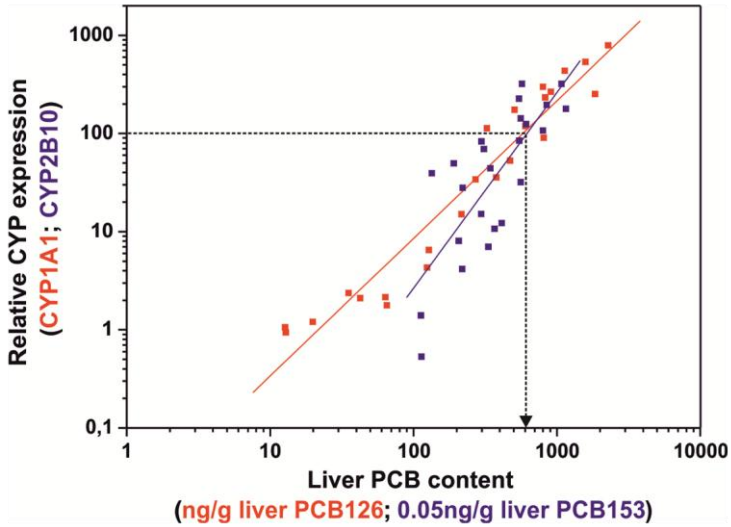

Figure 32: summarizes the relative Cyp1a1/2b10 mRNA expression levels determined in the preliminary experiment and associated liver PCB 126 and PCB 153 contents on a logarithmic scale. Indicated by the arrow is the relative CYP expression level set to ~100 and corresponding equipotent liver PCB 126, PCB 153 contents to be reached in the main experiment.

CYP induction factor of 100 was converted back to dosages by simple dose response extrapolation. Therefore, mice were either treated with 124µg/kg b.w. PCB 126 (relating to ~600ng/g liver PCB 126 content) or 135mg/kg b.w. PCB 153 (relating to ~12µg/g liver PCB 153 content) or corn oil only as control. Mice were then given weekly sustaining doses of 19µg/kg b.w. (PCB 126) or 21mg/kg b.w. (PCB 153) to maintain constant PCB levels. In addition, treatment groups with mice receiving only half the PCB doses were established (low dose groups) in order to examine possible synergistic effects at low dose levels that could be missed if the applied high dose PCB application would exceed a maximum response level. A second advantage would be that additive effects in the combined PCB 126/153 treatment group should be directly comparable to high dose treatment groups if the combined effects are additive in a linear fashion.

Tumor initiation-promotion study. The carcinogenicity study was conducted using DEN as initiator and the PCBs as tumor promoters. After 20 weeks, PCB or oil treatment was ended for all animals and about half the mice were killed one week later at a first point of time to study early tumor promotional effects. The remaining animals were killed 9 weeks later to unveil possible reverse effects of tumor promotion. To examine PCB activity, cytochrome P450 induction was measured in livers of animals killed at the first point in time. The results, summarized in Figure 33, showed that i) Cyp2b10 induction had taken place, not quite reaching the intended 100 fold induction margin in the PCB 153 high dose treatment group (H) and that the expression levels of Cyp1a1 exceeded the intended margin by ~6 fold in the high dose treatment group as compared to induction levels reached in the preliminary experiments at the same dosages (~600 fold induction in the PCB 126 high dose treatment group as compared to ~100 fold induction in the preliminary experiment) ii) CYP expression in low dose groups was less than half of that in high dose groups and iii) in the combined PCB 126/153 application group CYP induction was significantly higher than the respective expression in the low dose groups. To discriminate between a general gene expression increase or a specific Cyp1a1/2b10 inducing effect by the PCB mixture in livers of mice, mRNA expression levels of AhR and CAR as well as Cyp2e1 (a Ah-R induced target gene), GSTm3 (a PB induced target gene), and Ugt1a6 (a dioxin induced target gene) were analyzed (results are given in Figure 33).

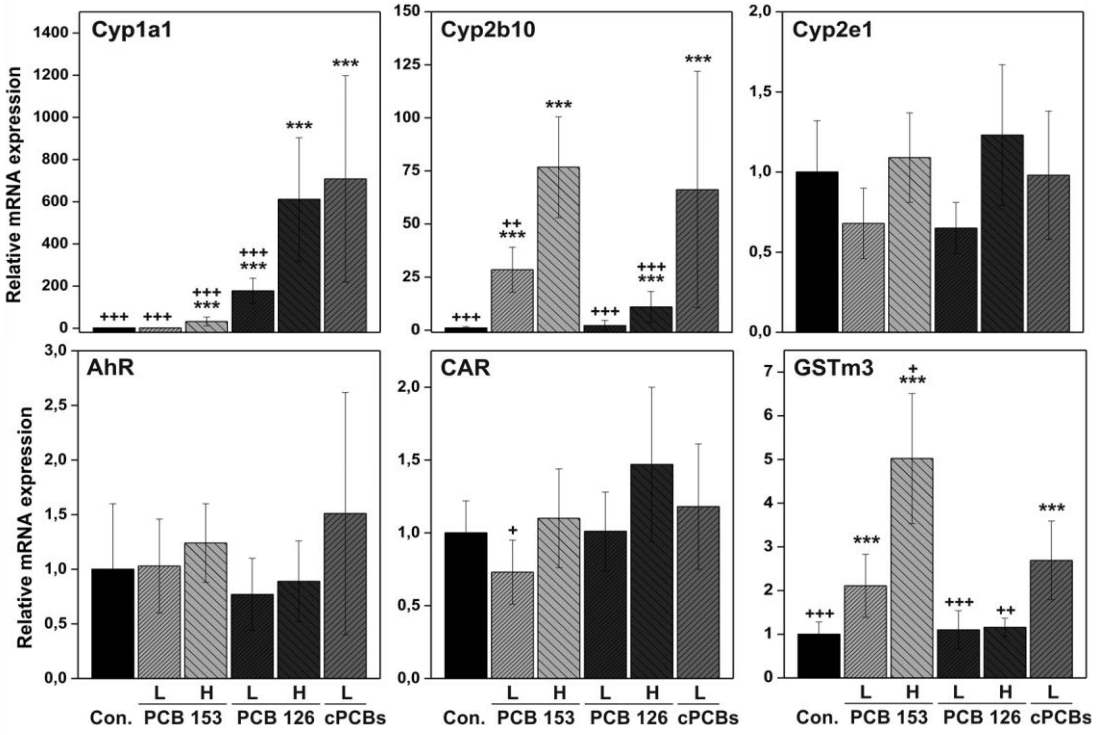

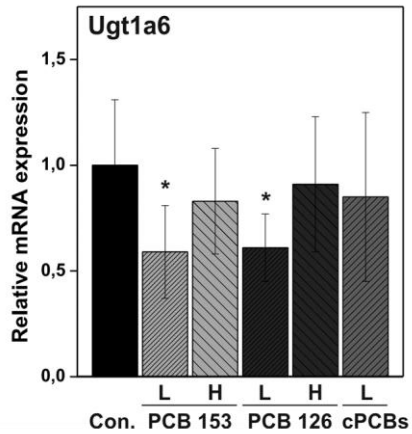

Figure 33: LC RT-PCR gene expression analysis of PCB 126 and PCB 153 target genes 25 weeks after DEN treatment. Results are presented as relative expression ratios of treatment groups against oil treated control animals. Statistically significant differences between oil control animals versus treatment groups are indicated by asterisks (* p≤0.05; *** p≤0.0001) and between combined PCB 126/153 treatment group versus the other groups by + (+ p≤0.05; ++ p≤0.001; +++ p≤0.0001). Treatment group sizes: n=16 (Oil control; PCB 153 L); n=11 (PCB 153 H); n=18 (PCB 126 L; PCB 153/126 L/L); n=12 (PCB 126 H). Abbreviations: Conc., control group; L, low dose; H, high dose; cPCBs, combined PCB 126/153 treatment group.

In summary, none of the measured mRNA expression levels showed the characteristic pattern of Cyp1a1 and 2b10 expression, pointing towards a specific, PCB 126/153 mixture dependent effect on Cyp1a1 and Cyp2b10 induction.

In addition western-blot analysis was performed with antibodies directed against Cyp1a1 as well as Cyp2b10 (Figure 34).

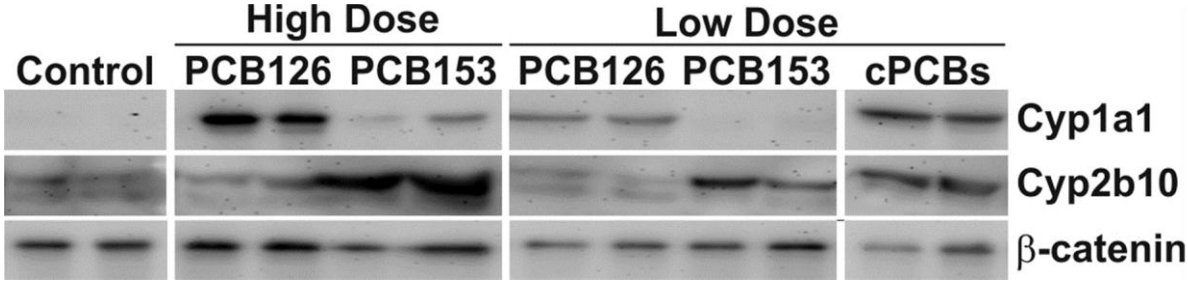

Figure 34: Western-blot analysis from PCB-treated non tumor tissue isolated 25 weeks after DEN treatment using antibodies directed against Cyp1a1, Cyp2b10 and the housekeeping protein β-catenin. Sample number: n=2 per treatment group.

Results of the western-blot analysis convincingly confirm the induced expression of Cyp1a1 by PCB126 and, to a lesser extent PCB153 (high dose) as well as Cyp2b10 by PCB153 and the increased induction of these CYP isoforms in the combined PCB126/153 treatment group.

Finally, enzymatic assays using fluorescent substrates specific for either Cyp1a1 (EROD) or Cyp2b10 (PROD) activity showed a significant increase of catalytic turnover (Table 8).

Table 8: Cytochrome P450 Enzyme activities in the livers of control- and PCB-treated mice

Treatment group	[a]EROD activity [pmol resorufin/min/mg protein]	[a]PROD activity [pmol resorufin/min/mg protein]
DEN/Oil	0.31 ± 0.07	0.09 ± 0.02
PCB 126 H	[b]11.11 ± 5.04	0.21 ± 0.06
PCB 153 H	1.59 ± 0.25	[b]0.75 ± 0.18
PCB 126 L	[c]5.33 ± 1.37	0.16 ± 0.02
PCB 153 L	0.45 ± 0.25	[b]0.50 ± 0.09
cPCBs	[d]8.05 ± 2.00	[b]0.47 ± 0.16

EROD/PROD activity of the respective treatment groups are given as mean ±SD.
[a]Kruskal-Wallis test is significant with p<0.001
[b]significantly different from oil control group (p<0.0001); Dunn´s multiple comparison test
[c] significantly different from oil control group (p<0.05); Dunn´s multiple comparison test
[d] significantly different from oil control group (p<0.001); Dunn´s multiple comparison test

Tumor multiplicity (mean number of tumors per animal) from animals killed 25 weeks after carcinogen treatment was close to zero for all treatment groups. There were only 3 tumors larger than 2mm in diameter, one in group 2 (DEN/oil treatment), the other in DEN/ PCB 153 low dose group 7 and the last in DEN/ PCB 126/153 mixture group 9. Tumor multiplicity differed in animals killed 30 weeks after carcinogen treatment, as summarized in Figure 35.

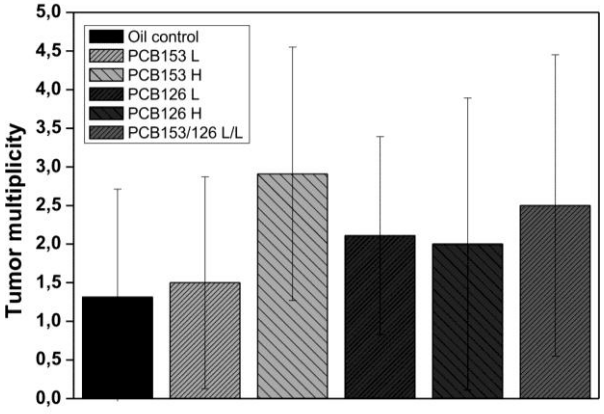

Figure 35: Tumor multiplicity 34 weeks after DEN treatment. PCB treatment does not lead to statistically significant differences in tumor number relative to control animals treated with oil only. Treatment group sizes: n=16 (Oil control; PCB 153 L); n=11 (PCB 153 H); n=18 (PCB 126 L; PCB 153/126 L/L); n=12 (PCB 126 H). Abbreviations: L, low dose; H, high dose.

The results demonstrated that i) high dose PCB 153 application led to a non-statistically significant increase in the mean tumor number per animal ii) high dose PCB 126 did not cause an increase in the occurrence of tumors as compared to low dose PCB 126 treatment and iii) PCB 126/153 mixture application led to a tumor

multiplicity between that seen in high dose treatment groups PCB 126 and PCB 153. However there was no statistically significant difference in the number of tumors between the treatment groups when using non-parametrical Kruskal-Wallis test followed by Dunn´s multiple comparison test. Tumor size distribution of tumors is given in figure 36.

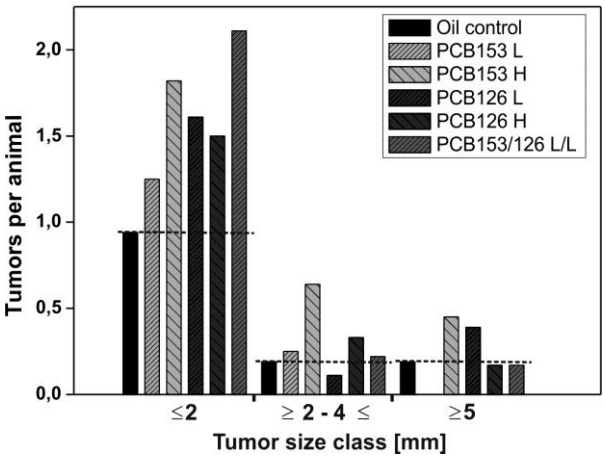

Figure 36 Tumor size distribution 34 weeks after DEN treatment. Tumor size of the oil control group is indicated by a dotted line (---).Treatment group sizes: n=16 (Oil control; PCB 153 L); n=11 (PCB 153 H); n=18 (PCB 126 L; PCB 153/126 L/L); n=12 (PCB 126 H). Abbreviations: L, low dose; H, high dose.

Morphometric analysis. Two-dimensional sizes of intersections of tumors identified by alterations in G6Pase-activity were determined thus allowing the quantification of the percentage of tumor tissue in animals. The volume fraction (summarized in table 9 and figure 37) as well as number of lesions per cm^2 and cm^3 (displayed in Table 9) show statistically significant differences when applying non-parametric Kruskal-Wallis test. Interestingly, only the combined PCB126/153 treatment group showed statistically significant differences to oil treated control animals when applying Dunn´s multiple group comparison test.

Table 9: Volume fraction of enzyme-altered lesions

	25 weeks after DEN				
Treatment group	[a]Volume fraction (%)	[a]Volume fraction GS - (%)	Volume fraction GS + (%)	[a]Average number of lesions per cm^2	[a]Average number of lesions per cm^3
DEN/Oil	0.04 (± 0.08)	0.04 (± 0.08)	0.00 (± 0.00)	0.73 (± 1.07)	28.04 (± 49.85)
PCB 153 L	0.43 (± 1.07)	0.42 (± 1.07)	0.01 (± 0.02)	1.87 (± 1.58)	55.15 (± 58.39)
PCB 153 H	0.28 (± 0.52)	0.27 (± 0.50)	0.01 (± 0.03)	1.95 (± 2.33)	53.48 (± 64.66)
PCB 126 L	0.10 (± 0.13)	0.10 (± 0.13)	0.00 (± 0.00)	2.29 (± 2.15)	90.27 (± 83.68)
PCB 126 H	0.11 (± 0.11)	0.11 (± 0.11)	0.00 (± 0.00)	2.15 (± 1.97)	76.91 (± 73.58)
PCB 126/153 L/L	[b]0.69 (± 1.26)	[b]0.68 (± 1.26)	0.01 (± 0.02)	[c]3.82 (± 1.90)	[d]140.78 (± 77.20)

Table 9: (continued)

	34 weeks after DEN				
Treatment group	Volume fraction (%)	Volume fraction GS - (%)	Volume fraction GS + (%)	Average number of lesions per cm^2	[a]Average number of lesions per cm^3
DEN/Oil	6.31 (± 10.94)	5.89 (± 11.05)	0.43 (± 1.70)	3.16 (± 2.61)	59.75 (± 65.00)
PCB 153 L	4.21 (± 5.72)	4.16 (± 5.70)	0.04 (± 0.11)	3.91 (± 1.91)	98.53 (± 69.94)
PCB 153 H	4.44 (± 3.80)	4.30 (± 3.94)	0.14 (± 0.26)	4.83 (± 2.16)	89.43 (± 53.59)
PCB 126 L	10.47 (± 14.75)	10.18 (± 14.22)	0.29 (± 1.15)	4.99 (± 3.26)	124.12 (± 115.06)
PCB 126 H	4.64 (± 5.08)	4.64 (± 5.08)	0.00 (± 0.00)	4.19 (± 1.82)	82.70 (± 40.15)
PCB 126/153 L/L	3.84 (± 4.35)	3.80 (± 4.36)	0.04 (± 0.11)	[b]6.06 (± 2.91)	[b]145.55 (± 98.24)

Volume fractions (Total, GS negative (-), GS positive (+)) as well as average number of G6Pase changed lesions per cm^2 and cm^3 of the respective phenotypes are given as mean ±SD.
[a]Kruskal-Wallis test is significant with $p<0.05$
[b]significantly different from oil treated control group ($p<0.05$); Dunn´s multiple comparison test
[c] significantly different from oil treated control group ($p<0.001$); Dunn´s multiple comparison test
[d] significantly different from oil treated control group ($p<0.01$); Dunn´s multiple comparison test

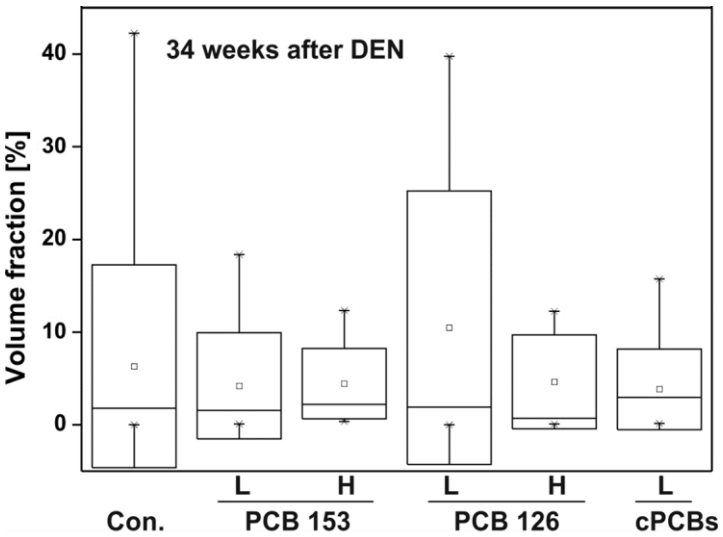

Figure 37: Lesion volume fractions of G6Pase altered lesions of animals 34 weeks after DEN treatment. The high standard deviation in control and PCB 126 low dose treated animals is due to one extremely large tumor within a single animal in each of the two groups. Abbreviations: L, low dose; H, high dose.

In addition, cell proliferation of corn oil- and PCB-treated animals either treated with DEN or NaCl as control was assessed using an antibody directed against bromo-desoxyuridine which was given to all mice in drinking water 3 days prior to organ isolation at 34 weeks after DEN initiation. The outcome of the analysis, displayed in figure 38, showed a statistically significant difference for group comparison using Kruskal-Wallis test (p≤0.001) but no significantly different BrdU-labeling indices when comparing individual treatment groups against each other using Dunn´s multiple comparison test.

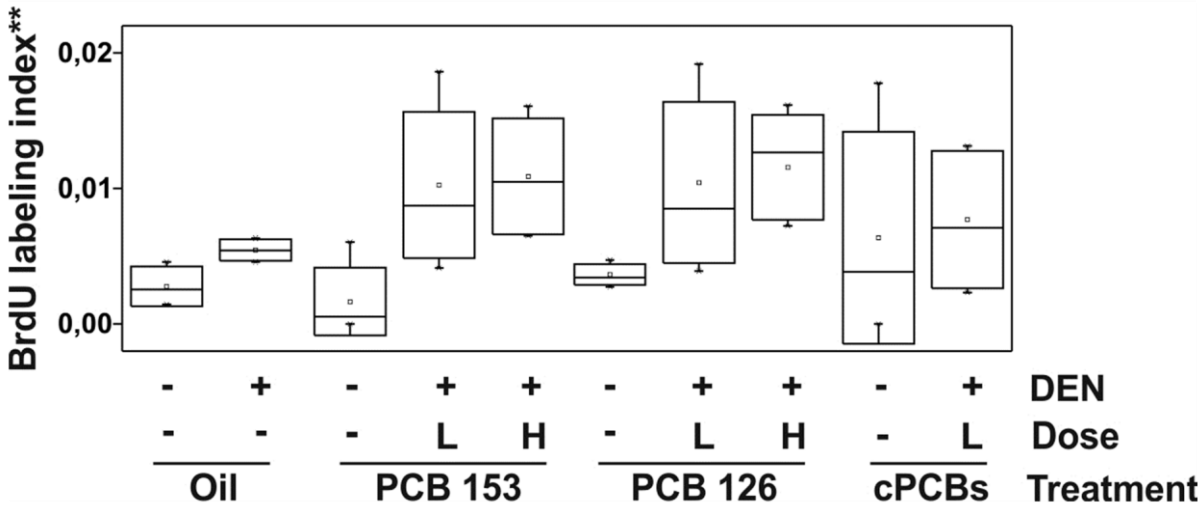

Figure 38: BrdU labeling index given as fraction of BrdU-positive labeled nuclei divided by the total nuclei number. Statistical analysis was significantly positive for non-parametric Kurskal-Wallis test (indicated by asterisks), however, there were no statically significant differences when comparing individual treatment groups, using Dunn´s multiple comparison test, against each other. Analyzed animals = 5 per treatment group. Analyzed liver slices = 5 per animal. Abbreviations: L, low dose; H, high dose.

Proteome analysis. 2D-PAGE gels of oil- and PCB-treated non-tumor tissue were fluorescently stained and subsequently statistically analyzed. On average, 2782 protein spots per run were detected in the tissue samples. When applying threshold levels of p≤0.05 and |log2 ratio| ≥0.6, a total of 68 protein spots were found to be significantly altered in intensity in mice treated with DEN and corn oil only as compared to mice treated with either PCB in high or low dose or in a combination of both PCBs. All significantly altered spots were isolated and subsequently identified using MALDI-TOF-TOF analysis. To verify correct spot picking and subsequent identification, a second set of identical protein spots from different gels were picked. Proteins that did not match between the first and second analysis were excluded from the evaluation. In summary 51 spots were unambiguously identified as a single

significantly altered protein. Another 8 spots represented two or more isoforms of the same protein. (For a complete list of proteins affected by the treatment regimens in hepatocytes see Rignall *et al*., manuscript in preparation). About half the proteins were de-regulated only once in the study (27 proteins), whereas the others (32 proteins) were de-regulated in more than one comparison of treatment groups.

Low dose treatment of mice with either PCB 126 or PCB 153 led to a significant alteration of 8 and 6 proteins, counting protein isoforms which could not be differentiated by the analysis as a single protein, respectively. The number for analysis between high dose gavage and control were 12 (PCB 126) and 15 (PCB 153). When comparing low- to high dose treatment within the same PCB treatment groups, PCB 126 high dose affected only 1 additional protein in comparison to low dose PCB 126 treatment. The numbers for PCB 153 treatment were about the same. Here dose increase led to the de-regulation of an additional 3 proteins. A total of 22 proteins were de-regulated in comparison between combined PCB 126/153 application group and controls, of which the majority (19) were up-regulated.

Among the proteins significantly de-regulated in the study was α-1-antitrypsin. Whereas one protein spot was down-regulated on 2D-SDS polyacrylamide gels in animals either treated with PCB 126 in high dose or the combined PCB 126/153 application group compared to controls a second protein spot, possibly representing a differently post-translational modified version of the same protein, was up-regulated in PCB 153 high dose treated animals and in the combined PCB 126/153 treatment group. Other proteins de-regulated in more than one treatment group when compared to oil treated controls included pyruvate kinase isozyme R/L (P53657; down-regulated in every PCB 153 and PCB 126 treatment group, irrespective of dose), UDP-glucose 6-dehydrogenase (O70475, up-regulated in PCB 153 high dose and PCB 126 high dose treatment groups, and strongest in the combined PCB 126/153 treatment group), GSTA2/A3 (P30115/P10648, down-regulated in PCB 126 high dose treatment group as well as PCB 153 high dose treatment group), GSTm1/3 (P10649/P19639, up-regulated in PCB 153 high dose- and combined PCB 126/153 treatment groups). A protein family exclusively up-regulated in the combined PCB 126/153 treatment group but not in high dose PCB 153 or high dose PCB 126 as compared to controls were the 14-3-3 protein isoforms sigma (O70456, relative expression of 1,54), beta/alpha (Q9CQV8, 1,72) and zeta/delta (P63102, 1,82). However there was no difference in gene expression of 14-3-3 protein isoforms

beta/alpha and zeta/delta between oil treated controls and combined PCB 126/153 treatment group (Figure 39).

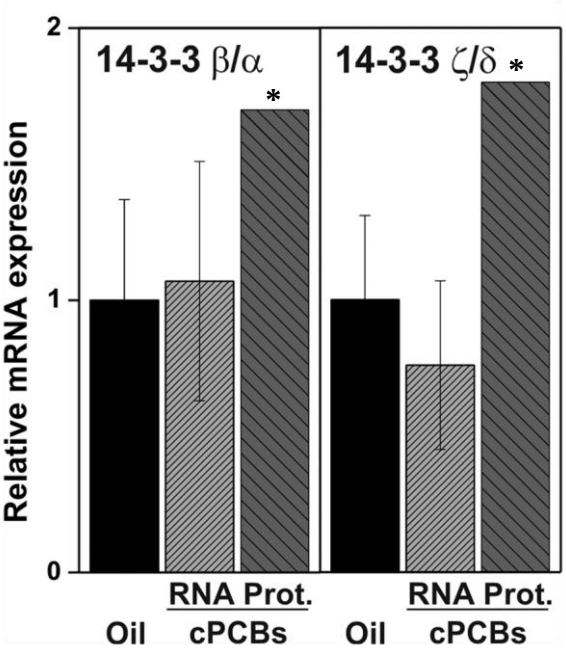

Figure 39: LC RT-PCR gene expression and protein expression analysis of 14-3-3 isoforms β/α and ζ/δ 25 weeks after DEN treatment. Expression values are given as relative expression to oil treated control animals. Protein expression levels are given as median expression values and are taken from the proteome analysis. Significant differences are indicated by an asterisk (p≤0.05). Abbreviations: Oil, oil treated control group; RNA, mRNA expression; Prot., protein expression; cPCBs, combined PCB 126/153 treatment group. Treatment group sizes: n=16 (Oil control); n=18 (mRNA); n= 4 (protein).

4E. Quantitative analysis of growth kinetics of chemically-induced mouse liver tumors by non-invasive magnetic resonance imaging

At the laboratory of Prof. Bernd Pichler and Andreas Schmid, chemically-induced liver tumors of mice, generated by single injection of the liver carcinogen DEN either in 2 weeks old (experiment 1) or 6 weeks old (experiment 2) male C3H mice at the laboratory of Prof. Michael Schwarz by me, followed by chronic treatment with PB in experiment 2 according to an initiation/promotion protocol, mice were routinely scanned by magnetic resonance imaging (MRI) in intervals between 2-3 weeks by Andreas Schmid. Liver tumors became detectable in both experiments 1 and 2 when they exceeded a diameter of ~1mm. Exponential increases in total tumor volume per liver was observed in both experiments but the onset of tumor development was much earlier in experiment 1 (Figure 40). While mice in experiment 1 had developed a mean total tumor volume of ~400 mm^3 at an age of ~27 weeks, it took ~5 weeks longer to reach this tumor mass in experiment 2 (when relating to the time of DEN treatment).

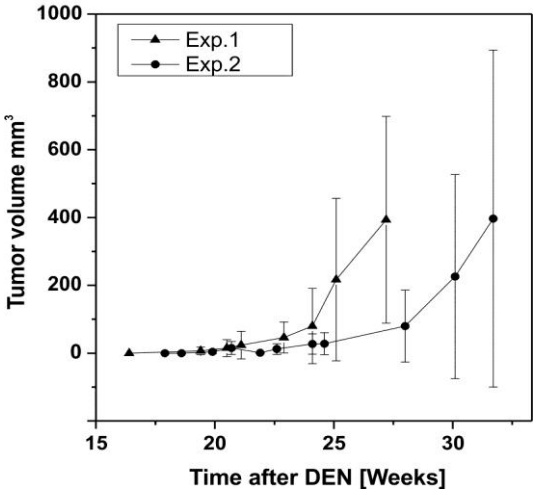

Figure 40: Mean tumor volume increase after DEN application in mice treated with DEN at the age of 2 weeks (Exp.1) or 6 weeks and subsequent chronic PB treatment until the end of the experiment (Exp.2). Tumors were visible at ~17 weeks after DEN treatment. Average maximal tumor size was ~400mm³ in both studies but with a delay of 5 weeks in study 2 to reach maximum size. Taken from (Schmid *et al.*, in preparation).

Determination of time-dependent growth of individual tumors demonstrated strong tumor heterogeneity (Figure 41).

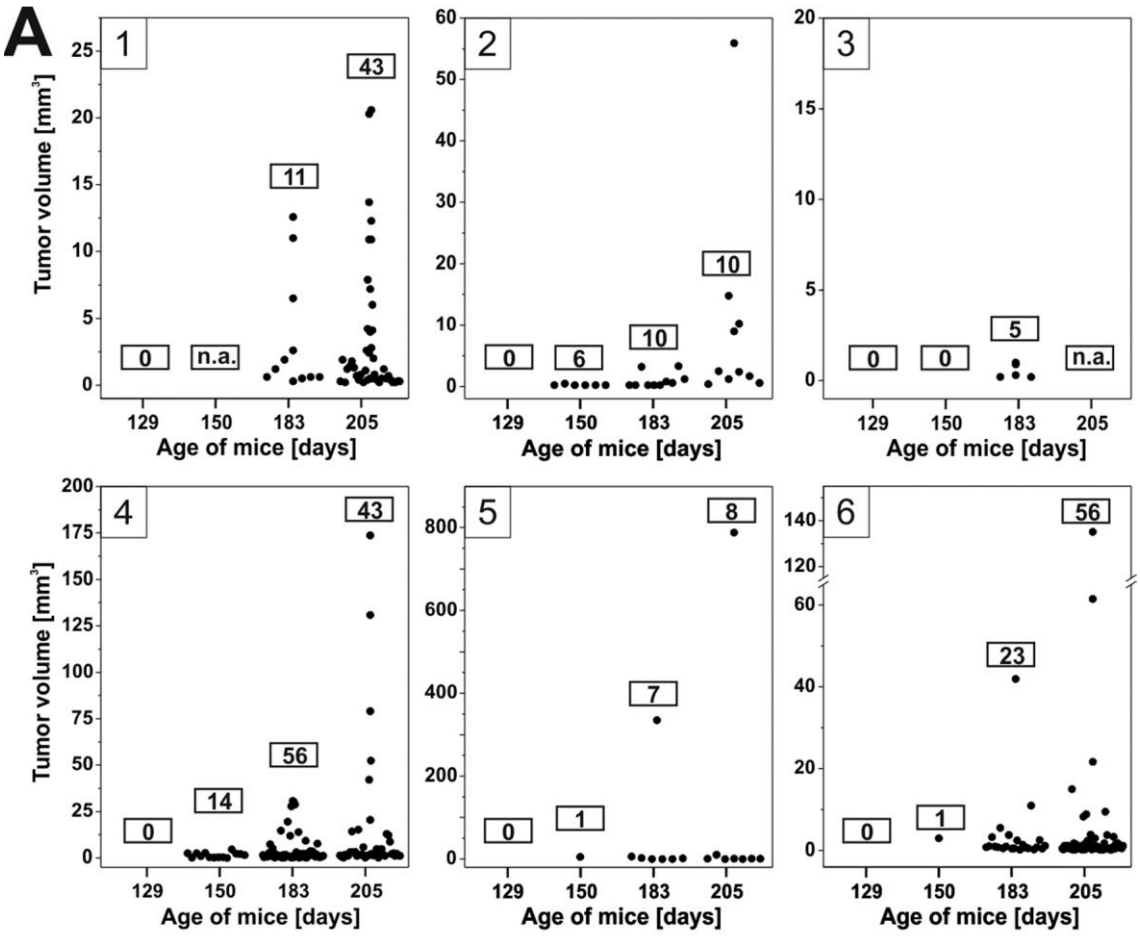

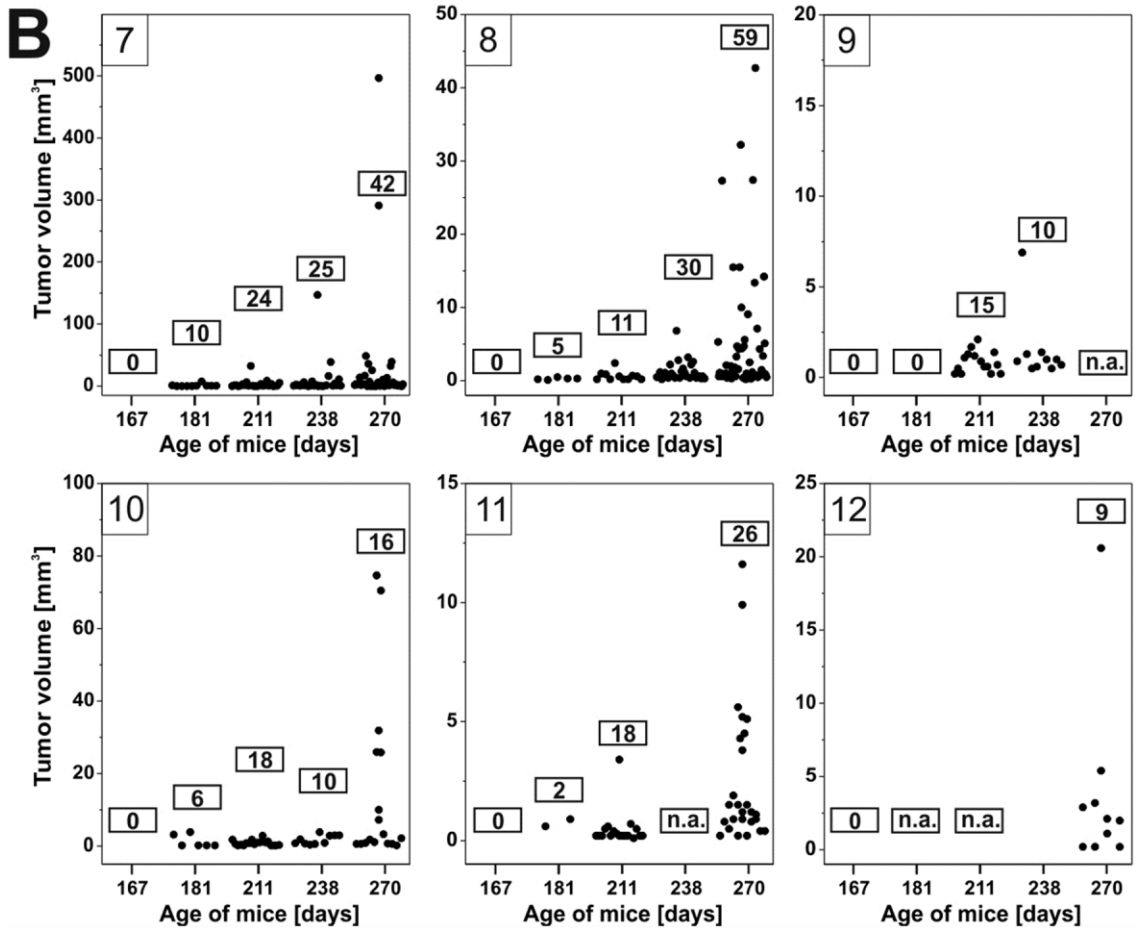

Figure 41: Tumor size distribution based on measurements from individual animals. A) Displays the outcome for experimental group 1 (animals 1-6) and B) the outcome for experimental group 2 (animals 7-12). Boxed numbers indicate the number of tumors recorded for the individual animal at the time of MRI. Abbreviation: n.a. no data available. Taken from (Schmid *et al.*, in preparation).

Phenotypes of tumors differed strongly between the two experiments but results showed that tumors were reliably detected independent of their phenotype when they exceeded a certain size and that growth behavior of individual tumors could be monitored over time.

5. Discussion

The present dissertation comprised work on 4 different projects. Project A addressed the comparison of two different types of mouse liver tumors, one mutated in the proto-oncogene encoding *Ha-ras* and the other in *B-raf*, on a proteome wide scale. In addition, the outcome was compared to data from a genome expression analysis of the same tumor types. The second project (B) was intended to analyze the importance of β-catenin, a proto-oncogene and part of Wnt-signaling pathway, in PB-dependent tumor promotion. Two different mouse strains were available for investigation, one expressing a constitutively active form of β-catenin in the liver, the other homozygously lacking in liver a functional form of *Ctnnb1*, the gene encoding β-catenin. Whereas the strain expressing activated β-catenin was chronically treated with PB only, the other was submitted to an initiation-promotion protocol using DEN as initiating agent and PB as tumor promoter. Subsequently, tumor promotion was assessed by analyzing tumor burden and genetic analysis of isolated tumor tissue. In addition a proteome analysis of mouse liver tissue from WT and KO-mice either receiving a PB containing diet or control diet was conducted. The most laborious project (C) dealt with the effect of a PCB mixture, containing two differently acting tumor promoting substances (PCB 126 and PCB 153), on tumor development in mouse liver. The outcome of this experiment was ought to elucidate the unresolved question whether mixtures of tumor promoting substances affecting the same organ (liver) but by differently acting signal transduction pathways may act in an antagonistic, additive or even synergistic mode of action with respect to tumor development. Major objectives were to define equipotent doses of the PCBs in order to achieve comparable effects in PCB-treated mice as well as to determine the half-life of both compounds, enabling the application of constant PCB levels during the entire period of the main experiment. The outcome was assessed by tumor burden, gene expression-, proteome-, Western-blot-, immunohistochemistry and cell proliferation analysis. The last project (D), in great parts carried out in cooperation with the laboratory of Prof. Bernd Pichler, assessed the possibility of life imaging mouse liver tumors utilizing MRI technology. To generate tumors, animals were treated with DEN as initiator only at the age of two weeks or with DEN at the age of six weeks followed by chronic PB treatment and were scanned for tumor development at the Laboratory for Preclinical Imaging and Imaging Technology of the

Werner Siemens-Foundation, Department of Radiology, University of Tübingen by Andreas Schmid.

Comparative Transcriptome and Proteome Analysis of *Ha-ras* and *B-raf* Mutated Mouse Liver Tumors

In this project, a proteome analysis was conducted using tissues from mouse liver tumors either carrying an activating point mutation in the proto-oncogenes encoding *Ha-ras* or *B-raf*. Development of these tumors types is initiated by a single intraperitoneal application of DEN in mice at the age of two weeks. At the end of the experiment, 70% of all tumors showed a point mutation in either of the two proto-oncogenes (Jaworski *et al*., 2005; Buchmann *et al*., 2008). Mutations in *ras* genes are in general non-overlapping with mutations in *B-raf*, neither in mouse liver tumors (Jaworski *et al*., 2005; Buchmann *et al*., 2008) nor in human cancers (Brose *et al*., 2002) suggesting that both types of oncogenes are equivalent in promoting tumor development. Ha-ras and B-raf are both part of MAP kinase signaling, Ha-ras operating as the molecular switch connecting receptor activation to cytosolic effector molecules and B-raf as MAP3 kinase, transducing activation from Ha-ras to kinases further down-stream of the signal transduction pathway (Krishna and Narang, 2008). In contrast to B-raf, which is believed to be involved in MAPK signaling only, Ha-ras potentially activates a broader set of signal transduction pathways (Malumbres and Barbacid, 2003). As a consequence, activation of Ha-ras would be expected to affect a larger set of transcriptional regulators which should result in significant differences in the mRNA and protein expression signatures of *Ha-ras* and *B-raf* mutated tumors. However, this potential is not reflected when comparing global gene expression between the proto-oncogenes (Jaworski *et al*., 2007). This finding was verified by the here conducted proteome analysis. In fact, there are no significant differences between protein expression of *Ha-ras* and *B-raf* mutated mouse liver tumors, when evaluating the proteome data with the respective cut-off values chosen for the analysis. Therefore *Ha-ras* and *B-raf* mutated tumors show the same characteristic changes in metabolic pathway activity. One of these changes affects cholesterol levels in hepatocytes. Whereas enzymes involved in biosynthesis of cholesterol are up-regulated (hydroxymethylglutaryl-CoA synthase 2; farnesyl pyrophosphate synthase) enzymes involved in the degradation of cholesterol are down-regulated (3-oxo-5-beta-steroid 4-dehydrogenase; 3-ketoacyl-CoA thiolase). In fact, an increase in

intracellular cholesterol levels within these tumor types has been demonstrated (Jaworski *et al*., 2007). In addition, proteome data was compared to the outcome of two recently conducted microarray analyses which used the same tumor material as in the proteome study (Jaworski *et al*., 2007; Stahl *et al*., 2005). The outcome shows that protein and mRNA expression appears well-correlated, both in *Ha-ras* and *B-raf* mutated tumors, with a few exceptions. The extent of protein expression changes was more pronounced than that of their mRNAs. Overall, the correlation between protein and mRNA expression was much better for proteins down-regulated in tumors than for those up-regulated in the tumors. In fact, 22/57 (39%) of significantly up-regulated proteins showed unaltered or even slightly decreased expression of their encoding mRNAs suggesting that the respective proteins are regulated at the post-transcriptional level affecting, for example, their stability and half-life. However, some technical aspects have to be considered as well. The applied 2D-SDS-PAGE technique shows some bias toward middle and highly abundant proteins with long half-lives (Futcher *et al*., 1999). Therefore, fairly long-lived enzymes of the intermediary metabolism may be identified reliably, whereas low-abundance proteins involved in cell signaling, DNA replication or regulation of the cell-cycle and gene transcription are missed, even though they may be de-regulated in the tumors. Apart from this, proteins that are too basic, acidic or hydrophobic are lost during the separation process (Greenbaum *et al*., 2003) and membrane associated proteins may be lost during the isolation procedure. For example, changes in microsomal cytochrome P450 enzymes were not detected in the study, even though it is well-known from studies based on methods other than 2D-SDS-PAGE that they are strongly down-regulated in *Ha-ras* mutated mouse liver tumors (e.g., Hailfinger *et al*., 2006; Braeuning *et al*., 2007).

B-raf, like its family member C-Raf, possesses serine-threonine kinase activity, leading to activation of MEK, a dual-specificity kinase, which activates the MAP kinase ERK (Hagemann and Rapp, 1999; Wellbrock *et al*., 2004). Phosphorylated ERK is able to shuttle from cytosol into the cell nucleus, ultimately stimulating transcription factors like Elk1, SRF, ATF2 and Jun (Treisman , 1996). Because *Ha-ras* and *B-raf* mutated mouse liver tumors showed an identical protein expression pattern, it seemed obvious that both tumor types would show the same activation of ERK. Surprisingly, this is not the case. Using an immunohistochemical approach, *Ha-ras* mutated mouse liver tumors showed positive staining for phospho-ERK (p-ERK)

whereas their B-raf mutated cousins were negative. This discrepancy was also detected using a reverse-phase protein microarray approach, utilizing the same tumor material as used in the proteome and microarray analyses, performed recently by Knorpp, *et al*. (dissertation Knorpp). This lack of p-ERK positive staining in *B-raf* mutated tumors is absolutely puzzling, precisely because p-ERK is, to our current knowledge, the ultimate transducer of MAP kinase activity. Although an experimental explanation cannot be cited, a theoretical approach is possible (summarized in Figure 42). MAP kinase activity is regulated by kinases (activating the protein) and phosphatases (inactivating the protein). A well-known transcriptional target of MAP kinase signaling is the dual-specificity phosphatase (Dusp)-6, creating a negative feedback loop by de-phosphorylation of p-ERK (Keyse 2008; Bluethgen *et al*., 2009). *Dusp6* was shown to be significantly overexpressed in both *Ha-ras* and *B-raf* mutated mouse liver tumors on the mRNA level, but without significant expression differences between the tumor types (Jaworski *et al*., 2007). However, Dusp6 contains catalytic essential cysteine residues that are vulnerable to reactive oxygen species (ROS)-dependent oxidation, rendering the enzyme inactive (Chan *et al*., 2008). Whereas both oncogenes induce transcription of NADPH-dependent oxidase 1 (Nox1), a ROS forming enzyme, by a GATA-6-dependent pathway (Adachi *et al*., 2008), only Ha-ras potentially activates the small G-protein Rac which is, together with β-pix, essential for Nox1 activity (Park *et al*., 2004). Hence, there could be a Ha-ras/Rac-dependent generation of ROS leading to inactivation of Dusp6. However, it remains puzzling why there is no difference in the protein expression pattern between the tumor types.

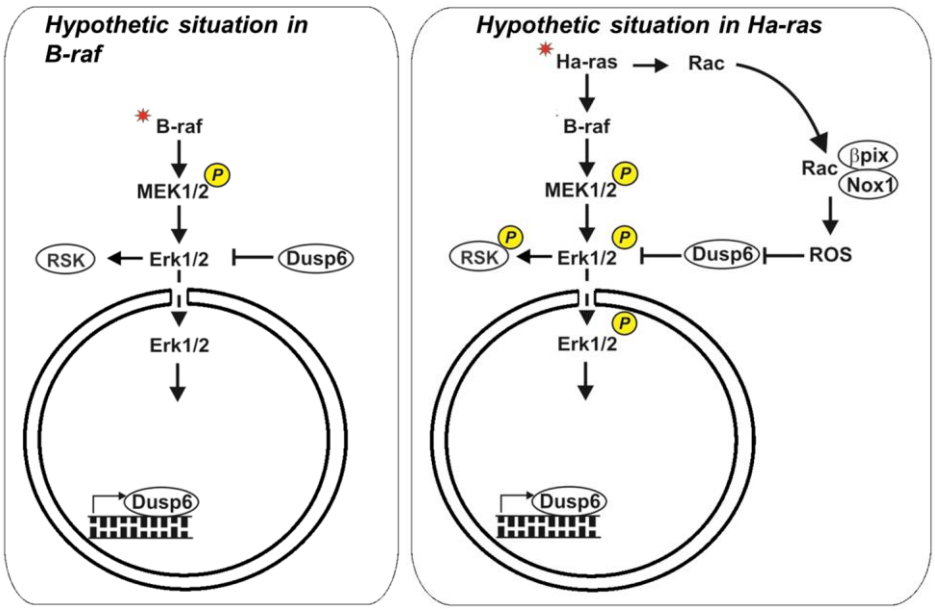

Figure 42: Theoretical situation in B-raf and Ha-ras mutated mouse liver tumors, possibly explaining the difference in p-ERK staining between the tumor types. A Ras/Rac-dependent generation of ROS may lead to Dusp6 inactivation, inhibiting de-phosphorylation of p-ERK. B-raf mutated mouse liver tumors may lack the generation of ROS, therefore expressing a functional form of Dusp-6.

The Importance of β-catenin in PB-Dependent Tumor Promotion

Recent studies have shown that initiation of mouse liver tumors with a single intraperitoneal injection of DEN causes the formation of mainly *Ha-ras* and *B-raf* mutated mouse liver tumors (Jaworski *et al*., 2005; Buchmann *et al*., 2008) whereas chronic treatment of DEN initiated mice with PB leads to the development of tumors mainly mutated in *Ctnnb1*, the gene encoding β-catenin (Aydinlik *et al*., 2001), that are associated with an over-expression of GS and a deficiency in G6Pase activity (Loeppen *et al*., 2002) when performing immunohistological staining. The positive selection for *Ctnnb1* mutated tumors by PB is dependent on the presence of CAR (Yamamoto *et al*., 2004) as well as connexin32 (Moennikes *et al*., 2000). It is still unknown whether β-catenin itself is essentially involved in this process, why and how PB stimulates the outgrowth of *Ctnnb1* mutated cells and what the consequences are for tumor cell metabolism. The latter has been analyzed earlier, performing a proteome wide analysis including GS-positively stained mouse liver tumors (Strathmann *et al*., 2007). To further analyze the importance of β-catenin in PB-dependent tumor promotion, a transgenic mouse line expressing a liver specific constitutively active form of β-catenin was exposed to chronic PB treatment. If β-catenin is an essential factor in this process, DEN initiation would be expected to be obsolete and developing tumors should express transgenic β-catenin. Before conducting the main experiment, livers of transgenic animals were analyzed for transgene expression, surprisingly showing that only a very small subpopulation of cells expressed GS and CYP2E1, marker proteins for active β-catenin signaling, scattered throughout the liver in “non-central vein hepatocytes”. Yet, this low incidence was assumed to benefit the tumor promotion study, because only those few transgene positive cells would be anticipated to proliferate under PB treatment, potentially limiting tumor burden to a smaller extent as would be expected of a broader transgene expression incidence in the liver. However, results of the tumor promotion experiment did not display the expected significant difference in tumor response, although PB treatment displayed a tendency towards the development of more and larger tumors in transgene expressing animals as compared to their WT counterparts. In addition, immunohistological stainings for GS-marker expression did not reveal the same increase in number of GS-positive liver lesions in transgene animals when comparing the outcome to a recently conducted study of DEN initiated and PB promoted mice (Loeppen *et al*., 2002). However, the overall number of 5 GS-

altered lesions in this study was too low to conduct a comprehensive and convincing analysis.

Generally, tumor development is believed to start from a single initiated precursor cell which clonally expands to form a pre-neoplastic lesion that, on its way to malignancy, adopts further mutational changes (e.g. Moolgavkar and Knudson, 1981). Based on the observations that β-catenin mutated liver lesions from DEN/PB treated animals are associated with a positive staining for GS as well as the fact these lesions are mainly homogenously stained for GS leads to the assumptions that i) β-catenin mutation is an early, most likely the initiating event in the generation of these lesions and that ii) the lesions constitute cells that are clonally derived from the initiated precursor cell. Hence, it would be expected that if β-catenin mutated cells are positively selected for by PB, transgenic animals would, under PB treatment, develop tumors of which, due to clonal origin, 80% would be transgene expressing, display elevated GS levels as well as express target genes of β-catenin pathway signaling. Therefore, isolated tumors ≥2mm in size from transgenic/PB treated animals were analyzed for transgene recombination as well as β-catenin target gene expression. In summary, only a minor fraction of tumors displayed transgene recombination on the DNA level. In fact, recombination frequency was ~3 times higher in non-tumor tissue as compared to tumor tissue (on average 6.1% versus 2.4%). An explanation therefore might be that some of the tumors did originate from cells without recombined transgene DNA and that cells surrounding the tumor tissue, which were positive in patches for the recombined transgene, were accidently isolated together with tumor material. Surprisingly, transgene mRNA expression was significantly higher in tumor tissue than in corresponding non-tumor tissue ($p \leq 0.05$) but with very low overall expression levels when comparing these to WT *Ctnnb1* expression (~1 transgene mRNA molecule / 50 *Ctnnb1* mRNA molecules). However, GS and GPR49 expression levels, both β-catenin target genes, were unchanged between non-tumor tissue and tumors. In addition, Cre recombinase expression was measured showing no difference between the tissue types but with overall very low expression levels.

In conclusion, β-catenin transgene expression occurs unexpectedly rare in transgenic animals, which was anticipated to benefit the promotion study with PB, revealing no significant difference but a tendency towards more and larger tumors between transgene- and WT animals. In addition, a significant but low level increase of recombined transgene mRNA was not accompanied by the respective target gene

expression increases in transgenic animals, leaving the question unanswered whether β-catenin is essential for PB-dependent tumor promotion in this project.

In a second project use was made of a genetically manipulated *Ctnnb1* knockout mouse strain (obtained from Dr. Huelsken and described in Huelsken and Behrens, 2001), in which β-catenin signaling pathway is specifically inactivated in hepatocytes (Braeuning *et al.*, 2009). This model allowed to further test the hypothesis that PB-mediated tumor promotion is dependent on Wnt/β-catenin signaling pathway (Aydinlik *et al.*, 2001) which could not be resolved in the former project. It is well known that cytochrome P450 expression in the liver is in part regulated by Wnt/β-catenin signaling (Braeuning *et al*., 2009, 2010; Sekine *et al.*, 2006) and that among these CYP2E1 is responsible for metabolic activation of DEN (Kang *et al*., 2007), the initiating agent used in this experiment. Although CYP2E1 expression has been shown to be absent in livers of *Ctnnb1* KO-mice (Braeuning et al., 2009; Sekine et al., 2006) metabolic activation of DEN does take place, as indicated by the presence of O^6-ethylguanine-adducts (Figure 22, B), however, the specific perivenous location of this process has been expanded to the entire liver lobule. This might be explained by the following consideration: Wnt/β-catenin signaling regulates the expression of perivenous CYPs, whereas other CYP isoforms are expressed throughout the liver lobule (Braeuning *et al.*, 2009). DEN is mainly activated in the perivenous location of the liver lobule, most probable by CYPs, like isoform 2E1, that are induced by Wnt/β-catenin signaling. In *Ctnnb1* KO-mice the expression of perivenously located CYPs is lost and the activation of DEN must be catalyzed by CYP isoforms that are independent of β-catenin presence as well as being distributed throughout the entire liver lobule (Figure 22, B). Another result of the metabolic DEN-activation shift to midzonal and periportal hepatocytes is the increase in number of hepatocytes affected by DEN. In addition, it is known that cell replication is much higher in periportal than in periveneous hepatocytes (Blikkendaal -Lieftinck et al., 1977). Taken together, it is of lesser surprise that tumor response, though not statistically significant, was ~7-fold higher in KO-mice than in their WT counterparts. A similar finding has been reported very recently (Zhang *et al*., 2010). PB treatment led to the development of visible tumors on the surface of livers, which was increased ~80-fold in WT mice compared to the respective non-PB treated controls. However, no tumor promoting effect of PB was observed in KO-mice. Similarly enzyme-altered liver

lesions, stained for G6Pase and GS, showed an increase in G6Pase negative and GS positive lesions in livers of WT/PB-treated mice but not in KO mice. Mutations in *Ctnnb1* are associated with an over-expression of GS and a deficiency in G6Pase activity (Loeppen *et al*., 2002). In accordance, 90% of tumors isolated from PB-treated WT mice harbored *Ctnnb1* mutations. However, 2 out of 6 tumors isolated from PB-treated KO-mice were also *Ctnnb1*-mutated. The easiest explanation for the existence of tumors of this phenotype is that transgene recombination, thereby inactivating *Ctnnb1*, mediated by the albumin promoter-driven Cre recombinase was incomplete. In fact, partial leakiness of the albumin promoter has been reported by others (Sekine *et al*., 2009) and was also observed, by the presence of small β-catenin positive patches, in our laboratory when analyzing livers of 8-week-old *Ctnnb1* KO-mice. Therefore the presents of *Ctnnb1* positive tumors most likely arises from *Ctnnb1*-positive cells that escaped the knockout process catalyzed by the Alb-Cre recombinase. In livers of *Ctnnb1* KO-mice 7/12 animals receiving a PB-containing diet and 1/10 animals receiving control diet showed a severe pre-cirrhotic phenotype, including signs of liver fibrosis accompanied by infiltrating immune cells, whereas WT animals were phenotypically normal. Histological inspection as well as immunohistological staining of liver slices for glucose metabolism (glycogen storage) and lipid metabolism (fat storage) point towards abnormalities in intermediary metabolism within these livers. Increased injury and inflammation, unrestricted oxidative stress, fibrosis, and compensatory increase in hepatocyte proliferation secondary to platelet-derived growth factor receptor α/phosphoinositide 3-kinase/Akt activation and c-Myc overexpression has been reported in another study treating *Ctnnb1* KO-mice with DEN but not PB (Zhang *et al*., 2010). The molecular mechanisms leading to this severe phenotype are most likely linked to the absence of β-catenin in these animals. As outlined earlier, β-catenin is a key factor in the perivenous expression of drug metabolizing enzymes. Among the targets known to be induced by active Wnt/β-catenin signaling there are also detoxifying enzymes of phase-II, especially glutathione S-transferases (GSTs) (Braeuning *et al*., 2009; Giera *et al*., 2010). GSTs play a decisive role in the defense against electrophilic compounds and oxidative stress (Hayes *et al.*, 1999). The expression of GST-isoforms m2, m3 and m6 is strongly induced in WT mice treated with PB but to a much lesser extent in *Ctnnb1* KO-mice (Braeuning *et al.*, 2009). Another isoform, GSTm1, was also shown to be statistically significant down-regulated in KO-mice as

compared to their WT counterparts (Table 7). Given that PB-exposure of hepatocytes leads to increased oxidative stress (Diez-Fernandez *et al*., 1998; Scholz *et al*., 1990) and that GST expression is reduced in livers of *Ctnnb1* KO-mice, hepatocellular degeneration and subsequent changes in liver architecture might be a result of increased oxidative stress. In addition, GSTs are involved in detoxification of electrophilic intermediates, generated by phase-I detoxifying reactions. Therefore, exposure to xenobiotic substances, for example in the diet, and especially PB-exposure in the absence of optimal GST activity may lead to the observed phenotypes in livers of KO-mice.

In addition, proteome changes were analyzed in livers of WT- and KO-mice treated with PB or control diet. Key enzymes of the urea cycle and of the histidine degradation pathway were up-regulated in hepatocytes from *Ctnnb1* KO mice as compared to WT mice. Interestingly, several of these enzymes (Histidine ammonia lyase, Argininosuccinate synthetase, Arginase 1) have previously been found to be down-regulated in liver tumors with *Ctnnb1* mutations (Stahl *et al*., 2005). Both the urea cycle and the histidine degradation pathway are localized preferentially in periportal hepatocytes (Gebhardt, 1992). The fact that enzymes of these two metabolic pathways are suppressed by activated β-catenin in tumors and up-regulated in normal liver following elimination of β-catenin clearly indicates that the expression of these preferentially periportal proteins is negatively regulated by Wnt/β-catenin-signaling. This is in line with a previous formulated hypothesis that Wnt/β-catenin-signaling, which positively regulates the expression of perivenous marker proteins, counteracts the expression of periportal genes/proteins, which may be positively regulated, at least in part, by signals through Ras-dependent signaling pathways (Hailfinger *et al*., 2006; Braeuning *et al*., 2006, 2007, 2009). In addition, the level of phosphoenolpyruvat carboxykinase 1 (PEPCK), the key enzyme in gluconeogenesis, a periportal pathway, was up-regulated in liver of KO mice, as were two enzymes involved in the metabolic degradation of aromatic amino acids. Interestingly, many of the proteins with increased expression in liver of KO mice were reduced in their level by treatment of KO mice with PB, while they were not affected in liver of WT mice (Figure 27). This suggests that PB has an effect in mouse liver, which mimics to some extent that of Wnt/β-catenin signaling. The same becomes evident upon inspection of the glycolytic metabolic pathway. In addition, expression analysis of several genes de-regulated in the proteome analysis was conducted.

However, results were not as conclusive as the protein data. There was a tendency of perivenously expressed genes towards up-regulation followed by a decrease in their expression by PB-treatment in livers of KO-mice, consistent with the proteome results. This correlation between mRNA and protein expression was reflected by only 1/3 genes with a perivenous expression profile. In summary, the levels of several enzymes involved in glucose metabolism were lowered in livers of KO mice suggesting that β-catenin signaling, absent in livers of KO-mice, positively regulates their expression. This finding is in good agreement with earlier observations demonstrating (i) that perivenous hepatocytes have a higher capacity for glycolysis than periportal hepatocytes (Jungermann and Katz, 1989; Jungermann *et al*., 1995) and (ii) that the perivenous phenotype of hepatocytes is mainly governed by β-catenin signaling (Hailfinger *et al*., 2006; Braeuning *et al*., 2006; Benhamouche *et al*., 2006).

Tumor promotion effects of PB-like and non-PB-like tumor promoters after combined application in mice after DEN initiation.

The effect of a combined application of dioxin-like PCB 126 (3,3´,4,4´,5-pentachlorobiphenyl) and PB-like PCB 153 (2,2´,4,4´,5,5´-hexachlorobiphenyl) on tumor promotion in DEN induced mice was evaluated in this project. Recent studies, using mixtures containing PCB 126 and PCB 153 have shown varying results on tumor promotion including antagonistic (Dean *et al*., 2002, Haag-Grönlund *et al*., 1998), no statistical significant different (van der Plas *et al*., 1999), and synergistic effects (Bager *et al*., 1995). PCBs have been recognized as carcinogens long time ago (reviewed in Silberhorn *et al*., 1990) and it has been shown that both, AhR and CAR agonist PCB congeners, can act as promoters of carcinogenesis (Buchmann *et al*., 1991). In addition, carcinogenic effects of individual PCBs and PCB mixtures have been shown in long-term studies using laboratory animals (Mayes *et al*., 1998). Dioxin-like substances elicit biological effects comparable to TCDD including AhR binding, induction of Cyp1a1 and 1a2, thymic involution, impairment of immune responses, induction of a wasting syndrome, increased mortality, teratogenicity and a variety of other toxic effects in the liver including carcinogenesis (Safe , 1990). PB-like compounds are not as potent as AhR agonists but, like PB, induce CYP enzymes, especially isoform 2b10, mediated by the nuclear receptor CAR (Muangmoonchai et al., 2001), as well as Cyp1a1/2 (Safe 1994; Safe *et al*., 1985).

Additionally, tumor promoting activity of PCB 153 has been demonstrated (Strathmann *et al*., 2006) even at low doses (Hemming *et al*., 1993; van der Plas *et al*., 1999). In the present study a tumor promotion study using a combined PCB 126/153 mixture was conducted in mice treated with equipotent dosages and steady state levels of the PCB congeners. The PCB congeners specifically induced the expression of either Cyp1a1 (PCB 126) or Cyp2b10 (PCB 153) in a preliminary experiment, although PB-like inducers have been shown to induce expression of Cyp1a1/2, too (Safe 1994; Safe *et al*., 1985). In addition, PCB 126 displayed a ~1000-fold stronger CYP induction potency than PCB 153. Liver half-life was around 25 days for both congeners. Interestingly the PCB 126 dose necessary to evoke an effect in mice (10µg/kg b.w. - 40µg/kg b.w.) compared to the treatment regimen used by Dean (0.1 µg/kg b.w.) (Dean *et al*., 2002) and Bager (1µg/kg b.w.) (Bager *et al*., 1995) in rats is at least 10 times higher. Hence, it seems that mice are less sensitive to PCB treatment than rats. Although PCB treatment led to a CYP-isoform specific induction in the exploratory experiment, PCB 153 high dose treatment statistically significantly induced Cyp1a1 as well as PCB 126 high dose induced Cyp2b10 after 20 weeks of PCB treatment in the main experiment. In addition, combined PCB 126/153 application synergistically induced both, Cyp1a1 and, to a lower extent, Cyp2b10 expression on the mRNA level. This is in contrast to another study, showing that combined PCB 126/153 application leads to a dose-dependent reduction of CYP2B1/2 (the rat homologue of mouse CYP2B10) expression in the liver (Bager *et al.*, 1995). It is known that PCB 153 induces AhR levels in the liver, potentially leading to hepatic deposition of dioxin-like PCBs (Denomme *et al*., 1986; de Jongh *et al*., 1995) inducing indirectly the activity and protein level of CYP1A2 and EROD activity (Bannister and Safe, 1987; Leece *et al*., 1987; de Jongh *et al*., 1993). Vice versa, PCB 153 concentration was shown to be increased in liver by high dose TCDD treatment (van Birgelen *et al.*, 1996). When performing enzymatic activity assays in this project, a statistically significant increase in EROD activity in PCB 126 high and low dose as well as in the combined PCB 126/153 treatment group was displayed when compared to oil treated control animals. Interestingly, EROD activity levels of the combined treatment group were, although not statistically significant different, between the levels of low- and high dose PCB 126 treatment groups, showing a tendency towards synergistically increased EROD activity caused by combined PCB 126/153 treatment. Comparable statistically significant increases in enzyme activity

were displayed when performing PROD assays. Here low and high dose PCB 153 treatment as well as combined PCB 126/153 treatment differed significantly in enzyme activity in comparison to oil treated controls. However, the combined PCB 126/153 treatment group displayed PROD activity levels in comparable magnitude to low dose PCB 153 treatment. Hence, there is, in contrast to EROD activity, no tendency towards synergistic PROD activity in the combined PCB treatment group. These results were convincingly confirmed by western-blot analysis using non-tumor tissue of oil control and PCB treated animals. Therefore, PCB 126 or PCB 153 treatment leads to statistically significant increases in EROD or PROD activity, respectively. However a combined PCB 126/153 treatment causes a tendency to produce a synergistic effect on EROD activity but not on PROD activity. Most interestingly, total tumor volume fraction and GS-altered tumor volume fractions as well as the average number of lesions per cm^2 and cm^3 were statistically significantly altered only in the combined PCB 126/153 treatment group when compared to oil treated controls at 25 weeks after DEN application. However at 34 weeks after DEN application, there was no difference in tumor volume fraction, neither of G6Pase negative nor of GS-positive lesions, but still a statistically significant increase in the average number of lesions in the combined PCB 126/153 treatment group. This lack of statistically significant increase in tumor volume fraction of the combined PCB 126/153 treatment group is mostly likely impaired by single animals harboring one extremely large tumor in the oil control group as well as in PCB 126 low dose treated animals. Taken together, PCB 153 might enhance the tumor promotional effect of PCB 126 promoted lesions in the liver of mice treated with DEN at the age of 6 weeks.

In addition to the tumor initiation-promotion experiment, a proteome analysis was performed using non-tumor tissue from DEN initiated PCB 126, 153, 126/153 or corn oil treated animals. A total of 68 protein spots were statistically significantly de-regulated of which 59 were unambiguously identified. About 50% of the identified proteins were de-regulated in more than one comparison, showing that i) dose increase partly de-regulated the same proteins within a treatment group (e.g. triosephosphate isomerase (P17751) for PCB 153 treatment and serum para-oxanase/arylesterase (P52430) for PCB 126 treatment) and ii) both PCB congeners partly de-regulated the same proteins (e.g. pyruvate kinase isozyme R/L (P53657)). Interestingly, comparison of high dose PCB 126 to high dose PCB 153 treatment

revealed a change in expression of 21 proteins, only 3 of these higher expressed in PCB 126 treated animals as compared to PCB 153 treated mice. This tendency towards inhibition of protein expression was also evident when comparing PCB 126 application to oil control treated animals, were 75% (9/12) of significantly de-regulated proteins were lower in expression in PCB 126 treated mice as compared to controls. 3 proteins, statistically significantly up-regulated by combined PCB126/153 treatment when compared to controls, were the 14-3-3 proteins beta/alpha (β/α), the α-isoform representing the phosphorylated form of β, zeta/delta (ζ/δ) and sigma (σ). 14-3-3 proteins constitute a highly conserved protein family involved in vital cellular processes (for recent reviews see Morrison 2009) controlling for example Raf-kinase activity (Rushworth *et al*., 2006; Garnett *et al*., 2005) and oncogenic B-raf signal transduction (Wan *et al*., 2004; Wellbrock *et al*., 2004), mediating Wnt/β-catenin signaling inhibition (Li *et al*., 2008; Takemaru *et al*., 2009), anti-apoptosis (Porter *et al.*, 2006), cell cycle regulation by 14-3-3σ (Hermeking *et al*., 1997) and mitotic translation (Wilker *et al*., 2007). Especially the importance of 14-3-3σ as a tumor suppressor has been recognized. Although low-abundant proteins are not expected to be detected by the method applied here, a recently conducted proteome analysis using the same technique for protein separation and identification found 14-3-3 proteins to be de-regulated in the esophagus squamous epithelial cell line Eca109 in a β-catenin dependent manner (Ren *et al*., 2010). The de-regulation of 14-3-3β/α as well as 14-3-3ζ/δ was also analyzed using RT-LC PCR. Although a de-regulation could not be verified on the transcript level, 14-3-3 proteins are known to be regulated post-translationally, which cannot be displayed by the gene expression analysis. However, further analysis is needed to analyze the consequences of 14-3-3 protein de-regulation in combined PCB 126/153 treated mice initiated with DEN.

In conclusion, the combined application of dioxin-like and non-dioxin-like (PB-like) tumor promoters PCB 126 and PCB 153 in DEN initiated mice caused a synergistic transcriptional as well as translational induction of Cyp1A1/2B10 accompanied by statistically significant elevated EROD and PROD activities, associated with a statistically significant increase of liver lesions in the combined PCB 126/153 treatment group only. This effect, also characterized by the absence of GS-altered lesions and hence a lack of PB-like tumor promotion activity, is most likely based upon an influence of PCB 153 on PCB 126 facilitated tumor promotion. Using a proteome analytic approach, 59 proteins, among these members of protein family 14-

3-3, were unambiguously identified as de-regulated in livers of DEN/PCB treated mice as compared to oil control animals. Based on these results, the concept of risk assessment may need to be adjusted. It is based upon the Toxic equivalence factor (TEF) which assumes that substances acting by the same molecular mechanism, here AhR binding and activation, induce additive effects and that TCDD, the most potent inducer, is used as a standard and set as 1. Other dioxin-like chemicals are assigned TEFs that are fractions thereof. The toxicological equivalence (TEQ) of a mixture is the sum of the individual potencies. This concept assumes that dioxin-like substances act in an additive mode of action only, even though non-additive PCB interactions have been reported. Most importantly CAR agonists are not included in this concept, although PB-like substances are known tumor promoters and combined dioxin-like/PB-like treatment has shown synergistic effects in this study.

Quantitative analysis of growth kinetics of chemically-induced mouse liver tumors by non-invasive magnetic resonance imaging

To better understand the molecular mechanisms of HCC and other types of tumors as well as to monitor tumor initiation and tumor growth *in vivo*, techniques for *in vivo* monitoring of animal tumor models would be of high value, simultaneously minimizing the number of experimental animals needed for statistically significant analyses. Magnetic Resonance Imaging (MRI) is routinely used for organ and tissue visualization in humans. Additionally, it is also feasible to study animal organ and tissue structure. In fact, MRI technology was used for visualization of protein expression in experimental mice (Cohen *et al*., 2007). In addition, MRI was used for *in vivo* imaging of tumor development in transgenic and chemical mouse models of HCC (Freimuth *et al*., 2010), demonstrating that the visualization of small single nodules with a diameter of 2mm is basically feasible in c-myc transgenic animals but 100% detection was reached at a size ≥4mm. In contrast, DEN initiated mouse liver tumors were not detected 24 weeks after initiation but after 45 weeks which may have been due to multi-nodular tumor appearance and low contrast of the specimen (Freimuth *et al*., 2010). This is in contrast to our experiment, were tumors of ~2mm in size in DEN only treated animals were visible from week 16 onwards. Interestingly tumor onset in DEN/PB treated animals was delayed by ~5 weeks when compared to tumors occurring in mice treated with DEN at 2 weeks of age. However, tumor volume increase and maximum tumor size of ~400mm^3 were equal at the point in

time when animals had to be killed in order to prevent suffering due to tumor burden. However, it is highly remarkable how strongly tumor incidence differed in individual animals as well as how growth kinetics of individual tumors differed within the same animal. This finding emphasizes more than ever how important it would be to monitor tumor development in single animals as well as to discover the molecular differences in growth kinetics between tumors within the same animal.

6. Summary (english)

Chemically induced mouse liver tumors are frequently mutated in genes encoding *Ha-ras*, *B-raf* or *Ctnnb1*, leading to constitutive activation of signaling pathways downstream of the respective regulatory proteins affected by mutation of their genes. While *Ctnnb1* mutations are highly prevalent in tumors induced by a treatment regimen including PB or a PB-like liver tumor promoter, *Ha-ras* or alternatively *B-raf* mutations are seen in up to 70% of spontaneously occurring liver tumors or in tumors induced by exclusive treatment with a genotoxic liver carcinogen like DEN.

Analyzing the global protein expression pattern of *Ha-ras* and *B-raf* mutated mouse liver tumors discovered no significantly differentially expressed proteins between these tumors types. Furthermore the expression profiles were highly correlated to a recently performed micro-array analysis of the same tumor material. Despite the high similarity in global protein and gene expression, the tumor types differed in the phosphorylation state of ERK1/2, albeit without apparent consequences on protein or gene expression levels.

Using two transgenic mouse strains, one expressing a liver specific constitutively active form of β-catenin and the other lacking a functional form of the proto-oncogene, the importance of β-catenin in PB-dependent tumor promotion was assessed *in vivo*, showing that β-catenin is an essential molecule in this process. Analyzing the liver-proteomes of these animals revealed that PB induces a β-catenin-mimetic effect in livers of β-catenin-KO mice treated with the tumor promoter.

To assess the impact of a mixture containing dioxin-like and PB-like tumor promoters, equipotent doses of PCB 126 and PCB 153 were given, either as a single substance or in a mixture of both substances, to mice initiated with DEN at the age of 6 weeks. As a result, animals receiving the combined mixture of PCB126 and PCB 153 displayed a statistically significant increase in relative lesion size and number when compared to control animals or treatment groups receiving either PCB 126 or PCB 153 only. The increased tumor promotional effect was accompanied by statistically significant and synergistic increases in Cyp1A1 as well as Cyp2B10 gene expression levels. However, protein levels, enzyme assays specific for CYP1A1 and CYP2B10 as well as immunohistochemical analysis revealed increased expression/ activity levels for CYP1A1 in the combined PCB treatment group only. Therefore it seems possible that in a combined PCB 126/153 application PB-like PCB 153 enhances

PCB 126 dependent tumor promotion in livers of mice initiated with DEN at the age of 6 weeks.

Finally, MRI-technology was utilized for *in vivo* visualization of mouse liver tumors, showing that tumors as small as 2mm in diameter can be displayed by this technology and that tumor growth varies substantially within and between animals.

7. Zusammenfassung (deutsch)

Durch Chemikalien induzierte Mauslebertumoren weisen häufig eine Mutation in den Genen *Ha-ras*, *B-raf* oder *Ctnnb1* auf, was zu einer konstitutiven Aktivierung von Signalwegen unterhalb des von der Mutation betroffenen regulatorischen Proteins führt. Während die Induktion von *Ctnnb1* Mutationen häufig in Tieren durch eine Behandlung mit PB oder PB-ähnlichen Substanzen mit tumorpromovierender Wirkung induziert wird, kommen *Ha-ras* oder alternativ *B-raf* Mutationen in 70% von spontan entstehenden Tumoren oder nach Behandlung mit dem gentoxischen Leberkanzerogen DEN vor.

Die Untersuchung des gesamten Proteinexpressionsmusters von *Ha-ras* und *B-raf* mutierten Mauslebertumoren ergab, dass es keine signifikanten Unterschiede in der Proteinexpression zwischen diesen Tumortypen gibt. Darüber hinaus waren die Proteinexpressionsprofile im Vergleich zu einer erst kürzlich durchgeführten RNA-Mikro-Array-Analyse desselben Tumormaterials hoch korreliert. Ungeachtet der ausgeprägten Übereinstimmung in der Protein- und Geneexpression wiesen die Tumortypen einen Unterschied im Phosphorylierungsstatus von ERK1/2 auf, der jedoch keine erkennbaren Auswirkungen auf die Protein- und Genexpression hatte.

Der Einfluss von β-Catenin auf die PB-abhängige Tumorpromotion wurde mit Hilfe von zwei transgenen Mausstämmen untersucht, von denen einer eine konstitutiv aktive Form von β-Catenin exprimierte während bei dem anderen eine funktionsfähige Form des Proto-onkogens fehlte. Die Ergebnisse des Versuchs zeigten, dass β-Catenin ein essentielles Protein in diesem Prozess ist. Eine Untersuchung des Leber-proteoms dieser Tiere zeigte darüber hinaus, dass PB in Lebern von β-Catenin-defizienten Tieren eine β-Catenin-mimetische Wirkung besitzt.

Um den Einfluss einer Mischung aus einem Dioxin-ähnlichen und einem PB-ähnlichen Tumorpromotor zu untersuchen, wurden equipotente Dosierungen von PCB 126 und PCB 153 entweder als Einzelsubstanzgabe oder im Gemisch beider Substanzen Tieren verabreicht, welche im Alter von 6 Wochen mit DEN behandelt worden waren. Die Ergebnisse des Versuchs zeigten, dass Mäuse, welche mit der Mischung aus PCB 126 und PCB 153 behandelt wurden, eine statistisch signifikante Erhöhung der relativen Lesionsgrößen und Anzahl, im Vergleich zu Kontrolltieren oder Tieren welche eine Einzelsubstanzgabe erhielten, aufwiesen. Der erhöhte tumorpromovierende Effekt wurde durch eine statistisch signifikante erhöhte Genexpressionsrate von Cyp1A1 und Cyp2b10 begleitet. Sowohl das Ausmaß der

Proteinexpression sowie enzymatische Tests der CYP1A1 und CYP2B10 Aktivität als auch immunohistochemische Analysen wiesen eine erhöhte Expression bzw. Aktivität für CYP1A1 nur in der kombinierten PCB126/153-Behandlungsgruppe auf. Daher wäre es möglich, dass bei gemeinsamer Applikation von PCB 126/ PCB 153 das PB-ähnliche PCB 153 einen verstärkenden Effekt auf die PCB 126-abhängige Tumorpromotion in der Mauslebern bewirkt.

Als letztes wurde die MRI-Technologie eingesetzt, um Mauslebertumore unter *in vivo* Bedingungen zu beobachten. Es konnte zum einen gezeigt werden, dass Tumore ab einem Durchmesser von ~2mm dargestellt werden können, zum anderen, dass sich das Tumorwachstum zwischen, aber auch innerhalb eines Tieres substantiell voneinander unterscheiden kann.

8. Literature

Adachi, Y., Y. Shibai, J. Mitsushita, W. H. Shang, K. Hirose, and T. Kamata. "Oncogenic Ras Upregulates Nadph Oxidase 1 Gene Expression through Mek-Erk-Dependent Phosphorylation of Gata-6." *Oncogene* 27, no. 36 (2008): 4921-32.

Aydinlik, H., T. D. Nguyen, O. Moennikes, A. Buchmann, and M. Schwarz. "Selective Pressure During Tumor Promotion by Phenobarbital Leads to Clonal Outgrowth of Beta-Catenin-Mutated Mouse Liver Tumors." *Oncogene* 20, no. 53 (2001): 7812-6.

Bager, Y., H. Hemming, S. Flodstrom, U. G. Ahlborg, and L. Warngard. "Interaction of 3,4,5,3',4'-Pentachlorobiphenyl and 2,4,5,2',4',5'-Hexachlorobiphenyl in Promotion of Altered Hepatic Foci in Rats." *Pharmacol Toxicol* 77, no. 2 (1995): 149-54.

Bandiera, S., S. Safe, and A. B. Okey. "Binding of Polychlorinated Biphenyls Classified as Either Phenobarbitone-, 3-Methylcholanthrene- or Mixed-Type Inducers to Cytosolic Ah Receptor." *Chem Biol Interact* 39, no. 3 (1982): 259-77.

Bannister, R., and S. Safe. "Synergistic Interactions of 2,3,7,8-Tcdd and 2,2',4,4',5,5'-Hexachlorobiphenyl in C57bl/6j and Dba/2j Mice: Role of the Ah Receptor." *Toxicology* 44, no. 2 (1987): 159-69.

Bauer-Hofmann, R., F. Klimek, A. Buchmann, O. Muller, P. Bannasch, and M. Schwarz. "Role of Mutations at Codon 61 of the C-Ha-Ras Gene During Diethylnitrosamine-Induced Hepatocarcinogenesis in C3h/He Mice." *Mol Carcinog* 6, no. 1 (1992): 60-7.

Behrens, J., B. A. Jerchow, M. Wurtele, J. Grimm, C. Asbrand, R. Wirtz, M. Kuhl, D. Wedlich, and W. Birchmeier. "Functional Interaction of an Axin Homolog, Conductin, with Beta-Catenin, Apc, and Gsk3beta." *Science* 280, no. 5363 (1998): 596-9.

Behrens, J., and B. Lustig. "The Wnt Connection to Tumorigenesis." *Int J Dev Biol* 48, no. 5-6 (2004): 477-87.

Benhamouche, S., T. Decaens, C. Perret, and S. Colnot. "[Wnt/Beta-Catenin Pathway and Liver Metabolic Zonation: A New Player for an Old Concept]." *Med Sci (Paris)* 22, no. 11 (2006): 904-6.

Blikkendaal-Lieftinck, L. F., M. Kooij, M. F. Kramer, and W. Den Otter. "Cell Kinetics in the Liver of Rats under Normal and Abnormal Dietary Conditions. An Autoradiographic Study by Means of [3h]Thymidine." *Experimental and molecular pathology* 26, no. 2 (1977): 184-92.

Bluthgen, N., S. Legewie, S. M. Kielbasa, A. Schramme, O. Tchernitsa, J. Keil, A. Solf, M. Vingron, R. Schafer, H. Herzel, and C. Sers. "A Systems Biological Approach Suggests That Transcriptional Feedback Regulation by Dual-Specificity Phosphatase 6 Shapes Extracellular Signal-Related Kinase Activity in Ras-Transformed Fibroblasts." *FEBS J* 276, no. 4 (2009): 1024-35.

Braeuning, A., C. Ittrich, C. Kohle, A. Buchmann, and M. Schwarz. "Zonal Gene Expression in Mouse Liver Resembles Expression Patterns of Ha-Ras and Beta-Catenin Mutated Hepatomas." *Drug Metab Dispos* 35, no. 4 (2007): 503-7.

Braeuning, A., C. Ittrich, C. Kohle, S. Hailfinger, M. Bonin, A. Buchmann, and M. Schwarz. "Differential Gene Expression in Periportal and Perivenous Mouse Hepatocytes." *FEBS J* 273, no. 22 (2006): 5051-61.

Braeuning, A., R. Sanna, J. Huelsken, and M. Schwarz. "Inducibility of Drug-Metabolizing Enzymes by Xenobiotics in Mice with Liver-Specific Knockout of Ctnnb1." *Drug Metab Dispos* 37, no. 5 (2009): 1138-45.

Braeuning, A., and M. Schwarz. "Beta-Catenin as a Multilayer Modulator of Zonal Cytochrome P450 Expression in Mouse Liver." *Biol Chem* 391, no. 2-3 (2010): 139-48.

Brose, M. S., P. Volpe, M. Feldman, M. Kumar, I. Rishi, R. Gerrero, E. Einhorn, M. Herlyn, J. Minna, A. Nicholson, J. A. Roth, S. M. Albelda, H. Davies, C. Cox, G. Brignell, P. Stephens, P. A. Futreal, R. Wooster, M. R. Stratton, and B. L. Weber. "Braf and Ras Mutations in Human Lung Cancer and Melanoma." *Cancer Res* 62, no. 23 (2002): 6997-7000.

Buchmann, A., R. Bauer-Hofmann, J. Mahr, N. R. Drinkwater, A. Luz, and M. Schwarz. "Mutational Activation of the C-Ha-Ras Gene in Liver Tumors of Different Rodent Strains: Correlation with Susceptibility to Hepatocarcinogenesis." *Proc Natl Acad Sci U S A* 88, no. 3 (1991): 911-5.

Buchmann, A., Z. Karcier, B. Schmid, J. Strathmann, and M. Schwarz. "Differential Selection for B-Raf and Ha-Ras Mutated Liver Tumors in Mice with High and Low Susceptibility to Hepatocarcinogenesis." *Mutat Res* 638, no. 1-2 (2008): 66-74.

Buchmann, A., S. Ziegler, A. Wolf, L. W. Robertson, S. K. Durham, and M. Schwarz. "Effects of Polychlorinated Biphenyls in Rat Liver: Correlation between Primary Subcellular Effects and Promoting Activity." *Toxicol Appl Pharmacol* 111, no. 3 (1991): 454-68.

Burke, M. D., and R. T. Mayer. "Ethoxyresorufin: Direct Fluorimetric Assay of a Microsomal O-Dealkylation Which Is Preferentially Inducible by 3-Methylcholanthrene." *Drug Metab Dispos* 2, no. 6 (1974): 583-8.

Cadoret, A., C. Ovejero, S. Saadi-Kheddouci, E. Souil, M. Fabre, B. Romagnolo, A. Kahn, and C. Perret. "Hepatomegaly in Transgenic Mice Expressing an Oncogenic Form of Beta-Catenin." *Cancer Res* 61, no. 8 (2001): 3245-9.

Calvisi, D. F., S. Ladu, V. M. Factor, and S. S. Thorgeirsson. "Activation of Beta-Catenin Provides Proliferative and Invasive Advantages in C-Myc/Tgf-Alpha Hepatocarcinogenesis Promoted by Phenobarbital." *Carcinogenesis* 25, no. 6 (2004): 901-8.

Cavard, C., S. Colnot, V. Audard, S. Benhamouche, L. Finzi, C. Torre, G. Grimber, C. Godard, B. Terris, and C. Perret. "Wnt/Beta-Catenin Pathway in Hepatocellular Carcinoma Pathogenesis and Liver Physiology." *Future Oncol* 4, no. 5 (2008): 647-60.

Chan, D. W., V. W. Liu, G. S. Tsao, K. M. Yao, T. Furukawa, K. K. Chan, and H. Y. Ngan. "Loss of Mkp3 Mediated by Oxidative Stress Enhances Tumorigenicity and Chemoresistance of Ovarian Cancer Cells." *Carcinogenesis* 29, no. 9 (2008): 1742-50.

Chen, W., J. Ji, R. Zhao, and B. Ru. "Comparative Proteome Analysis of Human Temporal Cortex Lobes by Two-Dimensional Electrophoresis and Identification of Selected Common Proteins." *Neurochemical research* 27, no. 9 (2002): 871-81.

Cohen, B., K. Ziv, V. Plaks, T. Israely, V. Kalchenko, A. Harmelin, L. E. Benjamin, and M. Neeman. "Mri Detection of Transcriptional Regulation of Gene Expression in Transgenic Mice." *Nat Med* 13, no. 4 (2007): 498-503.

Cullen, P. J., and P. J. Lockyer. "Integration of Calcium and Ras Signalling." *Nat Rev Mol Cell Biol* 3, no. 5 (2002): 339-48.

Curran, P. G., and L. J. DeGroot. "The Effect of Hepatic Enzyme-Inducing Drugs on Thyroid Hormones and the Thyroid Gland." *Endocr Rev* 12, no. 2 (1991): 135-50.

De Jongh, J., M. DeVito, J. Diliberto, M. Van den Berg, and L. Birnbaum. "The Effects of 2,2',4,4',5,5'-Hexachlorobiphenyl Cotreatment on the Disposition of 2,3,7,8-Tetrachlorodibenzo-P-Dioxin in Mice." *Toxicol Lett* 80, no. 1-3 (1995): 131-7.

De Jongh, J., R. Nieboer, I. Schroders, W. Seinen, and M. Van den Berg. "Toxicokinetic Mixture Interactions between Chlorinated Aromatic Hydrocarbons in the Liver of the C57bl/6j Mouse: 2. Polychlorinated Dibenzo-P-Dioxins (Pcdds), Dibenzofurans (Pcdfs) and Biphenyls (Pcbs)." *Arch Toxicol* 67, no. 9 (1993): 598-604.

Dean, C. E., Jr., S. A. Benjamin, L. S. Chubb, J. D. Tessari, and T. J. Keefe. "Nonadditive Hepatic Tumor Promoting Effects by a Mixture of Two Structurally Different Polychlorinated Biphenyls in Female Rat Livers." *Toxicol Sci* 66, no. 1 (2002): 54-61.

Denomme, M. A., S. Bandiera, I. Lambert, L. Copp, L. Safe, and S. Safe. "Polychlorinated Biphenyls as Phenobarbitone-Type Inducers of Microsomal Enzymes. Structure-Activity Relationships for a Series of 2,4-Dichloro-Substituted Congeners." *Biochem Pharmacol* 32, no. 19 (1983): 2955-63.

Denomme, M. A., K. Homonko, T. Fujita, T. Sawyer, and S. Safe. "Substituted Polychlorinated Dibenzofuran Receptor Binding Affinities and Aryl Hydrocarbon Hydroxylase Induction Potencies--a Qsar Analysis." *Chem Biol Interact* 57, no. 2 (1986): 175-87.

Devereux, T. R., C. H. Anna, J. F. Foley, C. M. White, R. C. Sills, and J. C. Barrett. "Mutation of Beta-Catenin Is an Early Event in Chemically Induced Mouse Hepatocellular Carcinogenesis." *Oncogene* 18, no. 33 (1999): 4726-33.

Diez-Fernandez, C., N. Sanz, A. M. Alvarez, A. Wolf, and M. Cascales. "The Effect of Non-Genotoxic Carcinogens, Phenobarbital and Clofibrate, on the Relationship between Reactive Oxygen Species, Antioxidant Enzyme Expression and Apoptosis." *Carcinogenesis* 19, no. 10 (1998): 1715-22.

Downward, J. "Targeting Ras Signalling Pathways in Cancer Therapy." *Nat Rev Cancer* 3, no. 1 (2003): 11-22.

Ekerot, M., M. P. Stavridis, L. Delavaine, M. P. Mitchell, C. Staples, D. M. Owens, I. D. Keenan, R. J. Dickinson, K. G. Storey, and S. M. Keyse. "Negative-Feedback Regulation of Fgf Signalling by Dusp6/Mkp-3 Is Driven by Erk1/2 and Mediated by Ets Factor Binding to a Conserved Site within the Dusp6/Mkp-3 Gene Promoter." *Biochem J* 412, no. 2 (2008): 287-98.

Freimuth, J., N. Gassler, N. Moro, R. W. Gunther, C. Trautwein, C. Liedtke, and G. A. Krombach. "Application of Magnetic Resonance Imaging in Transgenic and Chemical Mouse Models of Hepatocellular Carcinoma." *Mol Cancer* 9 (2010): 94.

Futcher, B., G. I. Latter, P. Monardo, C. S. McLaughlin, and J. I. Garrels. "A Sampling of the Yeast Proteome." *Molecular and cellular biology* 19, no. 11 (1999): 7357-68.

Garnett, M. J., S. Rana, H. Paterson, D. Barford, and R. Marais. "Wild-Type and Mutant B-Raf Activate C-Raf through Distinct Mechanisms Involving Heterodimerization." *Mol Cell* 20, no. 6 (2005): 963-9.

Gebhardt, R. "Metabolic Zonation of the Liver: Regulation and Implications for Liver Function." *Pharmacol Ther* 53, no. 3 (1992): 275-354.

Gebhardt, R., and F. Gaunitz. "Cell-Cell Interactions in the Regulation of the Expression of Hepatic Enzymes." *Cell Biol Toxicol* 13, no. 4-5 (1997): 263-73.

Gebhardt, R., and D. Mecke. "Heterogeneous Distribution of Glutamine Synthetase among Rat Liver Parenchymal Cells in Situ and in Primary Culture." *The EMBO journal* 2, no. 4 (1983): 567-70.

Giera, S., A. Braeuning, C. Kohle, W. Bursch, U. Metzger, A. Buchmann, and M. Schwarz. "Wnt/Beta-Catenin Signaling Activates and Determines Hepatic Zonal Expression of Glutathione S-Transferases in Mouse Liver." *Toxicol Sci* 115, no. 1 (2010): 22-33.

Greenbaum, D., C. Colangelo, K. Williams, and M. Gerstein. "Comparing Protein Abundance and Mrna Expression Levels on a Genomic Scale." *Genome biology* 4, no. 9 (2003): 117.

Griffin, T. J., S. P. Gygi, T. Ideker, B. Rist, J. Eng, L. Hood, and R. Aebersold. "Complementary Profiling of Gene Expression at the Transcriptome and Proteome Levels in Saccharomyces Cerevisiae." *Molecular & cellular proteomics : MCP* 1, no. 4 (2002): 323-33.

Haag-Gronlund, M., N. Johansson, R. Fransson-Steen, H. Hakansson, G. Scheu, and L. Warngard. "Interactive Effects of Three Structurally Different Polychlorinated Biphenyls in a Rat Liver Tumor Promotion Bioassay." *Toxicol Appl Pharmacol* 152, no. 1 (1998): 153-65.

Hagemann, C., and U. R. Rapp. "Isotype-Specific Functions of Raf Kinases." *Experimental cell research* 253, no. 1 (1999): 34-46.

Hailfinger, S., M. Jaworski, A. Braeuning, A. Buchmann, and M. Schwarz. "Zonal Gene Expression in Murine Liver: Lessons from Tumors." *Hepatology* 43, no. 3 (2006): 407-14.

Hayes, J. D., and L. I. McLellan. "Glutathione and Glutathione-Dependent Enzymes Represent a Co-Ordinately Regulated Defence against Oxidative Stress." *Free radical research* 31, no. 4 (1999): 273-300.

Hemming, H., S. Flodstrom, L. Warngard, A. Bergman, T. Kronevi, I. Nordgren, and U. G. Ahlborg. "Relative Tumour Promoting Activity of Three Polychlorinated Biphenyls in Rat Liver." *Eur J Pharmacol* 248, no. 2 (1993): 163-74.

Hermeking, H., C. Lengauer, K. Polyak, T. C. He, L. Zhang, S. Thiagalingam, K. W. Kinzler, and B. Vogelstein. "14-3-3 Sigma Is a P53-Regulated Inhibitor of G2/M Progression." *Mol Cell* 1, no. 1 (1997): 3-11.

Hosseinpour, F., R. Moore, M. Negishi, and T. Sueyoshi. "Serine 202 Regulates the Nuclear Translocation of Constitutive Active/Androstane Receptor." *Mol Pharmacol* 69, no. 4 (2006): 1095-102.

Huang, W., J. Zhang, M. Washington, J. Liu, J. M. Parant, G. Lozano, and D. D. Moore. "Xenobiotic Stress Induces Hepatomegaly and Liver Tumors Via the Nuclear Receptor Constitutive Androstane Receptor." *Mol Endocrinol* 19, no. 6 (2005): 1646-53.

Huelsken, J., R. Vogel, B. Erdmann, G. Cotsarelis, and W. Birchmeier. "Beta-Catenin Controls Hair Follicle Morphogenesis and Stem Cell Differentiation in the Skin." *Cell* 105, no. 4 (2001): 533-45.

Ingelman-Sundberg, M., and A. L. Hagbjork. "On the Significance of the Cytochrome P-450-Dependent Hydroxyl Radical-Mediated Oxygenation Mechanism." *Xenobiotica* 12, no. 11 (1982): 673-86.

Jaworski, M., A. Buchmann, P. Bauer, O. Riess, and M. Schwarz. "B-Raf and Ha-Ras Mutations in Chemically Induced Mouse Liver Tumors." *Oncogene* 24, no. 7 (2005): 1290-5.

Jaworski, M., C. Ittrich, S. Hailfinger, M. Bonin, A. Buchmann, M. Schwarz, and C. Kohle. "Global Gene Expression in Ha-Ras and B-Raf Mutated Mouse Liver Tumors." *Int J Cancer* 121, no. 6 (2007): 1382-5.

Jin, H., X. Wang, J. Ying, A. H. Wong, Y. Cui, G. Srivastava, Z. Y. Shen, E. M. Li, Q. Zhang, J. Jin, S. Kupzig, A. T. Chan, P. J. Cullen, and Q. Tao. "Epigenetic Silencing of a Ca(2+)-Regulated Ras Gtpase-Activating Protein Rasal Defines a New Mechanism of Ras Activation in Human Cancers." *Proc Natl Acad Sci U S A* 104, no. 30 (2007): 12353-8.

Jirtle, R. L., G. R. Hankins, H. Reisenbichler, and I. J. Boyer. "Regulation of Mannose 6-Phosphate/Insulin-Like Growth Factor-Ii Receptors and Transforming Growth Factor Beta During Liver Tumor Promotion with Phenobarbital." *Carcinogenesis* 15, no. 8 (1994): 1473-8.

Jungermann, K. "Zonation of Metabolism and Gene Expression in Liver." *Histochem Cell Biol* 103, no. 2 (1995): 81-91.

Jungermann, K., and N. Katz. "Functional Specialization of Different Hepatocyte Populations." *Physiol Rev* 69, no. 3 (1989): 708-64.

Kang, J. S., H. Wanibuchi, K. Morimura, F. J. Gonzalez, and S. Fukushima. "Role of Cyp2e1 in Diethylnitrosamine-Induced Hepatocarcinogenesis in Vivo." *Cancer Res* 67, no. 23 (2007): 11141-6.

Katz, N., H. F. Teutsch, K. Jungermann, and D. Sasse. "Heterogeneous Reciprocal Localization of Fructose-1,6-Bisphosphatase and of Glucokinase in Microdissected Periportal and Perivenous Rat Liver Tissue." *FEBS Lett* 83, no. 2 (1977): 272-6.

Katz, N., H. F. Teutsch, D. Sasse, and K. Jungermann. "Heterogeneous Distribution of Glucose-6-Phosphatase in Microdissected Periportal and Perivenous Rat Liver Tissue." *FEBS Lett* 76, no. 2 (1977): 226-30.

Kellendonk, C., C. Opherk, K. Anlag, G. Schutz, and F. Tronche. "Hepatocyte-Specific Expression of Cre Recombinase." *Genesis* 26, no. 2 (2000): 151-3.

Keyse, S. M. "Dual-Specificity Map Kinase Phosphatases (Mkps) and Cancer." *Cancer Metastasis Rev* 27, no. 2 (2008): 253-61.

Kim, Y., R. C. Sills, and C. D. Houle. "Overview of the Molecular Biology of Hepatocellular Neoplasms and Hepatoblastomas of the Mouse Liver." *Toxicol Pathol* 33, no. 1 (2005): 175-80.

Klaunig, J. E., L. M. Kamendulis, and Y. Xu. "Epigenetic Mechanisms of Chemical Carcinogenesis." *Hum Exp Toxicol* 19, no. 10 (2000): 543-55.

Kodama, S., C. Koike, M. Negishi, and Y. Yamamoto. "Nuclear Receptors Car and Pxr Cross Talk with Foxo1 to Regulate Genes That Encode Drug-Metabolizing and Gluconeogenic Enzymes." *Mol Cell Biol* 24, no. 18 (2004): 7931-40.

Köhle, C., M. Schwarz, and K. W. Bock. "Promotion of Hepatocarcinogenesis in Humans and Animal Models." *Arch Toxicol* (2008).

Krishna, M., and H. Narang. "The Complexity of Mitogen-Activated Protein Kinases (Mapks) Made Simple." *Cell Mol Life Sci* 65, no. 22 (2008): 3525-44.

Krutovskikh, V., and H. Yamasaki. "The Role of Gap Junctional Intercellular Communication (Gjic) Disorders in Experimental and Human Carcinogenesis." *Histol Histopathol* 12, no. 3 (1997): 761-8.

Kuo, F. C., and J. E. Darnell, Jr. "Evidence That Interaction of Hepatocytes with the Collecting (Hepatic) Veins Triggers Position-Specific Transcription of the Glutamine Synthetase and Ornithine Aminotransferase Genes in the Mouse Liver." *Mol Cell Biol* 11, no. 12 (1991): 6050-8.

Leece, B., M. A. Denomme, R. Towner, A. Li, J. Landers, and S. Safe. "Nonadditive Interactive Effects of Polychlorinated Biphenyl Congeners in Rats: Role of the 2,3,7,8-Tetrachlorodibenzo-P-Dioxin Receptor." *Can J Physiol Pharmacol* 65, no. 9 (1987): 1908-12.

Li, F. Q., A. Mofunanya, K. Harris, and K. Takemaru. "Chibby Cooperates with 14-3-3 to Regulate Beta-Catenin Subcellular Distribution and Signaling Activity." *J Cell Biol* 181, no. 7 (2008): 1141-54.

Loeppen, S., D. Schneider, F. Gaunitz, R. Gebhardt, R. Kurek, A. Buchmann, and M. Schwarz. "Overexpression of Glutamine Synthetase Is Associated with Beta-Catenin-Mutations in Mouse Liver Tumors During Promotion of Hepatocarcinogenesis by Phenobarbital." *Cancer Res* 62, no. 20 (2002): 5685-8.

Lustig, B., and J. Behrens. "The Wnt Signaling Pathway and Its Role in Tumor Development." *J Cancer Res Clin Oncol* 129, no. 4 (2003): 199-221.

Malumbres, M., and M. Barbacid. "Ras Oncogenes: The First 30 Years." *Nat Rev Cancer* 3, no. 6 (2003): 459-65.

Mayes, B. A., E. E. McConnell, B. H. Neal, M. J. Brunner, S. B. Hamilton, T. M. Sullivan, A. C. Peters, M. J. Ryan, J. D. Toft, A. W. Singer, J. F. Brown, Jr., R. G. Menton, and J. A. Moore. "Comparative Carcinogenicity in Sprague-Dawley Rats of the Polychlorinated Biphenyl Mixtures Aroclors 1016, 1242, 1254, and 1260." *Toxicol Sci* 41, no. 1 (1998): 62-76.

Maziarz, M., C. Chung, D. J. Drucker, and A. Emili. "Integrating Global Proteomic and Genomic Expression Profiles Generated from Islet Alpha Cells: Opportunities and Challenges to Deriving Reliable Biological Inferences." *Molecular & cellular proteomics : MCP* 4, no. 4 (2005): 458-74.

Mercer, K. E., and C. A. Pritchard. "Raf Proteins and Cancer: B-Raf Is Identified as a Mutational Target." *Biochim Biophys Acta* 1653, no. 1 (2003): 25-40.

Mitsushita, J., J. D. Lambeth, and T. Kamata. "The Superoxide-Generating Oxidase Nox1 Is Functionally Required for Ras Oncogene Transformation." *Cancer Res* 64, no. 10 (2004): 3580-5.

Moennikes, O., A. Buchmann, A. Romualdi, T. Ott, J. Werringloer, K. Willecke, and M. Schwarz. "Lack of Phenobarbital-Mediated Promotion of Hepatocarcinogenesis in Connexin32-Null Mice." *Cancer Res* 60, no. 18 (2000): 5087-91.

Moennikes, O., S. Loeppen, A. Buchmann, P. Andersson, C. Ittrich, L. Poellinger, and M. Schwarz. "A Constitutively Active Dioxin/Aryl Hydrocarbon Receptor Promotes Hepatocarcinogenesis in Mice." *Cancer Res* 64, no. 14 (2004): 4707-10.

Moolgavkar, S. H., and A. G. Knudson, Jr. "Mutation and Cancer: A Model for Human Carcinogenesis." *J Natl Cancer Inst* 66, no. 6 (1981): 1037-52.

Morgan, E. T. "Regulation of Cytochrome P450 by Inflammatory Mediators: Why and How?" *Drug Metab Dispos* 29, no. 3 (2001): 207-12.

Morrison, D. K. "The 14-3-3 Proteins: Integrators of Diverse Signaling Cues That Impact Cell Fate and Cancer Development." *Trends Cell Biol* 19, no. 1 (2009): 16-23.

Muangmoonchai, R., D. Smirlis, S. C. Wong, M. Edwards, I. R. Phillips, and E. A. Shephard. "Xenobiotic Induction of Cytochrome P450 2b1 (Cyp2b1) Is Mediated by the Orphan Nuclear Receptor Constitutive Androstane Receptor (Car) and Requires Steroid Co-Activator 1 (Src-1) and the Transcription Factor Sp1." *Biochem J* 355, no. Pt 1 (2001): 71-8.

Nonomura, A., G. Ohta, M. Hayashi, R. Izumi, K. Watanabe, N. Takayanagi, Y. Mizukami, and F. Matsubara. "Immunohistochemical Detection of Ras Oncogene P21 Product in Liver Cirrhosis and Hepatocellular Carcinoma." *Am J Gastroenterol* 82, no. 6 (1987): 512-8.

Oinonen, T., E. Nikkola, and K. O. Lindros. "Growth Hormone Mediates Zone-Specific Gene Expression in Liver." *FEBS Lett* 327, no. 2 (1993): 237-40.

Oinonen, T., M. Ronis, T. Wigell, K. Tohmo, T. Badger, and K. O. Lindros. "Growth Hormone-Regulated Periportal Expression of Cyp2c7 in Rat Liver." *Biochem Pharmacol* 59, no. 5 (2000): 583-9.

Park, H. S., S. H. Lee, D. Park, J. S. Lee, S. H. Ryu, W. J. Lee, S. G. Rhee, and Y. S. Bae. "Sequential Activation of Phosphatidylinositol 3-Kinase, Beta Pix, Rac1, and Nox1 in Growth Factor-Induced Production of H2o2." *Mol Cell Biol* 24, no. 10 (2004): 4384-94.

Pegg, A. E. "Formation and Metabolism of Alkylated Nucleosides: Possible Role in Carcinogenesis by Nitroso Compounds and Alkylating Agents." *Adv Cancer Res* 25 (1977): 195-269.

Peraino, C., R. J. Fry, and E. Staffeldt. "Reduction and Enhancement by Phenobarbital of Hepatocarcinogenesis Induced in the Rat by 2-Acetylaminofluorene." *Cancer Res* 31, no. 10 (1971): 1506-12.

Phillips, J. M., Y. Yamamoto, M. Negishi, R. R. Maronpot, and J. I. Goodman. "Orphan Nuclear Receptor Constitutive Active/Androstane Receptor-Mediated Alterations in DNA Methylation During Phenobarbital Promotion of Liver Tumorigenesis." *Toxicol Sci* 96, no. 1 (2007): 72-82.

Porter, G. W., F. R. Khuri, and H. Fu. "Dynamic 14-3-3/Client Protein Interactions Integrate Survival and Apoptotic Pathways." *Semin Cancer Biol* 16, no. 3 (2006): 193-202.

Prough, R. A., M. D. Burke, and R. T. Mayer. "Direct Fluorometric Methods for Measuring Mixed Function Oxidase Activity." *Methods Enzymol* 52 (1978): 372-7.

Ren, H. Z., J. S. Wang, G. Q. Pan, H. Lv, J. F. Wen, G. Q. Luo, K. S. Wang, and P. F. Zhang. "Comparative Proteomic Analysis of Beta-Catenin-Mediated Malignant Progression of Esophageal Squamous Cell Carcinoma." *Dis Esophagus* 23, no. 2 (2010): 175-84.

Rignall, B., A. Braeuning, A. Buchmann, and M. Schwarz. "Tumor Formation in Liver of Conditional Beta-Catenin-Deficient Mice Exposed to a Diethylnitrosamine/Phenobarbital Tumor Promotion Regimen." *Carcinogenesis* 32, no. 1 (2011): 52-7.

Rignall, B., C. Ittrich, E. Krause, K. E. Appel, A. Buchmann, and M. Schwarz. "Comparative Transcriptome and Proteome Analysis of Ha-Ras and B-Raf Mutated Mouse Liver Tumors." *J Proteome Res* (2009).

Rushworth, L. K., A. D. Hindley, E. O'Neill, and W. Kolch. "Regulation and Role of Raf-1/B-Raf Heterodimerization." *Mol Cell Biol* 26, no. 6 (2006): 2262-72.

Safe, S. "Polychlorinated Biphenyls (Pcbs), Dibenzo-P-Dioxins (Pcdds), Dibenzofurans (Pcdfs), and Related Compounds: Environmental and Mechanistic Considerations Which Support the Development of Toxic Equivalency Factors (Tefs)." *Critical reviews in toxicology* 21, no. 1 (1990): 51-88.

Safe, S., S. Bandiera, T. Sawyer, L. Robertson, L. Safe, A. Parkinson, P. E. Thomas, D. E. Ryan, L. M. Reik, W. Levin, and et al. "Pcbs: Structure-Function Relationships and Mechanism of Action." *Environmental health perspectives* 60 (1985): 47-56.

Safe, S. H. "Polychlorinated Biphenyls (Pcbs): Environmental Impact, Biochemical and Toxic Responses, and Implications for Risk Assessment." *Crit Rev Toxicol* 24, no. 2 (1994): 87-149.

Schmidt, M. W., A. Houseman, A. R. Ivanov, and D. A. Wolf. "Comparative Proteomic and Transcriptomic Profiling of the Fission Yeast Schizosaccharomyces Pombe." *Molecular systems biology* 3 (2007): 79.

Scholz, W., K. Schutze, W. Kunz, and M. Schwarz. "Phenobarbital Enhances the Formation of Reactive Oxygen in Neoplastic Rat Liver Nodules." *Cancer Res* 50, no. 21 (1990): 7015-22.

Schulte-Hermann, R., I. Timmermann-Trosiener, G. Barthel, and W. Bursch. "DNA Synthesis, Apoptosis, and Phenotypic Expression as Determinants of Growth of Altered Foci in Rat Liver During Phenobarbital Promotion." *Cancer Res* 50, no. 16 (1990): 5127-35.

Schwarz, M., and K. E. Appel. "Carcinogenic Risks of Dioxin: Mechanistic Considerations." *Regul Toxicol Pharmacol* 43, no. 1 (2005): 19-34.

Schwarz, M., A. Buchmann, and K. W. Bock. "Role of Cell Proliferation at Early Stages of Hepatocarcinogenesis." *Toxicol Lett* 82-83 (1995): 27-32.

Sekine, S., B. Y. Lan, M. Bedolli, S. Feng, and M. Hebrok. "Liver-Specific Loss of Beta-Catenin Blocks Glutamine Synthesis Pathway Activity and Cytochrome P450 Expression in Mice." *Hepatology* 43, no. 4 (2006): 817-25.

Sekine, S., R. Ogawa, R. Ito, N. Hiraoka, M. T. McManus, Y. Kanai, and M. Hebrok. "Disruption of Dicer1 Induces Dysregulated Fetal Gene Expression and Promotes Hepatocarcinogenesis." *Gastroenterology* 136, no. 7 (2009): 2304-15 e1-4.

Silberhorn, E. M., H. P. Glauert, and L. W. Robertson. "Carcinogenicity of Polyhalogenated Biphenyls: Pcbs and Pbbs." *Crit Rev Toxicol* 20, no. 6 (1990): 440-96.

Stahl, S., C. Ittrich, P. Marx-Stoelting, C. Kohle, O. Altug-Teber, O. Riess, M. Bonin, J. Jobst, S. Kaiser, A. Buchmann, and M. Schwarz. "Genotype-Phenotype Relationships in Hepatocellular Tumors from Mice and Man." *Hepatology* 42, no. 2 (2005): 353-61.

Stinchcombe, S., A. Buchmann, K. W. Bock, and M. Schwarz. "Inhibition of Apoptosis During 2,3,7,8-Tetrachlorodibenzo-P-Dioxin-Mediated Tumour Promotion in Rat Liver." *Carcinogenesis* 16, no. 6 (1995): 1271-5.

Strathmann, J., K. Paal, C. Ittrich, E. Krause, K. E. Appel, H. P. Glauert, A. Buchmann, and M. Schwarz. "Proteome Analysis of Chemically Induced Mouse Liver Tumors with Different Genotype." *Proteomics* 7, no. 18 (2007): 3318-31.

Strathmann, J., M. Schwarz, J. C. Tharappel, H. P. Glauert, B. T. Spear, L. W. Robertson, K. E. Appel, and A. Buchmann. "Pcb 153, a Non-Dioxin-Like Tumor Promoter, Selects for Beta-Catenin (Catnb)-Mutated Mouse Liver Tumors." *Toxicol Sci* 93, no. 1 (2006): 34-40.

Swales, K., and M. Negishi. "Car, Driving into the Future." *Mol Endocrinol* 18, no. 7 (2004): 1589-98.

Takemaru, K., V. Fischer, and F. Q. Li. "Fine-Tuning of Nuclear-Catenin by Chibby and 14-3-3." *Cell Cycle* 8, no. 2 (2009): 210-3.

Tan, X., J. Behari, B. Cieply, G. K. Michalopoulos, and S. P. Monga. "Conditional Deletion of Beta-Catenin Reveals Its Role in Liver Growth and Regeneration." *Gastroenterology* 131, no. 5 (2006): 1561-72.

Taniguchi, K., L. R. Roberts, I. N. Aderca, X. Dong, C. Qian, L. M. Murphy, D. M. Nagorney, L. J. Burgart, P. C. Roche, D. I. Smith, J. A. Ross, and W. Liu. "Mutational Spectrum of Beta-Catenin, Axin1, and Axin2 in Hepatocellular Carcinomas and Hepatoblastomas." *Oncogene* 21, no. 31 (2002): 4863-71.

Thorgeirsson, S. S., and J. W. Grisham. "Molecular Pathogenesis of Human Hepatocellular Carcinoma." *Nat Genet* 31, no. 4 (2002): 339-46.

Treisman, R. "Regulation of Transcription by Map Kinase Cascades." *Current opinion in cell biology* 8, no. 2 (1996): 205-15.

Unwin, R. D., and A. D. Whetton. "Systematic Proteome and Transcriptome Analysis of Stem Cell Populations." *Cell Cycle* 5, no. 15 (2006): 1587-91.

van Birgelen, A. P., D. G. Ross, M. J. DeVito, and L. S. Birnbaum. "Interactive Effects between 2,3,7,8-Tetrachlorodibenzo-P-Dioxin and 2,2',4,4',5,5'-Hexachlorobiphenyl in Female B6c3f1 Mice: Tissue Distribution and Tissue-Specific Enzyme Induction." *Fundam Appl Toxicol* 34, no. 1 (1996): 118-31.

van der Plas, S. A., M. Haag-Gronlund, G. Scheu, L. Warngard, M. van den Berg, P. Wester, J. H. Koeman, and A. Brouwer. "Induction of Altered Hepatic Foci by a Mixture of Dioxin-Like Compounds with and without 2,2',4,4',5,5'-Hexachlorobiphenyl in Female Sprague-Dawley Rats." *Toxicol Appl Pharmacol* 156, no. 1 (1999): 30-9.

Verna, L., J. Whysner, and G. M. Williams. "N-Nitrosodiethylamine Mechanistic Data and Risk Assessment: Bioactivation, DNA-Adduct Formation, Mutagenicity, and Tumor Initiation." *Pharmacol Ther* 71, no. 1-2 (1996): 57-81.

Wachstein, M., and E. Meisel. "Histochemistry of Hepatic Phosphatases of a Physiologic Ph; with Special Reference to the Demonstration of Bile Canaliculi." *American journal of clinical pathology* 27, no. 1 (1957): 13-23.

Wan, P. T., M. J. Garnett, S. M. Roe, S. Lee, D. Niculescu-Duvaz, V. M. Good, C. M. Jones, C. J. Marshall, C. J. Springer, D. Barford, and R. Marais. "Mechanism of Activation of the Raf-Erk Signaling Pathway by Oncogenic Mutations of B-Raf." *Cell* 116, no. 6 (2004): 855-67.

Washburn, M. P., R. R. Ulaszek, and J. R. Yates, 3rd. "Reproducibility of Quantitative Proteomic Analyses of Complex Biological Mixtures by Multidimensional Protein Identification Technology." *Analytical chemistry* 75, no. 19 (2003): 5054-61.

Watson, M. A., T. R. Devereux, D. E. Malarkey, M. W. Anderson, and R. R. Maronpot. "H-Ras Oncogene Mutation Spectra in B6c3f1 and C57bl/6 Mouse Liver Tumors Provide Evidence for Tcdd Promotion of Spontaneous and Vinyl Carbamate-Initiated Liver Cells." *Carcinogenesis* 16, no. 8 (1995): 1705-10.

Waxman, D. J. "P450 Gene Induction by Structurally Diverse Xenochemicals: Central Role of Nuclear Receptors Car, Pxr, and Ppar." *Arch Biochem Biophys* 369, no. 1 (1999): 11-23.

Wei, P., J. Zhang, M. Egan-Hafley, S. Liang, and D. D. Moore. "The Nuclear Receptor Car Mediates Specific Xenobiotic Induction of Drug Metabolism." *Nature* 407, no. 6806 (2000): 920-3.

Wellbrock, C., M. Karasarides, and R. Marais. "The Raf Proteins Take Centre Stage." *Nat Rev Mol Cell Biol* 5, no. 11 (2004): 875-85.

Wilker, E. W., M. A. van Vugt, S. A. Artim, P. H. Huang, C. P. Petersen, H. C. Reinhardt, Y. Feng, P. A. Sharp, N. Sonenberg, F. M. White, and M. B. Yaffe. "14-3-3sigma Controls Mitotic Translation to Facilitate Cytokinesis." *Nature* 446, no. 7133 (2007): 329-32.

Willert, K., and R. Nusse. "Beta-Catenin: A Key Mediator of Wnt Signaling." *Curr Opin Genet Dev* 8, no. 1 (1998): 95-102.

Wong, C. M., and I. O. Ng. "Molecular Pathogenesis of Hepatocellular Carcinoma." *Liver Int* 28, no. 2 (2008): 160-74.

Wu, W., L. M. Graves, G. N. Gill, S. J. Parsons, and J. M. Samet. "Src-Dependent Phosphorylation of the Epidermal Growth Factor Receptor on Tyrosine 845 Is Required for Zinc-Induced Ras Activation." *J Biol Chem* 277, no. 27 (2002): 24252-7.

Yamamoto, Y., R. Moore, T. L. Goldsworthy, M. Negishi, and R. R. Maronpot. "The Orphan Nuclear Receptor Constitutive Active/Androstane Receptor Is Essential for Liver Tumor Promotion by Phenobarbital in Mice." *Cancer Res* 64, no. 20 (2004): 7197-200.

Zhang, X. F., X. Tan, G. Zeng, A. Misse, S. Singh, Y. Kim, J. E. Klaunig, and S. P. Monga. "Conditional Beta-Catenin Loss in Mice Promotes Chemical Hepatocarcinogenesis: Role of Oxidative Stress and Platelet-Derived Growth Factor Receptor Alpha/Phosphoinositide 3-Kinase Signaling." *Hepatology* 52, no. 3 (2010): 954-65.

9. Appendix

Table 10: Statistically significant altered proteins expressed in project D as analyzed by proteome analysis followed by MS identification.

	Protein ID	fc.median	Access
PCB 153 H vs Oil	Pyruvate kinase isozymes R/L	0,47	P53657
	S-adenosylmethionine synthetase isoform type-1	0,67	Q91X83
	Carboxylesterase 3	1,51	Q8VCT4
	Liver carboxylesterase 31	1,57	Q63880
	Ester hydrolase C11orf54 homolog	1,58	Q91V76
	Probable D-lactate dehydrogenase, mitochondrial	1,61	Q7TNG8
	UDP-glucose 6-dehydrogenase	1,64	O70475
	Peroxiredoxin-6	1,74	O08709
	Serum paraoxonase/arylesterase	1,84	P52430
	Selenium-binding protein 2	2,27	Q63836
	Selenium-binding protein 1	2,27	P17563
	Anionic trypsin-1	2,37	P00762
	Fructose-bisphosphate aldolase B	2,53	Q91Y97
	Triosephosphate isomerase	2,64	P17751
	Glutathione S-transferase Mu 1	2,67	P10649
	Glutathione S-transferase Mu 3	2,67	P19639
	Alpha-1-antitrypsin 1-4	3,66	Q00897
	Alpha-1-antitrypsin 1-4	3,66	Q00897
PCB 153 L vs oil	Aldehyde dehydrogenase, mitochondrial	0,33	P47738
	Pyruvate kinase isozymes R/L	0,53	P53657
	Glycine dehydrogenase [decarboxylating], mitochondrial	0,64	Q91W43
	3-oxoacyl-[acyl-carrier-protein] synthase, mitochondrial	0,64	Q9D404
	Fructose-bisphosphate aldolase B	1,77	Q91Y97
	Triosephosphate isomerase	2,03	P17751
PCB 126 H vs oil	Pyruvate kinase isozymes R/L	0,42	P53657
	Alpha-1-antitrypsin 1-5	0,55	Q00898
	Alpha-1-antitrypsin 1-1	0,55	P07758
	Alpha-1-antitrypsin 1-2	0,55	P22599
	Alpha-1-antitrypsin 1-4	0,55	Q00897
	Moesin	0,58	P26041
	Ezrin	0,58	P26040
	Radixin	0,58	P26043
	Valacyclovir hydrolase	0,58	Q8R164
	Methylcrotonoyl-CoA carboxylase subunit alpha, mitochondrial	0,59	Q99MR8
	Alanine--glyoxylate aminotransferase 2, mitochondrial	0,64	Q3UEG6
	Glyceraldehyde-3-phosphate dehydrogenase, testis-specific	0,65	Q64467
	Glutathione S-transferase A3	0,66	P30115
	Glutathione S-transferase A2	0,66	P10648
	S-adenosylmethionine synthetase isoform type-1	0,66	Q91X83
	Protein disulfide-isomerase A3	1,53	P27773
	UDP-glucose 6-dehydrogenase	1,80	O70475
	Serum paraoxonase/arylesterase	2,68	P52430

Table 10: (continued)

PCB 126 L vs oil	Aldehyde dehydrogenase, mitochondrial	0,47	P47738
	Pyruvate kinase isozymes R/L	0,52	P53657
	Moesin	0,60	P26041
	Ezrin	0,60	P26040
	Radixin	0,60	P26043
	Fumarylacetoacetate hydrolase domain-containing protein	0,64	Q3TC72
	Rho GDP-dissociation inhibitor 1	0,67	Q5XI73
	Carboxylesterase 3	1,58	Q8VCT4
	Keratin, type I cytoskeletal 10	1,66	P02535
	Serum paraoxonase/arylesterase	2,11	P52430
cPCBs vs oil	Aldehyde dehydrogenase, mitochondrial	0,23	P47738
	S-adenosylmethionine synthetase isoform type-1	0,48	Q91X83
	Alpha-1-antitrypsin 1-5	0,60	Q00898
	Alpha-1-antitrypsin 1-1	0,60	P07758
	Alpha-1-antitrypsin 1-2	0,60	P22599
	Alpha-1-antitrypsin 1-4	0,60	Q00897
	Protein disulfide-isomerase A3	1,57	P27773
	UDP-glucose 6-dehydrogenase	1,70	O70475
	14-3-3 protein sigma	1,54	O70456
	Glyoxylate reductase/hydroxypyruvate reductase	1,56	Q91Z53
	Flavin reductase	1,65	Q923D2
	Keratin, type I cytoskeletal 10	1,71	P02535
	14-3-3 protein beta/alpha	1,72	Q9CQV8
	Peroxiredoxin-6	1,76	O08709
	14-3-3 protein zeta/delta	1,82	P63102
	Fructose-bisphosphate aldolase B	1,85	Q91Y97
	Carboxylesterase 3	2,02	Q8VCT4
	Selenium-binding protein 2	2,05	Q63836
	Selenium-binding protein 1	2,05	P17563
	Anionic trypsin-1	2,06	P00762
	Glutathione S-transferase Mu 1	2,40	P10649
	Glutathione S-transferase Mu 3	2,40	P19639
	UDP-glucose 6-dehydrogenase	2,66	O70475
	Triosephosphate isomerase	2,88	P17751
	Serum paraoxonase/arylesterase	3,17	P52430
	Alpha-1-antitrypsin 1-4	4,36	Q00897
	Alpha-1-antitrypsin 1-1	4,36	P07758
	Alpha-1-antitrypsin 1-2	4,36	P22599
	Alpha-1-antitrypsin 1-5	4,36	Q00898
	Alpha-1-antiproteinase	4,36	P26595
	Alpha-1-antitrypsin 1-4	4,45	Q00897
	Alpha-1-antitrypsin 1-4	4,45	Q00897
PCB 153 L vs PCB 153 H	Staphylococcal nuclease domain-containing protein 1	0,54	Q78PY7
	Glutathione S-transferase Mu 1	0,54	P10649
	Glutathione S-transferase Mu 3	0,54	P19639
	Anionic trypsin-1	0,60	P00762

Table 10: (continued)

PCB 126 H vs PCB 153 H	Glutathione S-transferase Mu 1	0,42	P10649
	Glutathione S-transferase Mu 3	0,42	P19639
	Selenium-binding protein 2	0,42	Q63836
	Selenium-binding protein 1	0,42	P17563
	Fructose-bisphosphate aldolase B	0,43	Q91Y97
	Phenylalanine-4-hydroxylase	0,43	P16331
	Anionic trypsin-1	0,48	P00762
	Keratin, type I cytoskeletal 18	0,56	P05784
	Methylcrotonoyl-CoA carboxylase subunit alpha, mitochondrial	0,58	Q99MR8
	Glutathione S-transferase A3	0,58	P30115
	Glutathione S-transferase A2	0,58	P10648
	Glyoxylate reductase/hydroxypyruvate reductase	0,60	Q91Z53
	Proteasome activator complex subunit 1	0,60	P97371
	Proteasome activator complex subunit 2	0,60	P97372
	UDP-glucose 6-dehydrogenase	0,61	O70475
	Peroxiredoxin-6	0,63	O08709
	Anionic trypsin-1	0,64	P00762
	Apolipoprotein A-I	0,64	Q00623
	Liver carboxylesterase 31	0,65	Q63880
	FK506-binding protein 4	0,65	P30416
	Heat shock 70 kDa protein 1B	0,66	P17879
	Selenium-binding protein 2	0,67	Q63836
	Sarcosine dehydrogenase, mitochondrial	1,54	Q99LB7
	Ferritin light chain 1	1,52	P29391
	Ferritin light chain 2	1,52	P49945
	Dimethylglycine dehydrogenase, mitochondrial	1,65	Q9DBT9
PCB 126 L vs PCB 153 L	Fructose-bisphosphate aldolase B	0,52	Q91Y97
cPCBs vs PCB 153 L	S-adenosylmethionine synthetase isoform type-1	0,58	Q91X83
	Fructose-bisphosphate aldolase B	0,60	Q91Y97
	Serum paraoxonase/arylesterase	1,96	P52430
	UDP-glucose 6-dehydrogenase	2,02	O70475
	Alpha-1-antitrypsin 1-4	2,19	Q00897
	Alpha-1-antitrypsin 1-4	2,19	Q00897
	Keratin, type II cytoskeletal 8	2,54	P11679
PCB 126 L vs H	Keratin, type II cytoskeletal 8	0,54	P11679

Table 10: (continued)

cPCB vs PCB 126 L	Nuclear migration protein nudC	1,53	O35685
	14-3-3 protein sigma	1,55	O70456
	Phenylalanine-4-hydroxylase	1,55	P16331
	Alpha-1-antitrypsin 1-4	1,57	Q00897
	Endoplasmic reticulum resident protein ERp44	1,58	Q9D1Q6
	Peroxiredoxin-6	1,63	O08709
	14-3-3 protein zeta/delta	1,68	P63102
	Fructose-bisphosphate aldolase B	1,68	Q91Y97
	Keratin, type II cytoskeletal 8	1,74	P11679
	Glutathione S-transferase P 1	1,77	P19157
	Glutathione S-transferase P 2	1,77	P46425
	Anionic trypsin-1	1,84	P00762
	Triosephosphate isomerase	1,96	P17751
	Keratin, type II cytoskeletal 8	2,10	P11679
	Selenium-binding protein 2	2,19	Q63836
	Selenium-binding protein 1	2,19	P17563
	Glutathione S-transferase Mu 1	2,31	P10649
	Glutathione S-transferase Mu 3	2,31	P19639
	UDP-glucose 6-dehydrogenase	2,44	O70475

Abbreviations: L, low dose; H, high dose; cPCBs, combined PCB 126/153 treatment; fc median; median fold change.

Table 11: Liver-PCB contents measured in the exploratory experiment of project D

		Liver PCB Concentration					Liver PCB Concentration		
Probe number	Treatment	[PCB] [ng/g] wet weight	Average	S.D.	Probe number	Treatment	[PCB] [ng/g] wet weight	Average	S.D.
1	PCB126 Control day 4	0,25	0,1	0,2	31	PCB153 Control day 4	4,34	3,2	1,7
2	PCB126 Control day 4	0,00			32	PCB153 Control day 4	1,98		
3	PCB126 Control day 21	0,00	0,0	0,0	33	PCB153 Control day 21	1,35	2,0	0,9
4	PCB126 Control day 21	0,00			34	PCB153 Control day 21	2,58		
5	PCB126 Control day 42	-	-	-	35	PCB153 Control day 42	-	-	-
6	PCB126 Control day 42	-			36	PCB153 Control day 42	-		
7	PCB126 10µg/KBw day 4	63,52	64,3	1,1	37	PCB153 25mg/KBw day 4	6169,47	6057,9	157,8
8	PCB126 10µg/KBw day 4	65,11			38	PCB153 25mg/KBw day 4	5946,29		
9	PCB126 10µg/KBw day 21	42,48	38,8	5,2	39	PCB153 25mg/KBw day 21	2681,13	3246,8	800,0
10	PCB126 10µg/KBw day 21	35,19			40	PCB153 25mg/KBw day 21	3812,57		
11	PCB126 10µg/KBw day 42	19,86	16,4	4,9	41	PCB153 25mg/KBw day 42	2251,56	2258,9	10,4
12	PCB126 10µg/KBw day 42	12,88			42	PCB153 25mg/KBw day 42	2266,26		
13	PCB126 50µg/KBw day 4	377,90	424,5	65,9	43	PCB153 50mg/KBw day 4	11155,94	11163,1	10,1
14	PCB126 50µg/KBw day 4	471,09			44	PCB153 50mg/KBw day 4	11170,24		
15	PCB126 50µg/KBw day 21	270,19	243,1	38,3	45	PCB153 50mg/KBw day 21	4386,29	5614,2	1736,6
16	PCB126 50µg/KBw day 21	216,05			46	PCB153 50mg/KBw day 21	6842,19		
17	PCB126 50µg/KBw day 42	124,24	126,1	2,7	47	PCB153 50mg/KBw day 42	4124,16	4239,6	163,3
18	PCB126 50µg/KBw day 42	128,04			48	PCB153 50mg/KBw day 42	4355,07		
19	PCB126 100µg/KBw day 4	807,66	803,1	6,4	49	PCB153 75mg/KBw day 4	15921,68	16433,0	723,2
20	PCB126 100µg/KBw day 4	798,58			50	PCB153 75mg/KBw day 4	16944,40		
21	PCB126 100µg/KBw day 21	506,82	555,1	68,3	51	PCB153 75mg/KBw day 21	10833,62	11511,5	958,6
22	PCB126 100µg/KBw day 21	603,47			52	PCB153 75mg/KBw day 21	12189,30		
23	PCB126 100µg/KBw day 42	324,87	168,8	220,7	53	PCB153 75mg/KBw day 42	5924,36	6277,5	499,4
24	PCB126 100µg/KBw day 42	12,73			54	PCB153 75mg/KBw day 42	6630,61		
25	PCB126 200µg/KBw day 4	2273,12	2058,8	303,1	55	PCB153 100mg/KBw day 4	21443,59	22225,5	1105,8
26	PCB126 200µg/KBw day 4	1844,41			56	PCB153 100mg/KBw day 4	23007,36		
27	PCB126 200µg/KBw day 21	1582,85	1357,5	318,7	57	PCB153 100mg/KBw day 21	11382,18	11128,4	358,9
28	PCB126 200µg/KBw day 21	1132,20			58	PCB153 100mg/KBw day 21	10874,67		
29	PCB126 200µg/KBw day 42	907,13	867,3	56,3	59	PCB153 100mg/KBw day 42	8220,69	7773,0	633,1
30	PCB126 200µg/KBw day 42	827,46			60	PCB153 100mg/KBw day 42	7325,36		

Abbreviations: S.D., standard deviation; KBw, kilogram body weight.